



Province of British Columbia  
Ministry of Energy, Mines and  
Petroleum Resources  
Hon. Anne Edwards, Minister

*Energy, Mines and Petroleum Resources  
Victoria, B.C.*



0008004962

MINERAL RESOURCES DIVISION  
Geological Survey Branch

**ORIGIN AND TECTONIC SETTING OF  
OPHIOLITIC ULTRAMAFIC AND RELATED  
ROCKS IN THE ATLIN AREA, BRITISH  
COLUMBIA (NTS 104N)**

By Chris H. Ash, P.Geo.

Canadian Cataloguing in Publication Data  
Ash, Christopher, H. (Christopher Henry)  
*Origin and tectonic setting of ophiolitic ultramafic and related  
rocks in the Atlin area, British Columbia (NTS 104N)*

(Bulletin, ISSN 0226-7497 ; 94)

Issued by Geological Survey Branch.  
Includes bibliographical references: p.  
ISBN 0-7726-2215-9

1. Geology, Structural - British Columbia - Atlin Region. 2.  
Gold ores - Geology - British Columbia - Atlin Region. 3.  
Geology, Economic - British Columbia - Atlin Region. I. British  
Columbia. Ministry of Energy, Mines and Petroleum Resources.  
II. British Columbia. Geological Survey Branch. III. Title. IV.  
Series: Bulletin (British Columbia. Ministry of Energy, Mines and  
Petroleum Resources) ; 94.

QE611.5C3A83 1994

551.88'0971185

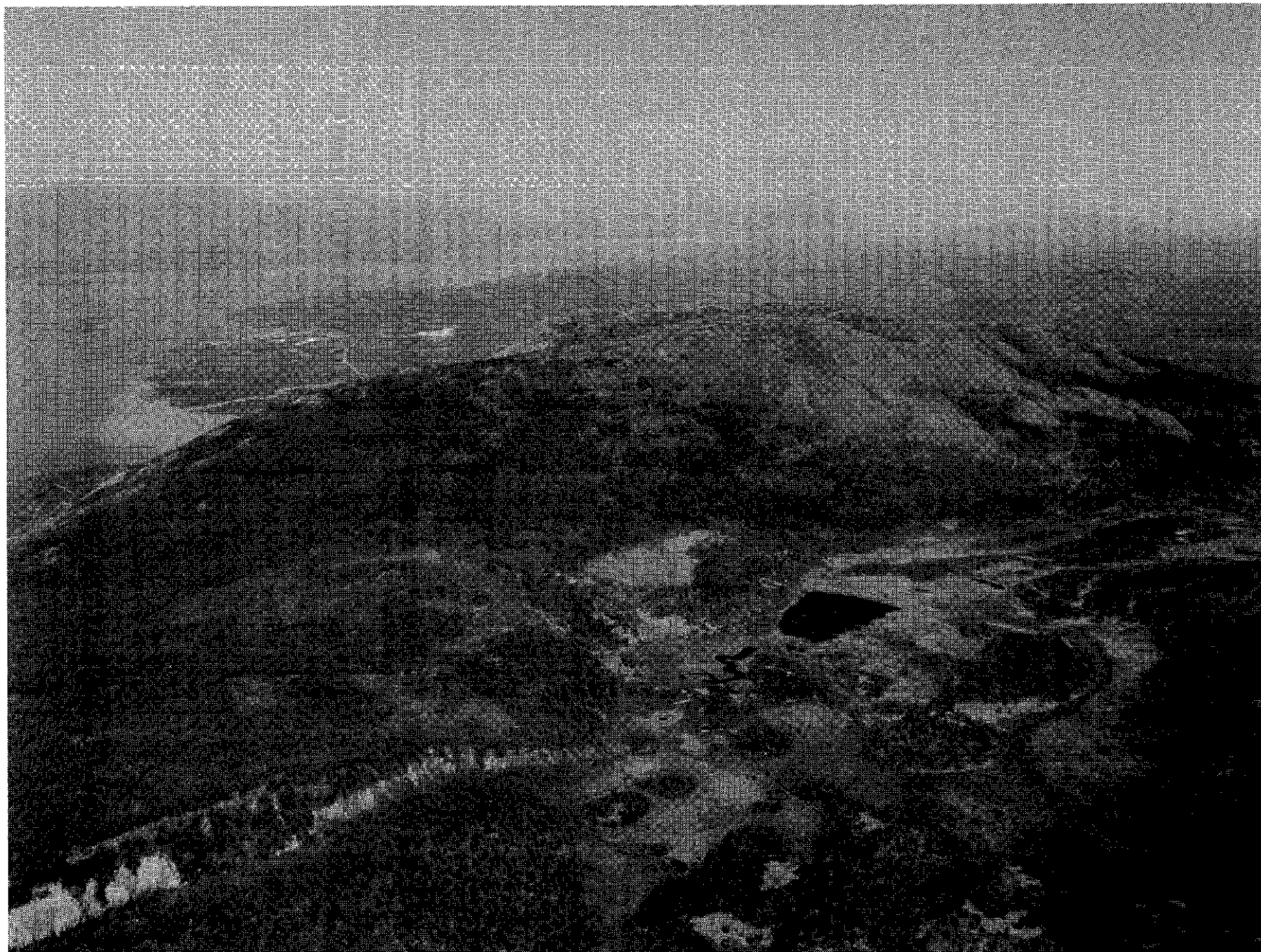
C94-960274-4



VICTORIA  
BRITISH COLUMBIA  
CANADA

JULY 1994

*Fieldwork for this research took place during the  
period 1989-1990.*



Frontispiece: Aerial view of Monarch Mountain and Atlin looking northwest.

## TABLE OF CONTENTS

	<i>page</i>		<i>page</i>
ABSTRACT.....	1	Origin of the Atlin Ultramafic Allochthon.....	41
CHAPTER 1		Emplacement of Atlin Ultramafic Allochthon.....	41
INTRODUCTION.....	3	Conclusions.....	43
Previous Work.....	5	REFERENCES.....	45
Present Study.....	5	FIGURES	
Acknowledgments.....	5	1-1. Top ten past-producing mesothermal gold vein deposits in British Columbia.....	3
CHAPTER 2		1-2. Top six gold-producing mining districts in British Columbia.....	3
GEOLOGY OF THE ATLIN AREA.....	7	1-3. Location of the Atlin map area.....	4
Regional Setting.....	7	2-1. Regional geological setting of the Atlin map area...	7
Local Geology.....	10	2-2. (A) Geology map of the Atlin area.....	8
Atlin Ophiolitic Assemblage.....	10	2-2. (B) Schematic geological cross section of the Atlin area.....	9
Ultramafic Rocks.....	10	2-3. Classification and nomenclature of ultramafic rocks.....	10
Harzburgite.....	10	3-1. Cross section of the Pictou showing.....	24
Serpentinite-bastite.....	12	3-2. Simplified model for ultramafic rocks.....	26
Petrography.....	13	3-3. Schematic representation of moderate, "A," and intense, "B," S <sub>2</sub> fabric development in harzburgite defined by bastite.....	27
Dunite.....	14	4-1. Composition of orthopyroxenes from harzburgite in the Atlin ultramafic allochthon.....	31
Petrography.....	15	4-2. Composition of chrome-spinels in harzburgite and dunite from the Atlin ultramafic allochthon compared to compositional fields for alpine-type peridotite.....	36
Pyroxenite Dikes.....	15	4-3. Molecular ratio plot for chrome spinels in harzburgites and dunites.....	36
Peridotite Cumulates (Wehrlite?).....	16	4-4. Classification of Atlin metabasalts.....	38
Petrography.....	16	4-5. Major element discrimination illustrating field of Atlin metabasalts.....	38
Metagabbro.....	17	4-6. Mobile element tectonomagmatic discrimination diagram illustrating field of Atlin metabasalts.....	38
Metabasaltic Rocks.....	17	4-7. Chondrite-normalized rare-earth-element distribution patterns for Atlin metabasalts.....	39
Petrography.....	18	4-8. Plot of Ti/1000 vs V, illustrating field of Atlin metabasalts.....	39
Atlin Accretionary Complex.....	18	4-9. Cr vs Y discrimination plot illustrating field of Atlin metabasalts.....	39
Intrusive Rocks.....	20	4-10. MORB normalized multi-element distribution patterns for Atlin metabasalts.....	39
Fourth of July Batholith.....	20	4-11. Genetic pathways on the Cr-Y plot for derivation of lavas in the Atlin area.....	40
Feldspar (Quartz) Porphyritic Dike Suite.....	21		
Melanocratic Dike Suite.....	21		
Surprise Lake Batholith.....	21		
CHAPTER 3			
STRUCTURE.....	23		
Atlin Accretionary Complex.....	23		
Atlin Ultramafic Allochthon.....	24		
Monarch Mountain Thrust.....	24		
Structure within the Allochthon.....	25		
Pre-Obduction Structures.....	26		
Obduction-Related Structures.....	26		
Serpentinite-Bastite Mylonite.....	27		
Post-Accretionary Structures.....	28		
Pine Creek Fault Zone.....	28		
CHAPTER 4			
LITHOGEOCHEMISTRY OF THE ATLIN OPHIOLITIC ASSEMBLAGE.....	31		
Phase Chemistry of the Ultramafic Rocks.....	31		
Olivine.....	31		
Orthopyroxene.....	31		
Chrome Spinel.....	36		
Geochemistry of the Atlin Metavolcanics.....	37		
Modeling the Mantle Source Region.....	40		
CHAPTER 5			
SUMMARY.....	41		

	<i>page</i>		<i>page</i>
5-1. Schematic representation for the origin and emplacement of ophiolitic and related rocks in the Atlin area .....	42	2-14. Light-coloured ribboned chert.....	19
<b>MAP</b>		2-15. Intensely sheared scaly argillite within the footwall of the Monarch Mountain thrust.....	20
Geological Map of the Atlin Area (1:250 000) scale.....	in pocket	2-16. Polymictic sedimentary/tectonic breccia south of Monarch Mountain .....	20
<b>PHOTOS</b>		2-17. Typical weathered surface of the potassium-feldspar megacrystic granitic phase of the Fourth of July batholith .....	
<b>FRONTISPIECE</b>		3-1. Lensoid chert fragments at the Beavis property .....	23
Aerial view of Monarch Mountain and Atlin looking northwest.....	<i>iii</i>	3-2. Intensely carbonatized ultramafic tectonic breccia 0.5 kilometre south of Atlin.....	25
2-1. Weathered appearance of harzburgite .....	11	3-3. Elongation of bastite mantling relict orthopyroxene .....	27
2-2. Tectonite banding .....	11	3-4. Well-banded mylonitic serpentinite-bastite fabric (S <sub>2</sub> ) with relict orthopyroxene porphyroclasts .....	27
2-3. Folded orthopyroxene banding in harzburgite tectonite .....	12	3-5. Serpentinite breccia with harzburgite knockers in a matrix of strongly sheared serpentinite .....	29
2-4. Mottled appearance of weathered serpentinite .....	12	<b>TABLES</b>	
2-5. Photomicrograph of partially serpentinized harzburgite.....	13	4-1A. Phase chemistry of olivine in harzburgite from the Atlin ultramafic allochthon.....	32
2-6. Photomicrograph of orthopyroxene-clinopyroxene-spinel cluster in harzburgite.....	13	4-1B. Phase chemistry of olivine in dunite from the Atlin ultramafic allochthon .....	32
2-7. Typical lenticular dunite body.....	14	4-2. Phase chemistry of orthopyroxene in harzburgite from the Atlin ultramafic allochthon .....	33
2-8. Close-up of contact between harzburgite and dunite pod.....	15	4-3A. Phase chemistry of chrome spinel in harzburgite from the Atlin ultramafic allochthon .....	34
2-9. Photomicrograph of partially serpentinized dunite.....	15	4-3B. Phase chemistry of chrome spinel in dunite from the Atlin ultramafic allochthon .....	35
2-10. Concordant and discordant pyroxenite dikes in harzburgite.....	16	4-4. Whole rock major, trace and rare earth elemental abundances for metavolcanic rocks in the Atlin area .....	37
2-11. Tightly folded pyroxenite dike in harzburgite .....	16		
2-12. Autobrecciation texture in well-washed exposure of metabasalt .....	17		
2-13. Well-preserved basaltic pillow lavas in the Lina Range.....	17		

---

# ABSTRACT

---

Mesothermal gold-bearing quartz veins throughout the Atlin placer camp of northwestern British Columbia are contained within or marginal to carbonate-altered ultramafic rocks (listwanites). These ultramafic rocks comprise individual thrust slices which form part of an imbricated package of late Paleozoic oceanic crust and upper mantle lithologies referred to as the Atlin ophiolitic assemblage. This ophiolitic assemblage was obducted onto a subduction-related accretionary complex, the Atlin accretionary complex, during the Middle Jurassic collision of Stikinia with North America.

Ultramafic rocks include both foliated harzburgite with subordinate dunite pods and peridotite cumulates, most likely wehrlite, that form individual thrust slices. The harzburgite is characterized by a medium to coarse-grained porphyroclastic texture. A well-developed primary foliation fabric ( $S_1$ ) and compositional banding with isoclinal folding of both banding and pyroxenite dikes. Features widely accepted to be indicative of ductile deformation at subsolidus to hypersolidus conditions during and subsequent to mantle partial melting.

Primary silicate phase chemistry of the harzburgite indicates that the unit is highly refractory with a very limited compositional range (En<sub>87.8-90.2</sub>, Fo<sub>89.5-90.7</sub>). Chrome spinels in the harzburgite form highly irregular amoeboid shapes and compositionally display a large reciprocal variation of chrome and alumina, which defines a partial melting trend. The texture, structure and the primary phase chemical

composition of the harzburgites indicate that they represent metamorphic mantle material formed by partial melting below a paleo-oceanic spreading centre. More specifically, the unit may be characterized as an abyssal peridotite formed within a mid-ocean ridge (MOR) paleotectonic setting as the chrome spinels have low Cr#[(Cr<sub>x</sub>100)/(Cr+Al); 23-47] and clinopyroxene contents are locally greater than 5%, indicating relatively fertile depleted mantle.

Whole-rock major, trace and rare-earth elemental (REE) data obtained for the metabasaltic rocks emplaced tectonically with the ultramafics, indicate that they are subalkaline tholeiitic in composition and also suggest a MOR paleotectonic eruptive setting for their origin. Petrogenetic modeling of the mantle source region using the basalt chemistry indicates that the basaltic liquids were derived by limited degrees of partial melting (10 to 15%). The ultramafic and metabasaltic rocks are therefore considered to be cogenetic.

The mantle section contains  $S_2$  emplacement-related fabrics that are defined by retrograde metamorphic assemblages after primary olivine and orthopyroxene. The distribution and variation in intensity of development of the  $S_2$  fabrics indicate that the ultramafic body has been affected by inhomogeneous bulk strain during tectonic emplacement in the solid state. Overprinting of these ductile fabrics by listwanite alteration along the basal thrust fault of the ultramafic body indicated subsequent influx of carbon-dioxide rich fluids.



## CHAPTER 1

## INTRODUCTION

The Listwanite Project was initiated in 1989 to establish the tectonic setting, origin and timing of ophiolite-related lode gold mineralization in British Columbia. The purpose of this research was to develop a metallogenic deposit model for mesothermal gold mineralization in the Province. Both lode deposits of this type and related placers are consistently associated with carbonatized ultramafic rocks known as listwanites (Ash and Arksey, 1990b). This association of ophiolitic ultramafic rocks and lode gold deposits, or their related placers, within and marginal to accreted oceanic terranes has been previously recognized (Hodgson *et al.*, 1982). The genetic relationship between the ultramafic rocks and gold deposits, however, has not been adequately evaluated to date. Provincial examples of gold camps with spatially associated ultramafic rocks include the Bridge River, Cassiar and Rossland lode gold and the Atlin and Dease Lake placer camps. Other examples in the Cordillera include both the Mother Lode gold belt of California and the Klondike area in the Yukon.

The economic significance of this deposit type in British Columbia is apparent from historic gold production (Schroeter *et al.*, 1989). Of the six gold camps producing more than 1 million ounces of gold (Figure 1-1), which together account for approximately 80% of the gold produced in the province, three are mesothermal vein districts with a clear ophiolitic association. Five of the top ten mesothermal vein deposits (Figure 1-2) have a known ophiolitic association. Added economic significance for this deposit type is reflected by the fact that the majority of placer gold camps in British Columbia are intimately associated with accreted ophiolitic terranes.

This association is fundamentally structural as the ultramafic rocks mark fault zones of deep crustal origin which are a first-order control on the development of this deposit type (Hoffman, 1990). Listwanites are distinctive indicators of sites along such structures where large volumes of CO<sub>2</sub>-rich fluids have been channeled. In addition to marking major hydrothermally active, transcrustal faults, the ultramafic rocks may also play a fundamental role as either the source of the gold or in triggering gold deposition, or both (Buisson and Leblanc, 1985, 1986). However, acceptance of a genetic link between the two remains a current topic of debate.

This paper presents the results of a detailed investigation of the tectonic setting and origin of ultramafic and related rocks in the Atlin area (Figure 1-3). A preliminary report and map (Ash and Arksey, 1990a, c) discussing initial results from the Atlin area have been published. Aspects of

the timing and structural setting of lode gold mineralization integrated with the regional tectonic history for this and the other camps studied in the province are published separately (Ash *et al.*, in preparation).

The Atlin area was selected for detailed study because of its excellent road access, the large number of listwanite-related lode gold occurrences and the extensive exploration database available for many of these occurrences. Following detailed mapping (1:25 000 scale) of the ultramafic rocks underlying the town of Atlin and Monarch Mountain in 1989 (Ash and Arksey, 1990a) the area was revisited in

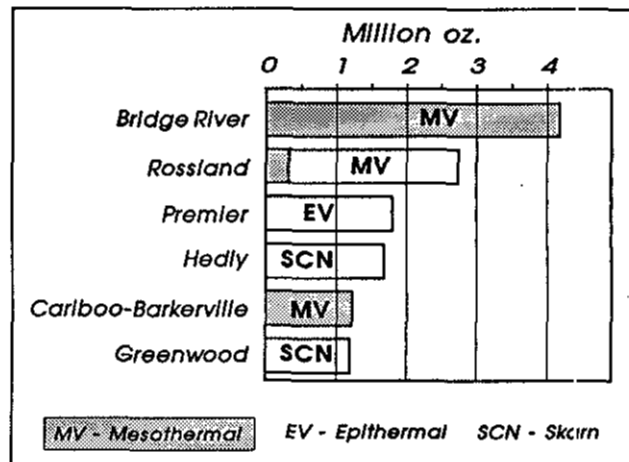


Figure 1-1. Top ten past-producing mesothermal gold vein deposits in British Columbia (data from Schroeter *et al.*, 1989).

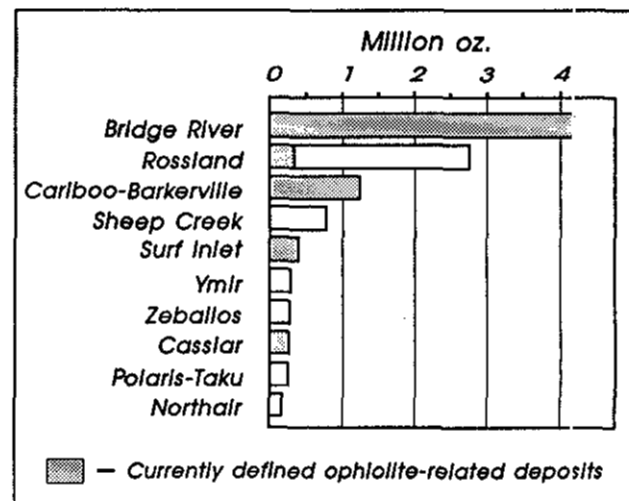


Figure 1-2. Top six gold-producing mining districts in British Columbia (data from Schroeter *et al.*, 1989).

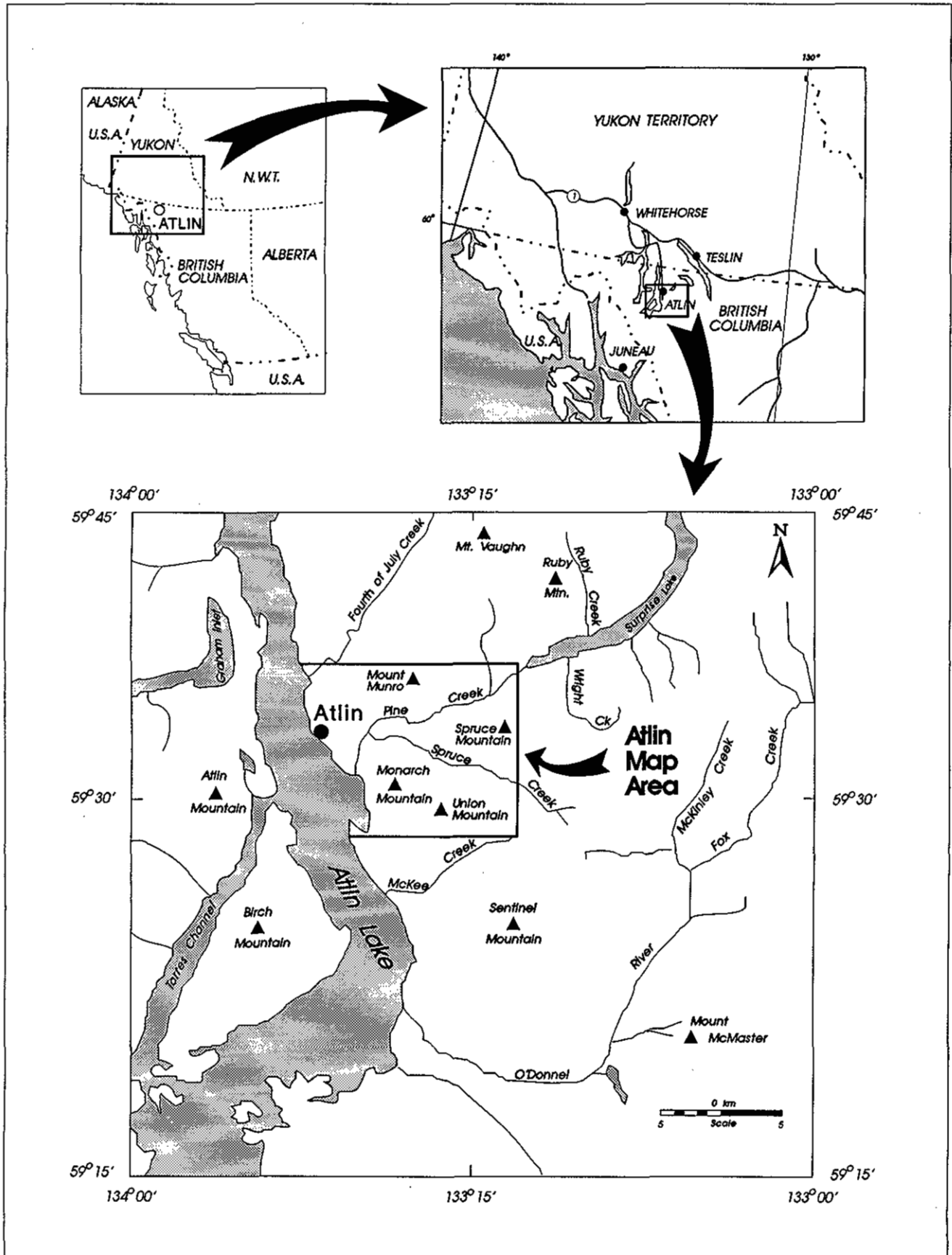


Figure 1-3. Location of the Atlin map area.

1990 and the map area extended in order to establish tectonic relationships between the ultramafic and surrounding lithologies to test the interpretations presented by Ash and Arksey (1990c).

Bedrock mapping of the immediate area at 1:25 000 scale, produced a geological map (in pocket) which incorporates results from both previously published maps and much of the available exploration information.

## PREVIOUS WORK

The first systematic geological mapping of the Atlin region was done by Aitken (1959) who produced a 1:250 000-scale map (NTS 104N) with an accompanying memoir. Monger (1975) mapped ten specific areas of the northern Cache Creek Terrane (Atlin Terrane) and provided the first regional overview and tectonic synthesis of the terrane. All these areas were, however, external to the present map sheet. Bloodgood *et al.* (1989a, b) conducted 1:50 000-scale geological mapping of the Surprise Lake (104N/11W) and Atlin (12E) map areas. Bloodgood and Bellefontaine (1990) mapped portions of the Dexi Lake and Teresa Island (104N/6 and parts 104N/5 and 12) map sheets at a similar scale. Lefebure and Gunning (1989) compiled a 1:20 000 geological map of the Atlin mining camp using information obtained chiefly from exploration assessment reports.

Studies relating specifically to aspects of lode gold mineralization in the Atlin camp have been made by several researchers. Newton (1985) studied the mineralogical and lithogeochemical character of listwanitic alteration assemblages from four lode-gold properties in the area. Lueck (1985) completed a similar study focusing specifically on the Anna claims. Andrew (1985) conducted a fluid inclusion and lead isotope study on mineralized quartz veins. A comparative study of the mineralogical and chemical characteristics of placer and lode gold was published by Ballantyne and MacKinnon (1986). Bozek (1989) investigated trace element signatures related to listwanitic alteration halos at both the Yellowjacket and Pictou properties and defined potential pathfinder elements indicative of gold mineralization. Lefebure and Gunning (1988), and Rees (1989) published property descriptions of the Yellowjacket and Pictou lode-gold showings respectively.

In addition to these publications, results of extensive exploration work conducted in the immediate area are given in assessment reports filed with the provincial government by mining and exploration companies. These reports include details of trenching, drilling and sampling programs as well as mapping and geophysical surveys.

## PRESENT STUDY

This paper presents the first detailed study of ultramafic and related rocks in the Atlin area. Detailed mapping has defined the setting and contact relationships of these units. From this a structural history of the ultramafic rocks underlying Monarch Mountain is proposed, then used to place constraints on their environment of formation and mode of emplacement.

The phase chemistry of the harzburgite and associated dunite have been investigated and are used to establish the origin of these units.

Whole-rock major, trace and rare-earth element chemistry is presented for basaltic rocks spatially associated with the ultramafics. These data are used to place constraints on the paleotectonic eruptive setting of the unit and to model the character of the mantle source from which these rocks was derived.

## ACKNOWLEDGMENTS

The writer is grateful to Ron Arksey for providing invaluable and competent assistance throughout the field and initial office component of this study. Robert Macdonald is thanked for providing assistance with petrographic descriptions of the mafic volcanic rocks. Thanks are extended to Darcy Marud and Joanne Bozek formerly of Homestake Mineral Development Company and Linda Dandy, formerly of Mark Management for their insightful discussions and for providing field visits and making maps and data readily available. Property visits provided by Brad White and John Harvey were greatly appreciated. Insightful discussions with Bruce Ballantyne of the Geological Survey of Canada helped to broaden the author's understanding of the chemical aspects of the mineralizing systems in the study area. Duncan McIvor of Homestake Mineral Development Company provided detailed observations and descriptions which significantly aided the present interpretation. Assistance in mapping provided by Mitch Mihalyuk, Jan Hammack, Bill McMillan and Keith Mountjoy helped to establish local lithotectonic relationships. Discussions with Chris Rees on aspects of the local geology were appreciated. Thanks are also extended to John Knight for his assistance during phase chemical analysis, conducted at The University of British Columbia. This work has been improved from reviews by Bill McMillan, Mitch Mihalyuk and Dave Lefebure. Editorial suggestions by John Newell and Brian Grant are greatly appreciated.



# CHAPTER 2

# GEOLOGY OF THE ATLIN AREA

## REGIONAL SETTING

The map area is situated near the northwestern margin of the northern Cache Creek Terrane in northwestern British Columbia (Figure 2-1). This terrane consists of the allochthonous remnants of a late Paleozoic to early Mesozoic Tethyan ocean (Monger, 1975, 1977a, b; Monger *et al.*, 1982). Destruction of this ocean basin during early Mesozoic subduction may have influenced the development of the island arc terranes of both Quesnellia and Stikinia which presently border the northern Cache Creek Terrane along the Teslin and Nahlin faults to the east and west respectively.

Middle Jurassic emplacement of oceanic Cache Creek rocks westward over Stikina is well constrained in northern British Columbia by both biostratigraphic evidence (Gabrielse, 1991; Ricketts *et al.*, 1992) and the age of cross-cutting plutons (Mihalynuk *et al.*, 1992). Relationships of the Cache Creek with Quesnellia arc rocks to the east, is less well constrained due to the effects of post-collisional, pre-Late Cretaceous dextral strike-slip faulting (Gabrielse, 1985, 1991).

The Cache Creek Terrane is a composite oceanic terrane that comprises two distinctive lithotectonic elements. Upper Triassic to early Jurassic accretionary prisms or sub-

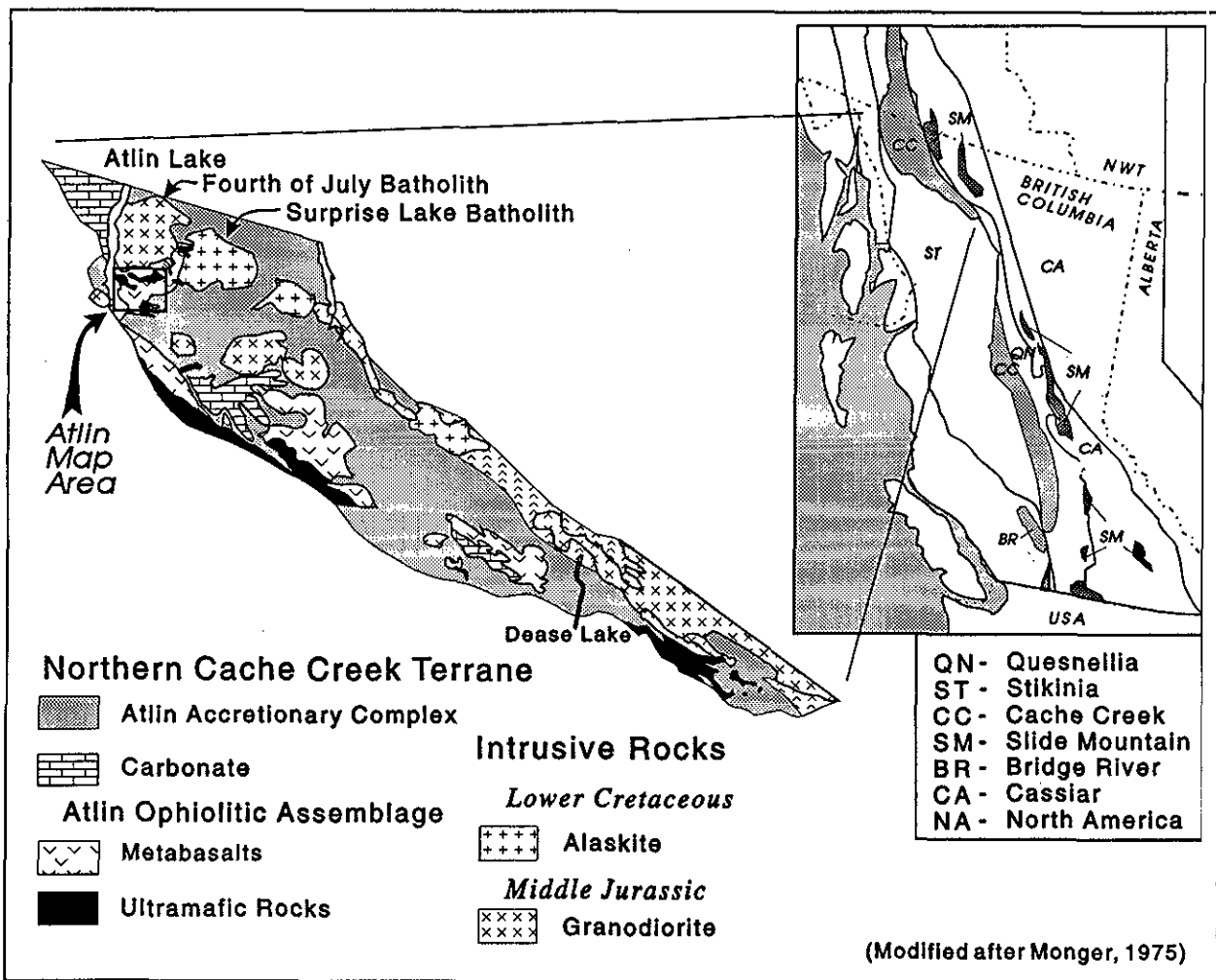


Figure 2-1. Regional geological setting of the Atlin map area. Map of the northern Cache Creek Terrane after Monger (1977a).

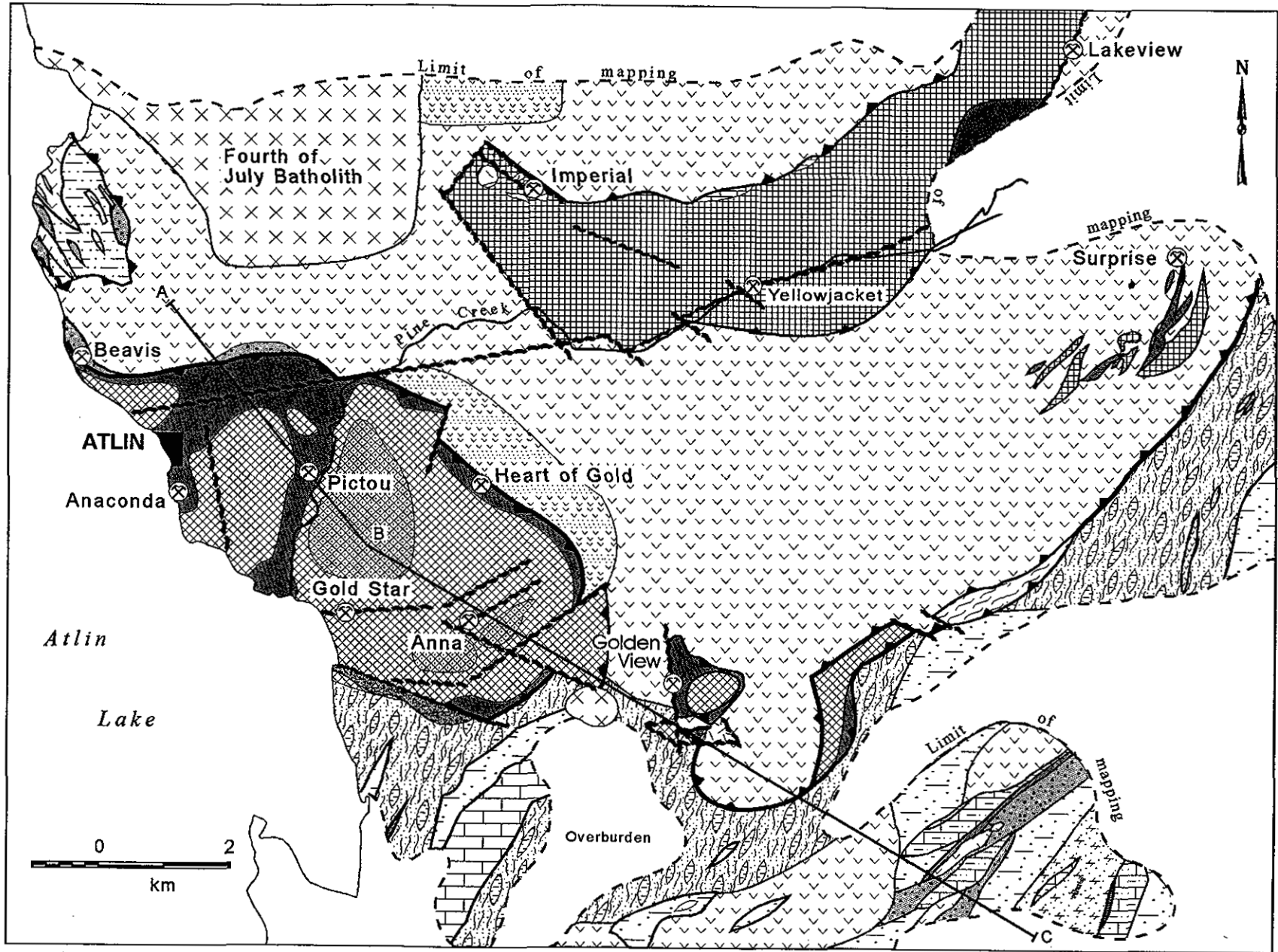


Figure 2.2. (A) Geology map of the Atlin area.

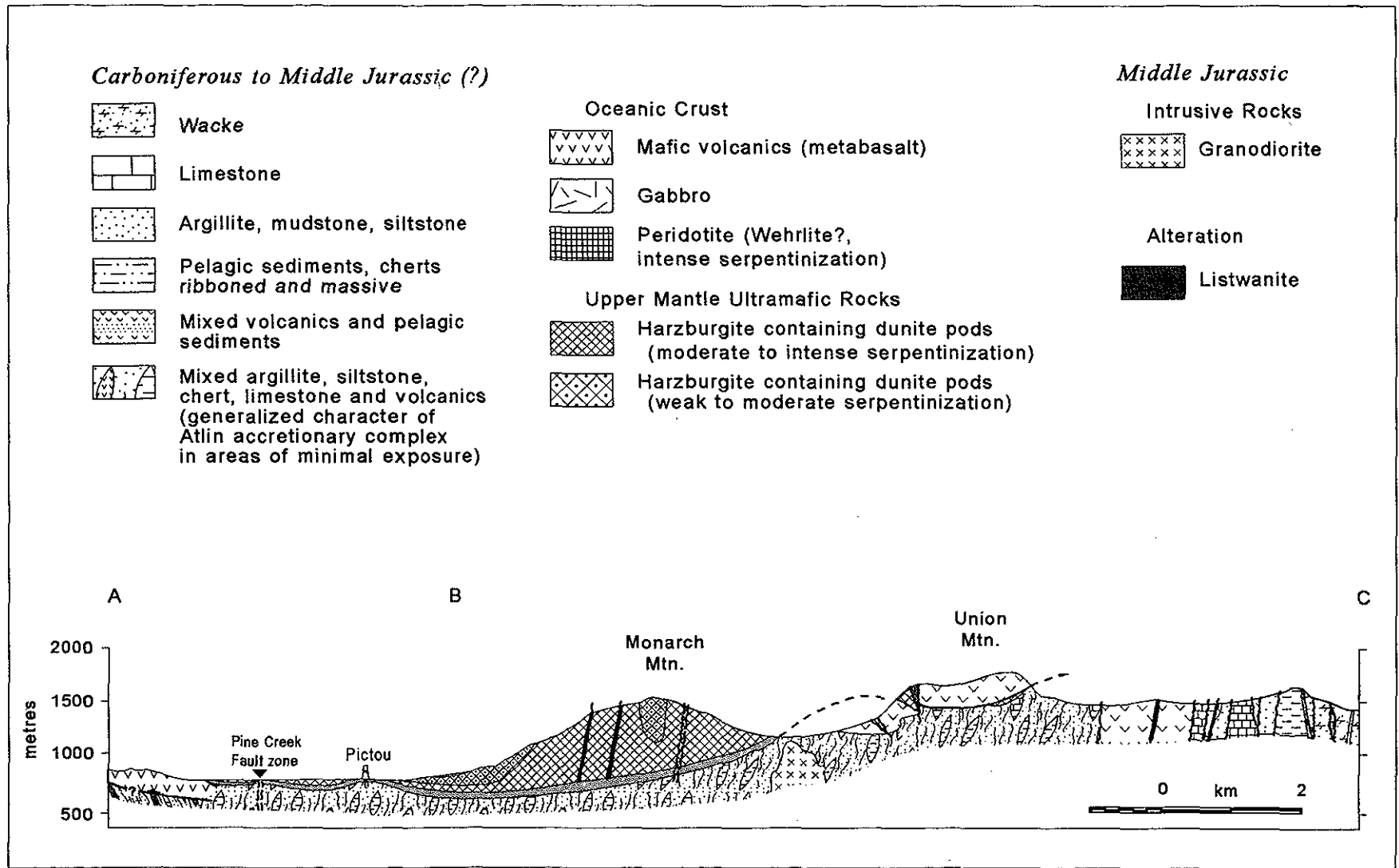


Figure 2.2. (B) Schematic geological cross section of the Atlin area.

duction-related accretionary complexes, generated by subduction of the oceanic lithosphere (Monger *et al.*, 1982; Monger, 1984; Gabrielse and Yorath, 1989; Coney, 1989), and dismembered ophiolitic assemblages emplaced by obduction of oceanic lithosphere, possibly by collision during final closure of the ancient ocean basin. These ophiolitic assemblages comprise a sequence of strongly disrupted sedimentary, crustal and upper mantle (alpine-type ultramafic) lithologies of oceanic origin, all of which are components of a typical ophiolite suite (Monger, 1977a). Also included are reefoidal limestones of equivocal origin, but suggested by Monger (1977a, b) and Souther (1977) to have formed on an ocean island or seamount. This interpretation is supported by recent investigation of Cache Creek rocks in the Stuart Lake area of central British Columbia which indicates that massive Permian limestones are associated with basaltic rocks of ocean island affinity (Ash and Macdonald, 1993).

## LOCAL GEOLOGY

The Atlin map area is located on the eastern shore of Atlin Lake (Figure 1-3 and frontispiece); it encompasses the town of Atlin and covers an area of roughly 270 square kilometres. Its geology is broadly divisible into two lithotectonic elements (Figure 2-2). A lower composite unit termed the Atlin accretionary complex crops out in the southern and northeastern areas of the map sheet. This complex is characterized by a structurally and lithologically diverse sequence of steeply to moderately dipping, tectonically imbricated slices of pelagic metasedimentary rocks with lesser amounts of metabasalt, limestone and wacke. The accretionary complex is tectonically overlain along the Monarch Mountain thrust by a series of imbricated units of dominantly metamorphosed oceanic crustal and upper mantle lithologies that collectively comprise the Atlin ophiolitic assemblage. Oceanic crustal lithologies are represented by metamorphosed basalt, gabbro and ultramafic rocks. Mantle lithologies are dominated by variably altered harzburgite (alpine-type peridotites).

Both these lithotectonic elements are intruded by the Middle Jurassic (Mihalynuk *et al.*, 1992) calcalkaline Fourth of July batholith and related dike rocks. Younger, Late Cretaceous dikes related to Surprise Lake plutonism may also be present.

The age of the Cache Creek Terrane is poorly constrained in the map area. Conodonts extracted from two isolated limestone exposures in the southern portions of the map area (map, in pocket) indicate Mississippian (late Visean-early Namurian) and Permian fossil ages. Regional fossil data however suggest that these rocks may range in age from Mississippian through to Lower Jurassic (Monger, 1975; Cordey, 1991; Orchard, 1991). During the present study attempts to obtain radiolaria from cherts, suitable for characterizing the age of the oceanic sediments, were unsuccessful. Although present, radiolaria were not suitable due a relatively high degree of recrystallization affecting the

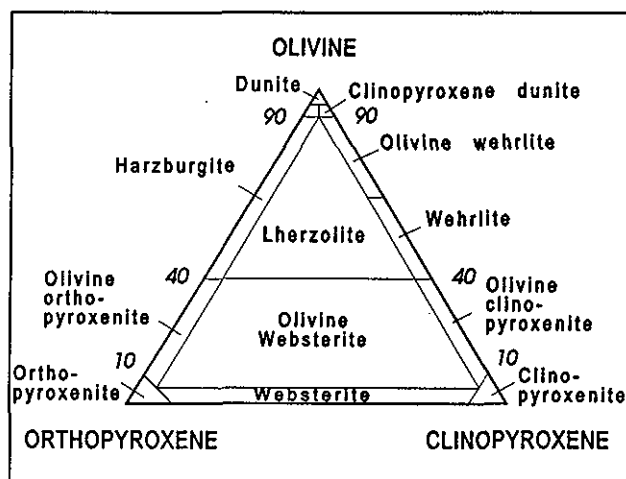


Figure 2-3. Classification and nomenclature of ultramafic rocks in the olivine-orthopyroxene-clinopyroxene prism (after Streckeisen, 1975).

samples collected (F. Cordey, personal communication, 1991).

## ATLIN OPHIOLITIC ASSEMBLAGE

### ULTRAMAFIC ROCKS

All ultramafic rocks in the Atlin map area were assigned to the Atlin intrusions by Aitken (1959) following the accepted pre-plate-tectonic view for the origin of such ultramafic bodies. This usage is discontinued here.

Peridotite comprising both harzburgite and wehrlite (Figure 2-3), or their serpentinized or carbonatized equivalents, represent the bulk of the ultramafic rocks exposed in the Atlin area. Other ultramafic rock types include minor dunite and lesser pyroxenite which are both hosted by the harzburgite. All ultramafic rocks are invariably serpentinized with complete to near complete serpentinization being common. Carbonate-altered ultramafics (listwanites) with varying assemblages of magnesite, ankerite and dolomite ( $\pm$ quartz, mariposite and gold) are also common, but restricted to fault zones, either within or marginal to the ultramafic bodies.

### HARZBURGITE

The most extensive exposure of harzburgite underlies both Monarch Mountain and the town of Atlin, and covers an area of roughly 35 square kilometres (Figure 2.2). Formerly considered one of the Atlin intrusions (Aitken, 1959), this body was termed the Atlin ultramafic allochthon by Ash and Arksey (1990a) following detailed mapping aided by exploration drill data that it is a relatively flat-lying, fault-bounded thrust slice. Harzburgite which is in general highly serpentinized and commonly brecciated is exposed on the northern and southern slopes of Union Mountain.

Where only partially serpentinized, the unit weathers reddish brown and retains relict primary textures. Evenly

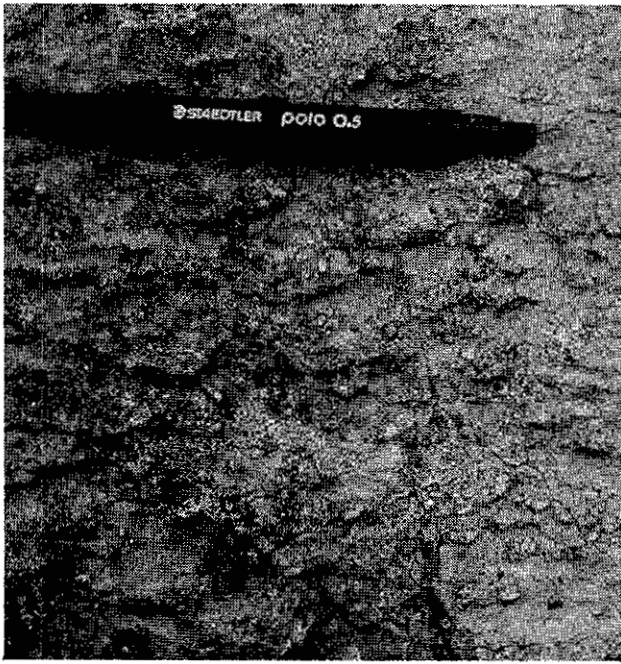


Photo 2-1. Weathered appearance of harzburgite with studded orthopyroxene in recessive dunite displaying a well-developed foliation fabric.

dispersed brown to bottle-green orthopyroxene grains or crystal aggregates, which constitute from 15 to 30 modal percent of the unit, are more resistant to weathering than the olivine groundmass (70 to 85 modal%) and stand out, producing a characteristic studded appearance on weathered surfaces (Photo 2-1; knobby peridotite of Bloodgood *et al.*, 1989 a, b). Fresh surfaces are dark green and massive but orthopyroxene grains are readily distinguishable due to their lustrous appearance. The rock is medium to coarse grained with a xenomorphic granular fabric. Clinopyroxene is a minor constituent, comprising from 3 to 7 modal percent. Accessory anhedral black, chrome spinel grains from 0.5 to 2 millimetres in size, range from trace to 2% and are easily identifiable on weathered surfaces.

Preferential orientation of the orthopyroxene grains throughout the harzburgite imparts a weak to moderate foliation to most of the unit. On the basis of the degree of fabric development, three types of harzburgite have been recognized. In decreasing order of abundance these are: foliated with no compositional banding, massive, and foliated with parallel compositional banding. Areas of compositional banding consist of alternating 1 to 2-centimetre pyroxene-poor and pyroxene-rich zones (Photo 2-2). Banding, though commonly laterally discontinuous and dis-



Photo 2-2. Tectonite banding ( $S_1$ ) defined by centimeter-scale alternating orthopyroxene-rich and poor bands.



Photo 2-3. Folded orthopyroxene banding in harzburgite tectonite. The marker, which is 14 centimetres long, is oriented parallel to the axial planar foliation fabric.

rupted, generally parallels the foliation defined by the elongated orthopyroxene grains in the surrounding harzburgite. The banding is isomodal, in that there is no identifiable variation in the proportions of the constituent minerals between individual bands or from band to band. Contacts between bands are diffuse and planar. Isolated localities of banding occur intermittently throughout the main body of harzburgite. The best exposure is on a north-trending knoll 0.5 kilometre southwest from the summit of Monarch Mountain. In a few outcrops the banding outlines isoclinal to open folds (Photo 2-3) with axial surfaces that parallel the dominant foliation fabric developed locally.

#### SERPENTINITE-BASTITE

Completely serpentinized harzburgite weathers a variety of colours ranging from dark to dull grey to light grey to olive green. Well-washed surfaces have a characteristic mottled or spotted appearance (Photo 2-4) with 2 to 5-millimetre dark grey to black bastite (serpentinized orthopyroxene) dispersed within a light grey matrix of serpentinized olivine reflecting the primary, coarse porphyroclastic texture. Unlike the rough, studded weathering surfaces of the partially serpentinized harzburgite, completely serpentinized exposures are smooth. In many cases the bastite forms ovoid wisps that surround the orthopyroxene grains and define a younger penetrative foliation fabric. The intensity of fabric development is highly variable and influences the overall appearance of the unit. Intensely deformed exposures have a distinctive mylonitic fabric with an alternating black and grey striped or ribboned appearance.

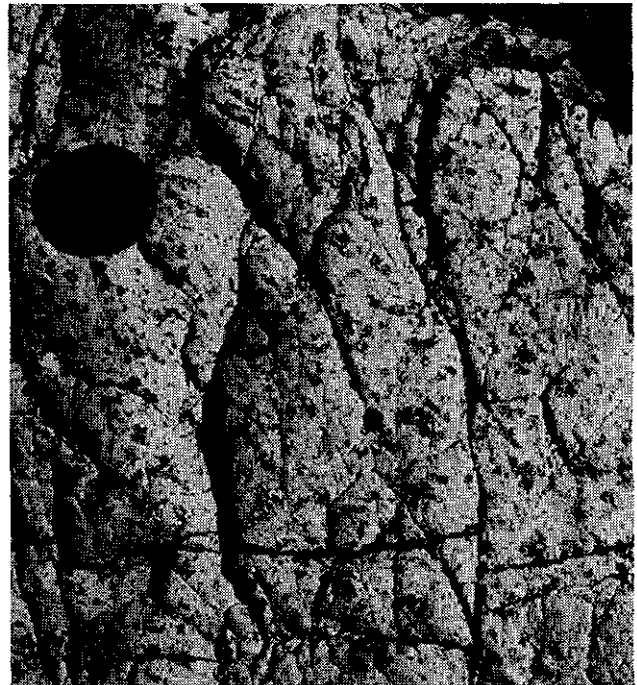


Photo 2-4. Mottled appearance of weathered serpentinite (light grey) - bastite (black).

Within the Atlin allochthon the least serpentinized rocks are exposed near the top of Monarch Mountain. Good exposure and steep topography on the west side provide a nearly continuous exposed section through the ultramafic body. Towards the structural base of the ultramafic sheet serpentinization becomes progressively more intense and



Photo 2-5. Photomicrograph of partially serpentinized harzburgite with relict olivine and orthopyroxene and amoeboid chrome-spinel. Field of view is 2 millimetres wide. Photo taken under plane polarized light.

pervasive. Along the base or sole thrust, where the ultramafic body is pervasively carbonatized and tectonized, it is characterized by a zone of listwanitic alteration. Thus a pseudostratigraphy is produced within the allochthon, defined by variations in both the degree and type of alteration. The distinctive mylonitic phase of the peridotite is exposed near the base of ultramafic body along this section.

#### PETROGRAPHY

In thin section the harzburgites display a medium to coarse-grained porphyroclastic texture (Harte, 1977). Olivine and orthopyroxene are invariably altered to secondary serpentine minerals. The degree of serpentinization varies from 40 to 100%, however, most samples are at least 75% serpentinized. Where alteration is incomplete, orthopyroxene is less affected than olivine.

Orthopyroxene of enstatite composition occurs as large, isolated anhedral grains, or as finer aggregates 2 to 8 millimetres in diameter, uniformly distributed throughout the harzburgite. Relict grains commonly form cores surrounded by bastite and lesser talc.

Clinopyroxene of diopsidic composition occurs both as lamellae and blebby exsolutions in orthopyroxene, and as anhedral grains 0.5 to 4 millimetres across that are commonly associated with enstatite.

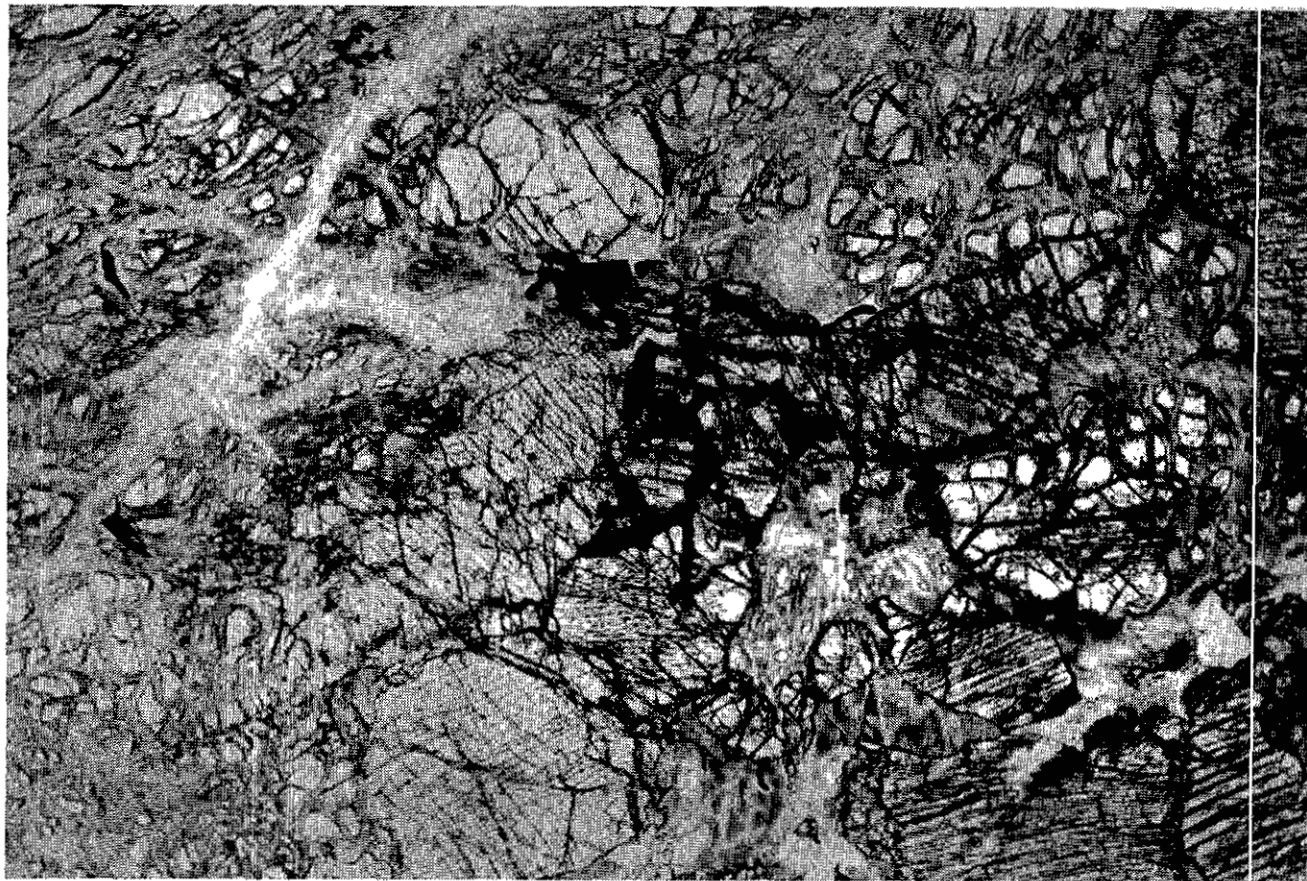


Photo 2-6. Photomicrograph of orthopyroxene-clinopyroxene-spinel cluster in harzburgite. Field of view is 3.5 millimetres wide. Photo taken under plane polarized light.

Olivine of forsteritic composition occurs as equant to moderately elongate, 1 to 7 millimetres anhedral grains. In general, serpentinization is associated with grain boundaries or cracks within the grains. With increasing degree of alteration, relics of original grains display a characteristic mosaic texture with remnant kernels of olivine set in a serpentine groundmass (antigorite). In most cases, the once contiguous grains maintain a constant optical orientation permitting estimates of original grain shape and size.

Some relatively fresh samples, examined petrographically, indicate that preserved relict clinopyroxene may exceed 5 modal percent; thus peridotite of lherzolitic composition (Figure 2-3) is also present. This minor difference between the two rock types is indistinguishable in the field. The limited number of samples sectioned, together with the generally strong serpentine alteration, precludes estimation of the relative abundance or distribution of these transitional peridotite subtypes. Throughout the remainder of the text the unit will be referred to as harzburgite, as the rock is either harzburgite or lherzolite approaching harzburgitic composition. However, the presence of lherzolite is important to the interpretation of the paleotectonic environment of formation of these ultramafic rocks. This feature will be reviewed further in a following chapter, during discussion of the phase chemistry of the unit.

Chrome spinel is a ubiquitous accessory phase in the harzburgite. It occurs as irregular amoeboid or cuspid grains interstitial to olivine and pyroxene (Photo 2-5) and as wormy intergrowths within the pyroxenes. Distinctive orthopyroxene-clinopyroxene-spinel clusters (Nicolas, 1986; Nicolas *et al.*, 1980) have been identified in some relatively fresh harzburgite samples (Photo 2-6).

#### DUNITE

This unit is everywhere hosted by harzburgite and occurs as isolated pods and bands throughout. Bands vary from several centimetres to tens of centimetres in width and are concordant to slightly discordant with the foliation fabric in the host harzburgite. Pods have moderate to high aspect ratios and vary from metres to several hundred metres in length, with their long axes concordant with the harzburgite foliation (Photo 2-7). Weathering of dunite produces smooth tan-brown to khaki-coloured surfaces containing 1 to 4% disseminated, black chromite grains. The dunite is easily distinguishable from the dark brown, rough-textured host harzburgite. Contacts with the enveloping harzburgites lack chilled margins and are defined by abrupt changes in orthopyroxene content over distances of less than a centimetre (Photo 2-8). On the margin of the larger dunite bodies, smaller 0.5 to 1-metre lobate pods or tongues of dunite invade the host harzburgite over distances of several metres from the main mass of dunite.

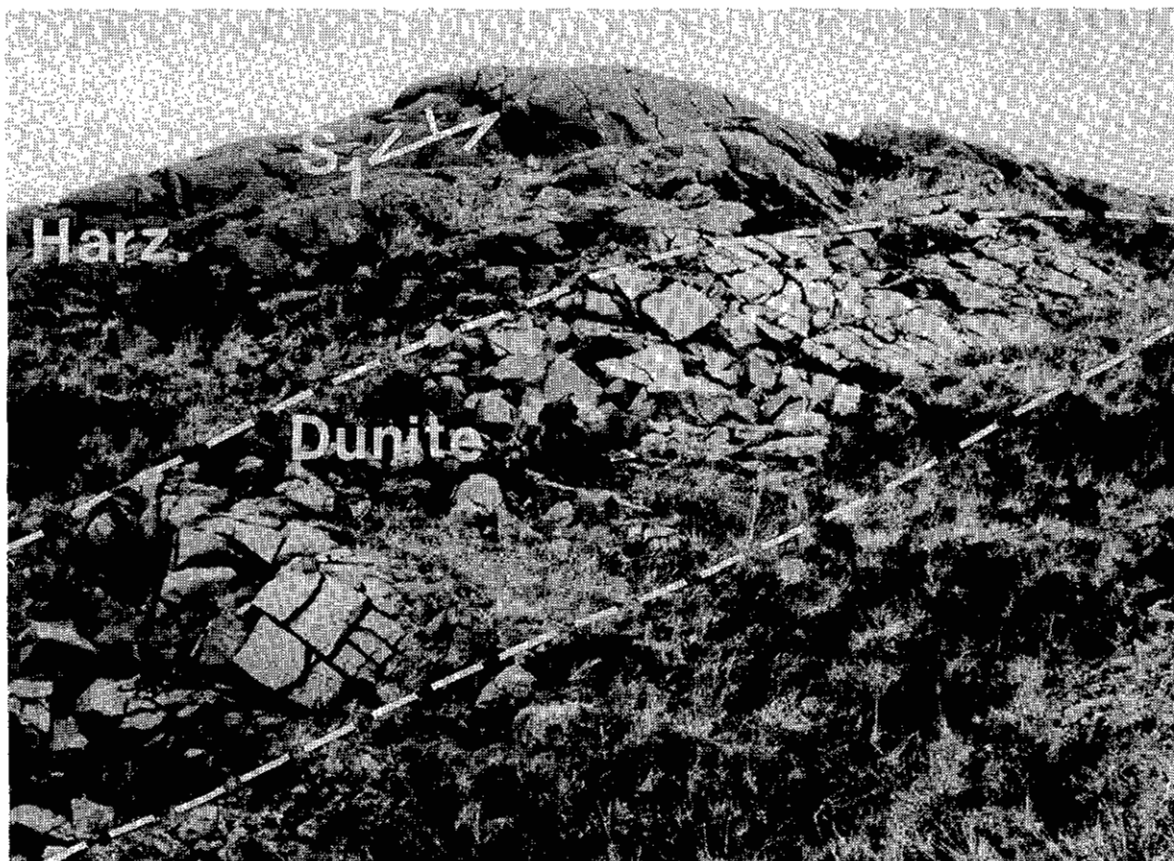


Photo 2-7. Typical lenticular (podiform) dunite body, with the long axis concordant with the  $S_1$  tectonite fabric in the host harzburgite.

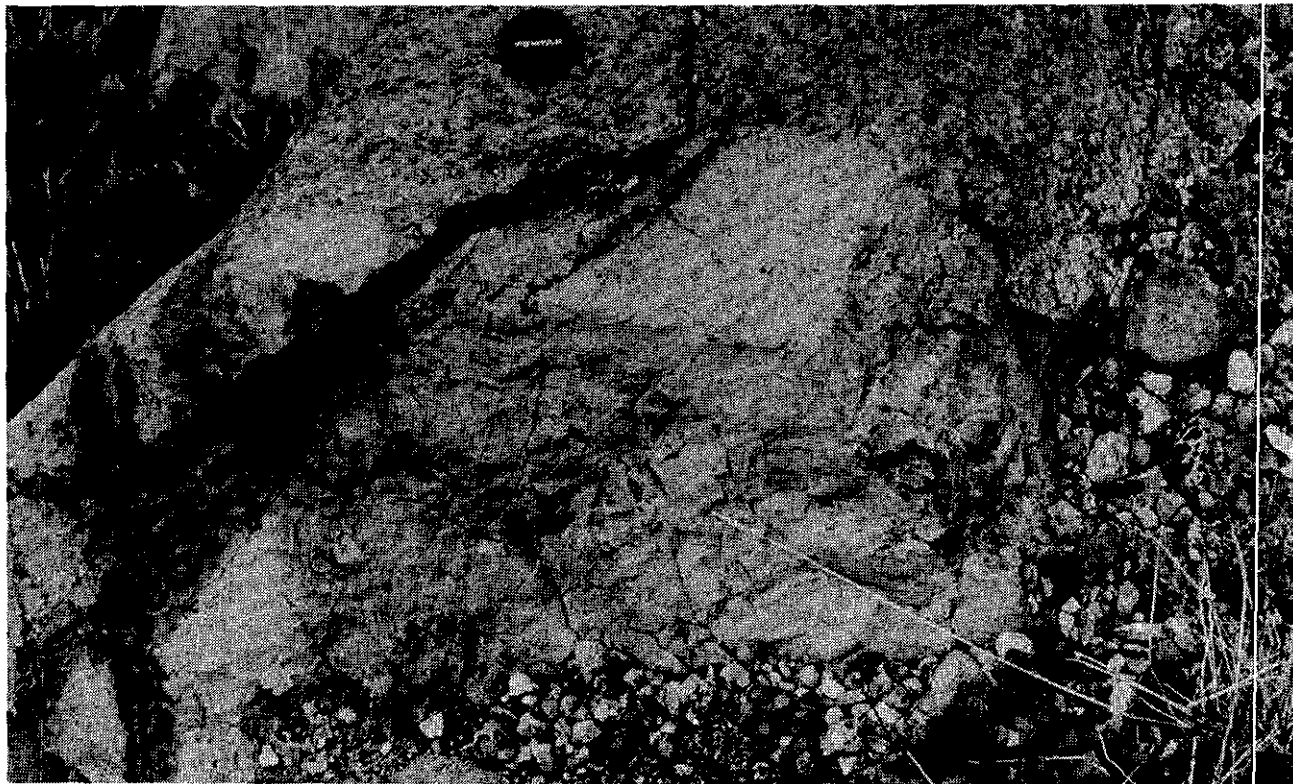


Photo 2-8. Close-up of contact between harzburgite and dunite pod shown in Photo 2-7.

#### PETROGRAPHY

Dunite is essentially monomineralic, composed of olivine (forsterite) with only trace amounts of accessory chrome spinel which locally increase to 4%. It has a medium to coarse-grained granular texture, with individual grains ranging from 1 to 6 millimetres in diameter. As in the harzburgite, olivine is invariably partially to completely replaced by secondary serpentine and where partially altered displays a characteristic mosaic texture (antigorite).

Dunite chrome spinels occur as disseminated euhedral to subhedral grains 0.5 to 4 millimetres across that are commonly opaque in thin section (Photo 2-9) and therefore texturally distinct from those observed in the harzburgite.

#### PYROXENITE DIKES

Pyroxenite dikes weather a homogeneous dark brown colour and range from 1 to 10 centimetres in width. The dikes are coarse grained to pegmatitic, lack chilled margins and have sharp contacts with harzburgitic country rock. Varying abundances of coarse-grained crystals of both clinopyroxene and orthopyroxene commonly form comb structures that grow perpendicular to dike walls. Dike orientations are predominantly concordant but occasionally are oblique to highly discordant with the foliation fabrics in the host harzburgite (Photo 2-10). This suggests emplacement before, during and after ductile deformation. Effects of synkinematic ductile deformation of some dikes are clearly evident where they have been isoclinally to tightly



Photo 2-9. Plane polarized view of partially serpentinized dunite with kernels of relict olivine and anhedral chrome-spinel in dunite. Field of view is 4 millimetres in width.



Photo 2-10. Concordant and discordant pyroxenite dikes in harzburgite.



Photo 2-11. Tightly folded pyroxenite dike in harzburgite. Well-developed tectonite fabric parallels the axial plane of the fold.

folded (Photo 2-11). Axial surfaces of these folds are invariably parallel to the foliation fabric in the host harzburgite.

#### PERIDOTITE CUMULATES (WEHRLITE?)

Serpentinized peridotite (wehrlite?) outcrops discontinuously along an east-trending belt 1 to 3 kilometres wide, on the south-facing slope of Mount Munro. It was also noted south of Fourth of July Bay and on the northeast side of Third Island, 1.3 kilometres west of the Atlin townsite.

This unit is characteristically strongly serpentinized and weathers a dull to dark grey colour. On well-washed surfaces, altered intercumulate pyroxene (clinopyroxene?) weathers a darker colour than the lighter grey cumulate olivine and displays ghost oikocrysts that range from 1 to 3 centimetres in diameter.

#### PETROGRAPHY

Cumulate olivine, which constitutes from 60 to 80% of the unit, occurs as equant to moderately elongate anhedral grains or as isolated rounded grains 1 to 4 millimetres across, poikilitically enclosed by secondary aggregates of antigorite and talc after clinopyroxene. The degree of retrograde metamorphism varies from 50 to 100% and comprises various proportions of antigorite and magnetite. In general, serpentinization is associated with grain boundaries or cracks within the grains. With increasing degree of alteration, relics of the original grain become more detached and replaced by roughly equal proportions of serpentine and magnetite displaying a characteristic mosaic texture. In most instances, the once contiguous grains maintain a constant optical orientation permitting estimates of original grain shape and size. Serpentinized olivine in the wehrlite typically has a much higher proportion of magnetite than was identified in serpentinized olivine in the harzburgite. Completely serpentinized olivines in the wehrlite have a characteristic aggregate structure and contain up to 40% magnetite.

The occurrence of relict clinopyroxene is extremely rare. The mineral is typically totally replaced by fibrous aggregates of serpentine (antigorite) and talc ( $\pm$ carbonate) with a distinctive lack of magnetite. Clinopyroxene is clearly much more susceptible to secondary alteration than olivine. In many thin sections which contain from 50 to 60% relict olivine, clinopyroxene is totally replaced by serpentine and talc.

Chromite occurs as an accessory phase comprising less than 1 modal per cent. It forms 0.2 to 0.5-millimetre subhedral grains and is typically associated with intercumulate clinopyroxene.

In thin section, the relict cumulate textures are readily identifiable in completely altered samples of wehrlite, due to the distinctive styles of secondary alteration affecting both primary phases. A lack of magnetite, combined with the association of talc in clinopyroxene pseudomorphs, distinguishes it from magnetite-rich talc-free retrograde metamorphic assemblages after olivine.

Variably serpentinized and carbonatized ultramafic rocks of undetermined peridotite type crop out on Spruce Mountain. Small ultramafic blocks and slivers are also present within mélangé zones associated with the Atlin accretionary complex, as along McKee Creek. To the south, near Sentinel Mountain, Monger (1975) noted that tectonized slivers of serpentinized ultramafic rocks are commonly present at major structural contacts.

#### METAGABBRO

Metagabbro is the least represented oceanic crustal component in the map area. It outcrops on the northern slope of Union Mountain and along the south-facing slope of Mount Munro. It is also well represented in drill core from the Yellow Jacket property along Pine Creek, where it occurs as isolated pods and lenses within the Pine Creek fault zone (Lefebure and Gunning, 1988; Marud, 1988 a; Marud and Southam, 1988). On Union Mountain, the gabbro is exposed along the Monarch Mountain thrust and forms isolated dismembered blocks with faulted contacts.

Metagabbro weathers a buff-white to dull grey colour and is typically medium to coarse grained and equigranular, consisting of roughly equal proportions of relict plagioclase and clinopyroxene ranging from 1 to 4 millimetres in size.

Review of a few thin sections indicates that plagioclase is completely replaced by sericite. Pyroxenes are typically replaced by secondary amphibole. In some instances relict clinopyroxene occurs as cores mantled by the secondary amphibole.

#### METABASALTIC ROCKS

Metabasaltic rocks that dominate the northern and central portion of the map area comprise the bulk of both Union and Spruce mountains and is the dominant rock type exposed on Mount Munro. It is also the most widely exposed rock type throughout the lowlands between Spruce and Monarch mountains and to the northeast of Atlin, and occurs as isolated tectonic lenses on a variety of scales throughout the accretionary complex. In the centre of the map area, east of Monarch Mountain, the extent of the metabasaltic rocks may not be as continuous as indicated on previous maps (Bloodgood *et al.*, 1989b; Lefebure and Gunning, 1989; Ash and Arksey, 1990c). Review of the limited drill-core data available from the area indicates that the basalts are commonly intercalated (on the order of metres to tens of metres) with pelagic sedimentary rocks, including both chert and argillite. Data are insufficient to permit estimates of the proportion of sedimentary to volcanic rocks. Whether the intercalation is mostly tectonic or primary is uncertain but most core logs examined suggest faulted contacts.

Metabasalts are generally massive, fine grained to aphanitic and weather a characteristic dull green-grey to dark green colour. Locally, the unit grades to medium-grained varieties or diabase. This gradation is sporadic and the diabasic phases of the unit have not been differentiated.



Photo 2-12. Autobrecciation texture in well-washed exposure of metabasalt.



Photo 2-13. Well-preserved basaltic pillow lavas, exposed on ridge in the Lina Range, 1.5 kilometres south of Union Mountain.

On Sentinel Mountain metabasalts gradational into mapable units of medium-grained diabase have been described by Monger (1975). In most exposures of metabasalt throughout the map area, the rock is covered by a thin growth of lichen so identification of primary features such as flow banding, autobrecciation and chilled margins is difficult. On well-washed exposures features indicative of both autobrecciation (Photo 2-12) and flow banding have been identified in some areas, otherwise the unit is characteristically massive. Locally metabasalts contain relict microphenocrysts of pyroxene and/or plagioclase as well as rare carbonate amydules.

Pillowed structures are rare and have been identified at only one locality during the present study (Photo 2-13). This occurrence is near the top of a small rounded hill in the Lay Range several kilometres south of Union Mountain. Pillow structures are typified by concentric textural zoning from a variolitic margin to a fine-grained core with up to 5% pyroxene microphenocrysts. Individual pillows range in size from 5 to 50 centimetres across. Pyroxene-phyric basalt is interstitial to the pillows. Well-developed pillow structures have also been described by Monger (1975) and Bloodgood and Bellefontaine (1990) on Sentinel Mountain several kilometres to the south of the present map area.

Basalt contacts are commonly faulted with sheared or brecciated zones sometimes intensely carbonatized. Primary contacts with both the cherts and limestones have also been noted throughout the area. Both sedimentary rock types are locally interlayered with the basalt. Basalts may also completely enclose massive lenses of chert, with both rock types appearing undeformed, suggesting primary stratigraphic relationships. This feature is particularly well developed along the south side of Union Mountain.

## PETROGRAPHY

In thin section, basalts are typically intensely altered. The dominant primary minerals are only recognized in the coarser grained samples (diabase) and include plagioclase, clinopyroxene, rare orthopyroxene and accessory magnetite.

Plagioclase occurs as both a phenocrystic and matrix phase and in both habits displays characteristic ophitic textures, enclosing mafic minerals. It constitutes 35 to 55% of the modal mineralogy and is almost entirely sericitized and only recognized by its characteristic lath-like shape and relict polysynthetic twinning.

Alteration of primary mafic phases is common, and characterized by rim replacement of individual grains by fine-grained aggregates of epidote, chlorite and pleochroic, pale green to green hornblende. Grain cores remain relatively unaltered and permit identification of primary phases. The finer grained volcanics are characterized by intense and pervasive alteration and their primary mineralogy can only be inferred by comparison with similarly altered mafic phases in the coarser grained rocks. In the finer grained

volcanics, larger, 1 to 2-millimetre, subhedral to anhedral tabular epidote or fibrous hornblende grains commonly "float" in a cryptocrystalline groundmass of sericite, epidote minerals and chlorite. These larger grains may be pseudomorphs of mafic phenocrysts but this cannot be clearly established. All mafic phases, both primary and secondary, are intergrown and vary in relative modal proportion from 40 to 65%. Most display an authigenic mineralogy indicating lower to subgreenschist facies metamorphism. Locally, such as on Mount Munro, basalts marginal to the Fourth of July batholith contain secondary amphibole indicating upper greenschist to amphibolite grade metamorphism, most likely the result of contact metamorphism surrounding the intrusion.

Most mafic volcanic samples examined are intensely fractured and all are veined to some degree. Chlorite, epidote, carbonate and quartz are the dominant vug and fracture-filling minerals. Chlorite and epidote veining are consistent with the secondary alteration mineralogy and suggest that their formation may be directly related to the subgreenschist facies metamorphic event affecting the unit as a whole. Carbonate and quartz veining clearly crosscuts and laterally displaces the chlorite and epidote veins and is therefore later.

## ATLIN ACCRETIONARY COMPLEX

The Atlin accretionary complex is a composite unit comprising a series of steeply to moderately dipping lenses and slices of structurally intercalated metasedimentary and metavolcanic rocks underlying the southern half and north-west corner of the map area. Pelagic metasedimentary rocks that dominate the package consist of cherts, cherty argillites, argillaceous cherts and argillites with lesser limestones and greywackes. Sparse fossils collected from limestones throughout the map area, as well as some from beyond its southern boundary, are predominantly middle to late Paleozoic and late Triassic in age.

Individual tectonic slices in the complex display a wide variation in size, ranging from metres to several hundreds of metres in width. Indications of internal deformation are moderate or lacking in many slices; internal contacts and original stratigraphic relationships are preserved. Contact relationships between many of the individual units of the complex have not been established due a lack of exposure, however, most are interpreted to be tectonic. Internal bedding within the individual lenses may parallel the external contacts, but is more often strongly discordant. This relationship argues against simple interbedding of different facies.

Cherts weather a variety of colours ranging from dark to light grey to buff-white to red-brown to black. They vary from massive to typically well bedded on a 1 to 10-centimetre scale and most are interbedded with grey to black, cleaved argillite or finely laminated siltstone (Photo 2-14).

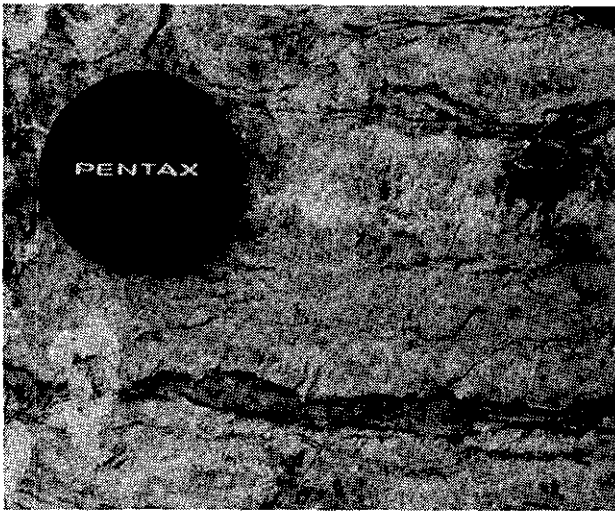


Photo 2-14. Typical appearance of light-coloured ribboned chert interbedded with thin, dark-coloured argillite.



Photo 2-15. Intensely sheared scaly argillite containing small rounded blocks of limestone, such as the one above the lens cap, occurring within the footwall of the Monarch Mountain thrust.

Less commonly, chert is interbedded with thin discontinuous lenses of millimetre to centimetre-scale pale grey weathering limestone or limy mudstone. Siliceous siltstone appears to grade locally into the chert unit. These rocks are very fine grained and vary from dark to pale grey or greenish grey to black in colour. Bedding in the siltstones is usually not as well defined as in the cherts.

Clastic sediments are dominated by argillite with lesser siltstone and greywacke. Argillite is typically very fine grained and grey to dark bluish grey in colour. It varies from

weakly cleaved to intensely sheared with a well developed scaly fabric.

Sedimentary carbonates include both limestone and dolostone. Both are typically massive and recrystallized, weathering a characteristic grey to mottled grey-white colour in outcrop. Locally the limestone contains bedding-parallel wisps and foliae of more argillaceous or graphitic carbonate.

Intermittent strongly disrupted zones of variable thickness occur between some of the tectonic slices. The general character of these zones, which contain a variety of competent lithologies in a finer grained matrix, suggests that they are best classified as *mélanges* (Raymond, 1984). Competent lithologies within these *mélange* zones, like chert and limestone, form lozenge-shaped or ovoid to rounded blocks set in a scaly argillaceous matrix. The argillaceous matrix is typically moderately to strongly foliated. This fabric is generally planar on an outcrop scale, but in detail follows the margins of enveloping clasts. Well-developed *mélange* is exposed in a number of localities throughout the map area. A road cut along Warm Bay road southeast of Monarch Mountain, provides a well exposed example (Photo 2-15). Exposures of the fissile argillaceous matrix material can be easily disaggregated into polished lenticular chips. Where zones of interbedded chert and argillite have been deformed they display a conspicuous penetrative foliation defined by a scaly fabric in the argillite and a planar distribution of lensoid fragments of chert with long axes paralleling the fabric. Such units are probably better defined as a broken formation as opposed to *mélange*.

Throughout the accretionary complex areas of varied lithologies outcrop in close juxtaposition with no clearly defined contact relationships. This may indicate that zones of *mélange* are more prevalent than currently recognized, as only the more competent clasts stand out as outcrop. The fissile and easily eroded argillaceous matrix is recessive and not exposed, particularly in areas of moderate overburden thickness.

A distinctive zone of brecciated sedimentary rocks (Photo 2-16) that appear to have been flooded and altered by hydrothermal carbonate is exposed over a distance of 2 kilometres along a prominent west-trending ridge south of Monarch Mountain. The unit crops out intermittently along the ridge and in a road cut several tens of metres long on Warm Bay road. The breccia contains angular to rounded fragments of variably bedded to massive siltstone, limy mudstone and limestone. Individual clasts vary from several centimetres to several metres in size. Weathered surfaces are a distinctive rusty red brown to a light tan brown, the latter also characteristic of fresh surfaces. Matrix iron-magnesite is typically recessive on weathered surfaces and the individual clasts stand out in relief. The structural position of the unit along the footwall of the Monarch Mountain thrust combined with its tectonized and altered character suggests



Photo 2-16. Polymictic sedimentary/tectonic breccia exposed on east-trending ridge south of Monarch Mountain.

that it was most likely generated during emplacement of the overlying ultramafic allochthon.

The Atlin accretionary complex is a disrupted and tectonically intercalated package of dominantly pelagic sedimentary rocks. It is interpreted to be an early Mesozoic subduction complex formed during destruction of the Cache Creek ocean basin. Lack of detailed mapping beyond the local area of investigation makes it difficult to establish the regional distribution of the unit. It is notable, however, that most of the northern Cache Creek Terrane comprises pelagic sediments with pods of volcanic rock and carbonate (Monger, 1975; Figure 2-1, stippled pattern) that may correlate with the complex.

## INTRUSIVE ROCKS

### FOURTH OF JULY BATHOLITH

The southern extension of the Middle Jurassic Fourth of July batholith (Aitken, 1959; Mihalynuk *et al.*, 1992) into the northeastern corner of the map sheet is the only major intrusive unit exposed in the study area. The potassium-feldspar megacrystic granitic phase of this composite pluton (Photo 2-17) is predominant. Pink potash feldspar megacrysts set in a coarse-grained equigranular ground-

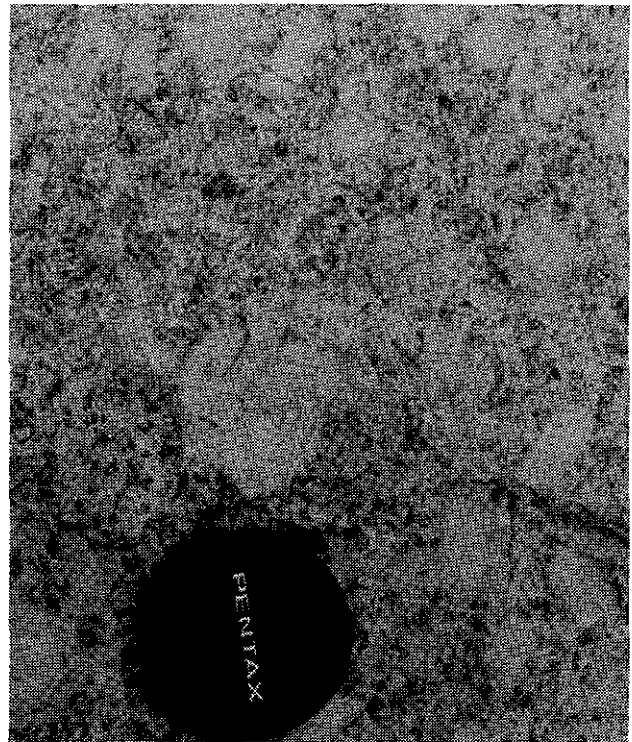


Photo 2-17. Typical weathered surface of the potassium-feldspar megacrystic granitic phase of the Fourth of July batholith exposed along the northern boundary of the map area.

mass of mottled light green to buff-white plagioclase and grey quartz typifies the unit in this area. Prismatic megacrysts range from 1 to 4 centimetres in length and comprise from 15 to 30% of the unit. Mafic minerals, restricted to the matrix, consist of both amphibole and biotite, with combined modal abundances of 5 to 20%. Primary clinopyroxene is also a common, but minor mafic phase. Where present it is typically mantled by amphibole. Accessory magnetite comprises 1 to 2% of the matrix mineralogy.

Uranium-lead analysis on zircon recently established the age of the pluton as 167 to 172 Ma (Mihalynuk *et al.*, 1992). Biotite from a small stock of potash feldspar megacrystic biotite granodiorite that crops out in the valley midway between Monarch and Union mountains yielded a K-Ar apparent age of  $167 \pm 3$  Ma (Sample DY-2958, Dawson, 1988). This cooling age is in excellent agreement with the Middle Jurassic age reported from the main body of the Fourth of July batholith. This date gives a minimum age of accretion and imbrication for the oceanic Cache Creek Complex. Notably a similar age and inferred tectonic relationship are reported for a granodiorite stock (K-Ar, biotite of  $173 \pm 4$  Ma) which intrudes sedimentary and ultramafic rocks of the northern Cache Creek Terrane near Tachilta Lakes, 58 kilometres to the northwest of Dease Lake (Stevens *et al.*, 1982).

#### FELDSPAR (QUARTZ) PORPHYRITIC DIKE SUITE

A suite of felsic, feldspar-porphyratic dikes, thought to be related to the Fourth of July batholith, outcrop throughout the map area. Typically they are 0.5 to 2 metres in width, have variable orientations and dip steeply. The dikes are undeformed and clearly crosscut both fabrics and deformed tectonic contacts between all lithological units of the Cache Creek Complex. Thus they postdate deformation and metamorphism related to accretion of the oceanic assemblage.

Typical dikes consist of randomly oriented, dull white prismatic plagioclase phenocrysts 1 to 4 millimetres long set in a grey aphanitic groundmass and comprising from 20 to 50% of the rock. Variable amounts of amphibole and quartz (0 to 20%) also occur as phenocrysts of comparable size.

#### MELANOCRATIC DIKE SUITE

A suite of melanocratic dikes crops out adjacent to, and locally intrudes the Fourth of July batholith. These dikes

vary from tens of centimetres to several metres in thickness. They generally trend northwest and are typically subvertical. The dikes are fine to medium grained and massive. In the field they are distinctively dark green to black in colour, a feature resulting from the high content of mafic minerals, which comprise up to 60% of the rock. Hornblende is the dominant mafic phase, occurring with lesser and variable amounts of biotite, pyroxene and magnetite. Sphene is a ubiquitous accessory mineral.

Mihalynuk *et al.* (1992) suggest that these dikes are late-stage magmatic residues related to the Fourth of July batholith. This appears to be reasonable as the mafic component of the dikes is mineralogically identical to that of the batholith, both containing amphibole, biotite and pyroxene, with the latter typically mantled by amphibole.

In addition to being mineralogically similar, a clear temporal relationship can also be established. Dikes are post-collisional and therefore must be at least mid-Jurassic in age. Dikes also cut alteration zones which have been dated at mid-Jurassic (Ash *et al.*, in preparation) and the dikes themselves are also altered suggesting that they too must be mid-Jurassic, consistent with the age of the Fourth of July batholith.

#### SURPRISE LAKE BATHOLITH

The Surprise Lake batholith, which hosts the Ruby Creek molybdenum deposit, is a Late Cretaceous, composite alkali granite intrusion that lies roughly 5 kilometres northeast of the map area. The granite is typically coarse grained and equigranular, consisting of smokey quartz, chalky plagioclase, potassium feldspar and accessory biotite (Bloodgood *et al.*, 1989a). The characteristic smokey appearance of the quartz is attributed to the anomalously high uranium content and radioactive character of the batholith. An average of six biotite K-Ar dates indicates an intrusive age of  $70.6 \pm 3.8$  Ma (Christopher and Pinsent, 1982). A recently obtained U-Pb zircon age of  $83.8 \pm 5$  Ma for the intrusion (Mihalynuk *et al.*, 1992) is in relatively good agreement with the K-Ar ages. No phases representative of this intrusion have been identified in the present map area. This brief description is included because the intrusion is exposed to the northeast and may have influenced local mineralization. Some of the felsic dikes in the map area may also be related to this younger intrusive event.



## CHAPTER 3

## STRUCTURE

Due to the protracted deformation history of the Cache Creek Terrane, the structure of the local map area is complex. The structural character of the Atlin accretionary complex is briefly described, however, no clear deformational history has been interpreted. The only unit for which a polyphase deformational history has been established is the harzburgite comprising the Atlin ultramafic allochthon.

### ATLIN ACCRETIONARY COMPLEX

The style and intensity of deformation within the accretionary complex is highly variable and reflects its heterolithic nature. This variability appears to result from differences in lithology and the respective competencies of the individual units. More massive, competent lithologies, such as basalt, chert and limestone, show limited evidence of internal penetrative deformation. In most cases, deformation is localized along the faulted or sheared margins of such bodies. Shear fabrics are typically well developed in the comparatively less competent argillite or mixed chert and

argillite units. They are often characterized by a moderate to well developed scaly fabric. Where interbedded with chert, the argillite may display a moderate to well developed bedding-parallel cleavage. The intensity of deformation in the bedded chert and argillite unit is clearly a function of its position relative to major faults. Remote from such structures the unit is either undeformed or displays only moderately developed fabrics. In the vicinity of major structures there is a progressive increase in stratal disruption and the chert layers become disaggregated and form isolated lenses enveloped in the scaly argillite matrix. Where such units are associated with major fault zones there is a preferred orientation of the long axes of the chert lenses parallel to the scaly fabric in the matrix argillite. This style of deformation is well exposed in a series of exploration trenches on the Beavis property on the northern outskirts of Atlin (Photo 3-1) where several hundred metres of chert and argillite occupy a faulted contact between hangingwall ultramafics and footwall metavolcanic rocks.



Photo 3-1. Lensoid chert fragments in scaly argillite, exposed in a trench at the Beavis property.

Throughout the Atlin accretionary complex the orientation of most of the shear fabrics, and the elongation direction of most of the individual units, has a dominant north-northeast to northeast structural grain. This orientation is markedly discordant to the regional northwestern trend, characteristic of the northern Cache Creek Terrane as a whole (Monger, 1975). This local structural grain is, however, consistent with that described in the Sentinel Mountain area to the immediate south-southeast (Monger, 1977c).

Later faults, on a variety of scales, are ubiquitous throughout the complex. Many tend to truncate or off-set preexisting tectonized contacts. Many of these structures cannot be represented at the scale of mapping.

## ATLIN ULTRAMAFIC ALLOCHTHON

The Atlin ultramafic allochthon is a compositionally uniform structural slice of oceanic mantle material which comprises the hanging wall of the Monarch Mountain thrust.

## MONARCH MOUNTAIN THRUST

The Monarch Mountain thrust defines the structural base of the ultramafic allochthon and the tectonic contact between the upper Atlin ophiolitic assemblage and the underlying Atlin accretionary complex. Based on the annular surface trace of the thrust, combined with drill-hole information, it is interpreted to be a relatively flat lying, undulating fault zone.

This basal thrust fault is characterized by a zone of tectonic brecciation and carbonatization, from several me-

tres to tens of metres in width, that affects both hangingwall and footwall lithologies. Hangingwall peridotites are the most intensely and pervasively altered due to their ultramafic composition and reactivity with fluids rich in carbon dioxide. The degree of alteration in footwall lithologies is highly variable, due to the heterolithic nature of the underlying composite complex. Basalts are typically carbonatized and, as in the ultramafic rocks, altered zones contain intermittent silicified shear zones which may host gold mineralization. Footwall cherts yield to brittle fracture and form tectonic breccias which are commonly cemented by variably mineralized assemblages including both hydrothermal carbonate and quartz. Argillaceous rocks within and adjacent to the thrust are intensely sheared and typically form gouge zones.

The arcuate surface trace of the Monarch Mountain thrust crosses the lower southern and eastern slopes of Monarch Mountain. The fault contact is not exposed, however, its approximate location is well constrained by contrasting lithologies, styles of deformation and superimposed carbonate alteration on either side of the faulted contact zone.

Along the northeastern side of the allochthon the thrust is covered by overburden. Its location, however, is well constrained by data from rotary-drill holes and by ground and airborne magnetometer surveys conducted on the Heart of Gold property (*see map in pocket*). Drill holes straddle and also penetrate the thrust contact. A fence of three holes, spaced 100 metres apart parallel to the contact, are all collared in variably serpentinized harzburgites (McIvor, 1988b). The succession of rock types penetrated by each hole is generally comparable: first serpentinized ul-

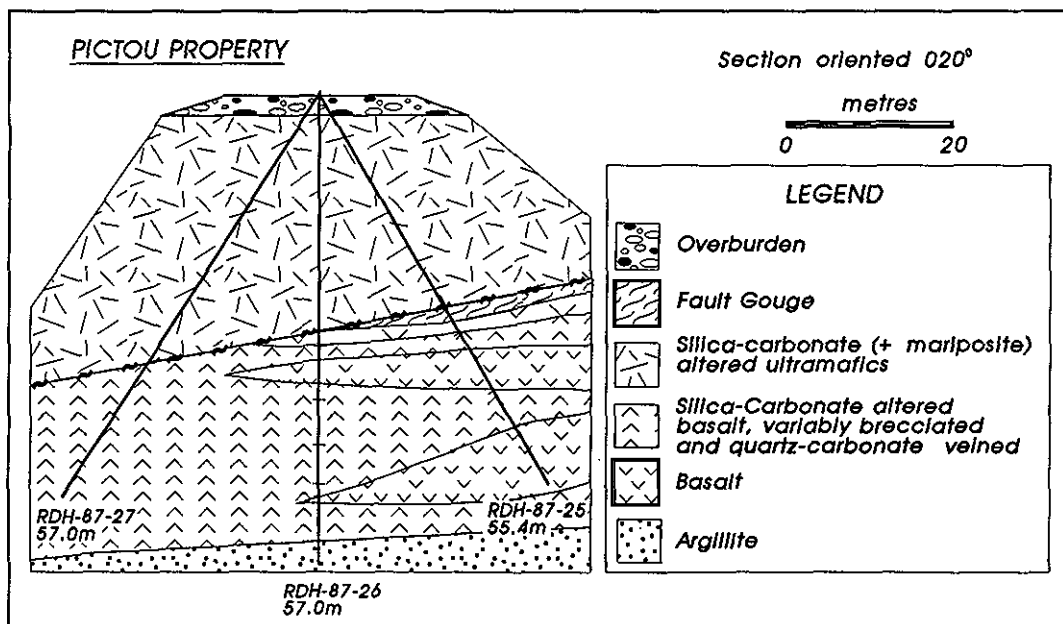


Figure 3-1. Cross section of the Pictou showing illustrating the relatively flat-lying nature of the Monarch Mountain thrust fault.

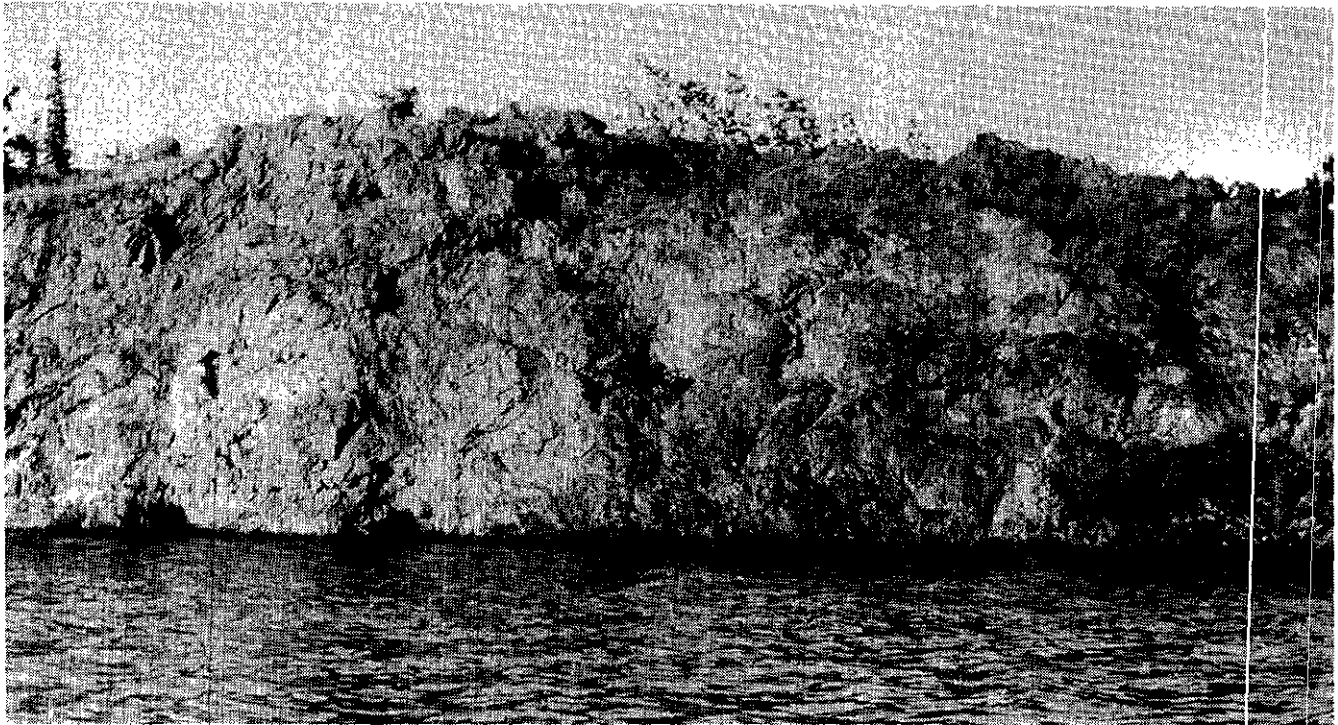


Photo 3-2. Intensely carbonatized ultramafic tectonic breccia within the hangingwall of the Monarch Mountain thrust exposed along the shore of Atlin Lake 0.5 kilometre south of Atlin.

tramafics, followed by an interval of carbonatized ultramafics with intermittent carbonatized shear zones, then into tectonically mixed zones of basalt, diabase and sediments, locally cut by felsic dikes, and ending in brecciated chert or strongly sheared mixed chert and argillaceous footwall lithologies.

Rotary drilling on the Pictou property (Figure 2-2a and b) intersected a somewhat similar sequence (McIvor, 1988a; Rees, 1989). There, an area of intensely carbonatized and variably silicified ultramafic rocks is exposed at the centre of the ultramafic body. Ten holes intersected a similar succession of rock types with comparable alteration characteristics. A representative section defined by three of these holes is illustrated in Figure 3-1. Each hole initially penetrated several tens of metres of silica-carbonate-mariposite-altered ultramafite. This lithology was followed by several tens of metres of intermittent fault zones dominated by silica-carbonate-altered basalt with lesser chert and argillite. Drill logs indicate a gradation into unaltered equivalents of these footwall lithologies.

Quartz-carbonate-altered ultramafics that crop out on the Pictou property are the exposed portion of an elongate north-northeast-trending band, corresponding to an aeromagnetic low which extends across the ultramafic body. This band is interpreted as the hinge zone of a broad, open antiform, (Figure 2-2b) presumably produced by post-thrust buckling.

Monolithic, pervasively carbonatized ultramafic tectonic breccias have been identified at two isolated localities. One crops out in a vertical cliff face, 6 to 8 metres high, over a distance of several hundred metres on the shore of Atlin Lake roughly a kilometre south of the Atlin townsite. The other exposure forms the southern tip of Third Island, where it crops out over a distance of 300 to 400 metres. The breccia in both areas consists of 1 to 5-metre rounded clasts in a tectonically fragmented matrix (Photo 3-2). Similar in character to ultramafic rocks described in Pictou property drill sections, both these exposures are thought to represent deformed and altered rocks in the hangingwall of the Monarch Mountain thrust. Footwall lithologies were not observed in either area, nor has there been any drilling which would help to establish if this potentially mineralized contact occurs in the subsurface.

### STRUCTURE WITHIN THE ALLOCHTHON

Three distinct deformational fabrics are defined within harzburgite of the Atlin ultramafic allochthon, these are related to events before, during and after obduction of these mantle rocks from their place of origin to their present crustal levels. Pre-obduction structures are restricted to the harzburgite unit where primary mantle metamorphic textures are preserved.

Syn-obduction structures include both localized fault zones and a penetrative foliation fabric defined by flattening and elongation of retrograde serpentine after primary har-

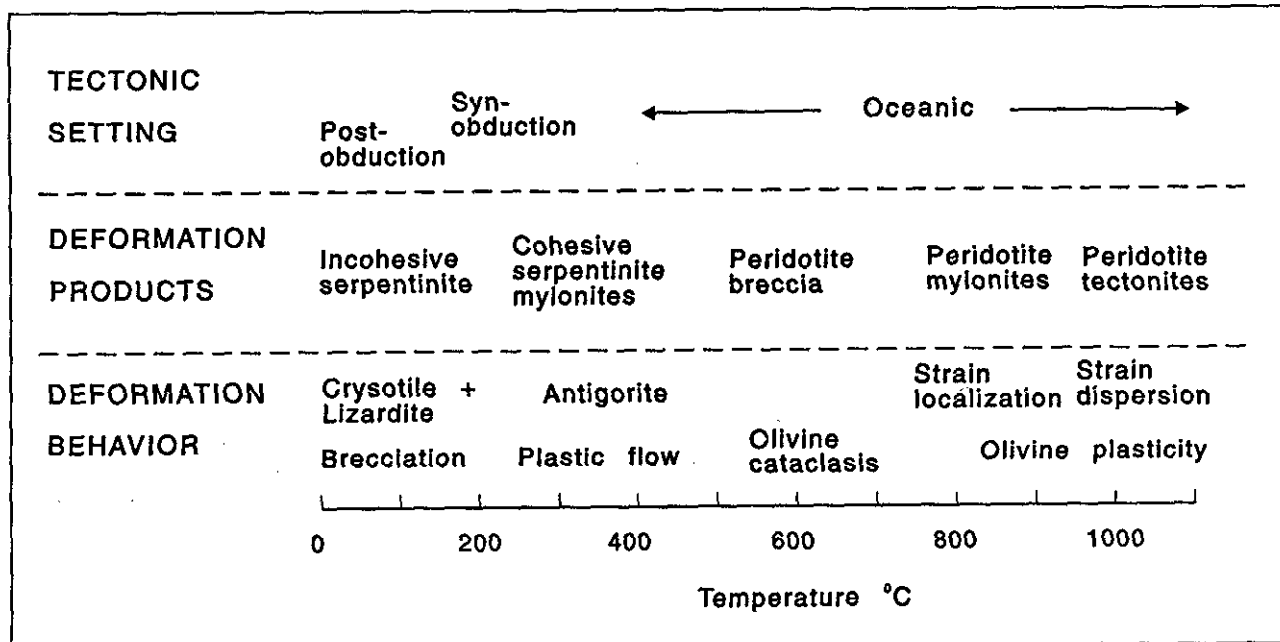


Figure 3-2. Simplified model illustrating relationship between deformation behavior, deformation product, deformation temperature and tectonic setting for ultramafic rocks (after Norrell *et al.*, 1989).

zburgite minerals. Post-obduction structures are restricted to brittle faults evident throughout the map area on a wide variety of scales. Recognition of syn and post-obduction faulting is based on differences in both the type of alteration and style of deformation affecting the ultramafic rocks. A simplified model after Norrell *et al.* (1989) illustrating the relationships between deformation behavior, deformation product, deformation temperature and tectonic setting (Figure 3-2) characterizes the differences in deformation style identified within the ultramafic rocks. Syn-emplacement-related structures are characterized by cohesive serpentine fabrics and are typically associated with carbonate alteration. Post-accretionary structures are, in contrast, characterized by incohesive serpentine fabrics and a lack of carbonate alteration. Late structures also commonly have millimetre-wide veinlets of chrysotile and asbestos which occupy dilational fractures within the later faults.

#### PRE-OBDUCTION STRUCTURES

Structures identified throughout the harzburgite as pre-emplacement are dominant in the interior parts of the body where the harzburgite is less affected by younger deformation and retrograde metamorphism.

Penetrative fabric elements which have been systematically mapped and interpreted to reflect pre-obduction deformation include:

- Foliation fabric ( $S_1$ ) defined by the preferred dimensional orientation and elongation of orthopyroxene or orthopyroxene aggregates.
- Compositional banding ( $S_0$ ) defined by diffuse centimetre-scale variations in the ratio of olivine and orthopyroxene.

- Dunitic lenses in the harzburgite.

The most prominent structural feature is the moderate to well-developed penetrative  $S_1$  fabric which is common throughout the body. Compositional banding ( $S_0$ ) is much less common. Where present, banding is invariably parallel to the  $S_1$  fabric, except in the hinge areas of rare isoclinal to open folds, in which case the axial surfaces of the folds parallel the  $S_1$  fabric in the surrounding harzburgite. Like the banding, the orientation of the long axes of the dunitic lenses consistently parallels the dominant  $S_1$  fabric in the surrounding harzburgite. The parallelism of all these structural elements appears to be consistent with a uniform and progressive deformational episode. Both compositional banding ( $S_0$ ) and foliation fabric ( $S_1$ ) are therefore attributed to pre-obduction deformation due to the common parallelism of the two  $S$ -planes.

Orientation of  $S$  fabrics throughout the harzburgite have a relatively homogeneous distribution pattern. There is a dominance of northeast to east-trending fabrics with steep to moderate dips to the north and northwest. Locally there is some variability; however, it has not been established whether the variation in orientation of the fabric is the result of pre-obduction folding or a function of rigid-body rotation of earlier  $S_1$  planar elements due to movement on later high angle faults.

#### OBDUCTION-RELATED STRUCTURES

Obduction-related structures are represented by both a penetrative foliation fabric ( $S_2$ ) and faulting. These fabrics are defined by a uniform elongation direction of retrograde metamorphic bastite which is commonly identified as rims mantling relict orthopyroxene grains from which it is de-

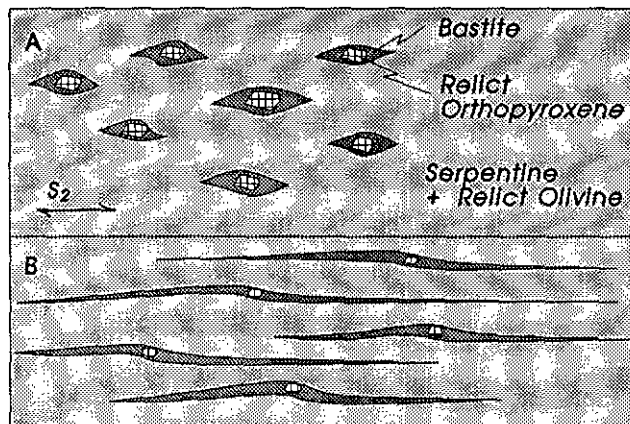


Figure 3-3. Schematic representation of moderate, "A," and intense, "B,"  $S_2$  fabric development in harzburgite defined by bastite.

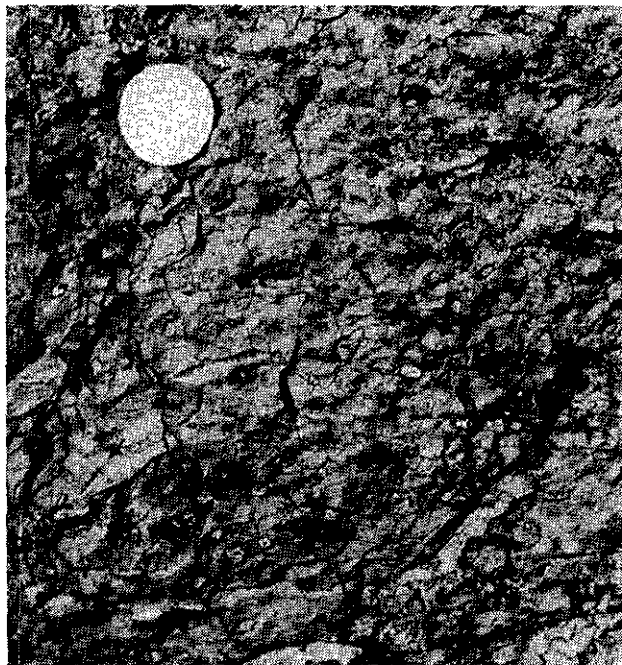


Photo 3-3. Elongation of bastite mantling relict orthopyroxene defines moderate  $S_2$  fabric in harzburgite.

rived. This fabric is clearly later as it is defined by a retrograde metamorphic assemblage after the orthopyroxene which defines the earlier high-temperature mantle-flow  $S_1$  fabrics that are attributed to oceanic, pre-emplacment deformation. The secondary bastite weathers black to dark grey, in contrast to the light grey serpentine after olivine, and is clearly visible on well-washed surfaces. These fabrics are identified throughout most of the body but the intensity of fabric development is highly variable. In most cases the fabric is only weakly to moderately developed (Figure 3-3A, Photo 3-3), however,



Photo 3-4. Well-banded mylonitic serpentinite-bastite fabric ( $S_2$ ) with relict orthopyroxene porphyroclasts.

very high strain zones with mylonitic fabrics occur locally (Figure 3-3B, Photo 3-4). Such high-strain zones are clearly best developed towards the margins of the body and near emplacement-related faults. The variation between the different types of alteration and deformation is everywhere transitional.

The dominant orientation of the  $S_2$  fabrics in the ultramafic rocks is consistent with the general structural grain of the Atlin accretionary complex. This implies that the Middle Jurassic collisional event which resulted in ophiolite obduction may be responsible for the overall structural grain defined locally.

#### SERPENTINITE-BASTITE MYLONITE

A structurally distinctive mylonitic phase of the harzburgite unit, characterized by a 1 to 3-millimetre banding of alternating light and dark grey to black layers of serpentinite and bastite (Photo 3-4) is exposed on the western side of Monarch Mountain. The unit outcrops intermittently over an area of several hundred square metres east of the Warm Bay road, 3.5 kilometres south of Atlin near the start of a well-marked hiking trail leading toward the summit of the Monarch mountain. Serpentinite-bastite mylonites are also well developed along the steeply dipping, east-trending normal fault which transects the ultramafic body and is host to the Goldstar lode gold showing.

These ultramafic rocks have a well developed gnessic fabric designed by segregation of serpentinite and bastite into bands, with augen-shaped orthopyroxene porphyroclasts common throughout the bastite. Many porphyroclasts contain cores of relict orthopyroxene mantled by fine-

grained aggregates of magnetite and serpentine (bastite). The mantled material commonly displays well-developed porphyroclast trails. Locally, the mylonitic banding is moderately to tightly folded with the axial planes of the folds coplanar with the dominant  $S_2$  fabric. Where exposed in the low-lying area east of the Warm Bay road, the fabric varies from subhorizontal to moderately dipping towards the northwest.

Ductile cohesive fabrics developed in the peridotite marginal to and paralleling the east-west trending high-angle fault dip steeply to the north. The presence of these fabrics along the fault suggests that the structure is most likely related to thrust emplacement of the ultramafic body. The fact that this fault is mineralized and displays well developed listwanitic alteration halos further supports a syn-obduction origin, as the timing of carbonate alteration follows closely emplacement of the ultramafic body (Ash *et al.*, 1992; Ash *et al.*, in preparation).

The significance of this high-angle fault within the ultramafic body is questionable, however, two possible mechanisms are suggested to account for its development. Simple-shear strain between simultaneously active upper and lower bounding faults of the ultramafic thrust slice during emplacement is possible. Alternatively, the structure may reflect internal imbrication of the ultramafic body.

The presence of rotated porphyroclasts in the unit could be useful in providing kinematic indicators for determining the direction and sense of transport of the ultramafic body during its emplacement. Sense of motion can only be determined if porphyroclasts display a consistent asymmetry in a plane containing the elongation lineation and normal to the foliation. Unfortunately no definite mineral lineation was identified. Detailed structural analysis of these serpentinite mylonites is warranted.

The timing of serpentinitization, whether it accompanied the deformational event or represents a later retrogression overprinting the fabric, has important implications for the physical character of the ultramafic body during emplacement. Based on textural criteria associated with the mylonite, it is suggested that the serpentinitization is indeed syndeformational. Serpentinitization under static conditions (*i.e.* postdeformation) would result in a random cross-mesh texture which characteristically crosscuts sutured grain boundaries. Within the mylonite, however, several features indicate that the serpentine has been deformed. Neocrystalline magnetite from the serpentinitization reaction forms monoclinic porphyroclast systems. In many cases enstatite has acted as rigid clasts, while neomineralized magnetite and bastite form asymmetric tails. In addition, the strong preferred crystallographic orientation of the serpentine minerals in the mylonite suggests that they have undergone deformation. These combined petrographic features are compatible with serpentinitization occurring during deformation suggested to be the result of obduction of the ultramafic mass.

## POST-ACCRETIONARY STRUCTURES

High-angle faults characterize the map area and occur on a wide variety of scales. The continuation of identified fault zones or the existence of such faults has often been inferred from either air photo linears or aeromagnetic data, or both. Many of the smaller scale faults appear to offset earlier thrust faults. These faults are particularly evident throughout the Monarch Mountain plateau where they form linear depressions. Development of intense serpentinitization, with or without carbonate alteration, adds evidence that such linears represent faults. Only one major and economically significant post-obduction structure, the Pine Creek fault zone will be discussed.

### PINE CREEK FAULT ZONE

The Pine Creek fault is a high-angle east-northeast-trending structure which parallels Pine Creek and is thought to extend across the entire map area. It crops out on the shore of Atlin Lake near the northern outskirts of Atlin. At this locality an exceptionally well developed tectonic serpentinite breccia is exposed (Photo 3-5) over a distance of approximately 50 metres along the lake shore, perpendicular to the fault trace. It is characterized by strongly sheared green-grey to olive-green serpentine hosting dark brown, angular to subangular clasts of serpentinitized harzburgite from 5 to 60 centimetres across and displaying well preserved primary textures. These serpentinites have a rough, disjunctive, anastomosing cleavage resembling "fish-scale" serpentines (Norrell *et al.*, 1989). The fabric, which locally wraps around individual clasts, is subvertical with an overall easterly trend. The entire exposed area lacks carbonate alteration. The structure is interpreted to postdate the alteration episode that is so prevalent in other faults cutting the ultramafic rocks throughout the area. Its trace is defined 8 kilometres to the east-northeast, at the Yellow Jacket property along Pine Creek. Within this general area the fault is well constrained by a total of 86 exploration drill holes (Lefebvre and Gunning, 1988; Marud, 1988a, b; Marud and Southam, 1988). It occurs along the southern margin of an east-trending ultramafic belt on the southern flank of Mount Munro. Drill-hole data indicate that it truncates an earlier system of northwest-dipping imbricate thrust faults at depth. The earlier low-angle thrust fault zone defines a tectonic contact between ultramafics and metabasaltic rocks. The zone of thrusting is characterized by up to 15 metres of carbonate alteration with intermittent zones of quartz-carbonate veining developed within the hangingwall metabasalts. Due to the low angle of this structural zone and the timing of associated carbonate alteration, at Middle Jurassic (Ash *et al.*, in press), it is interpreted to be a syn-obduction structure.

In the Yellow Jacket area the Pine Creek fault zone averages approximately 70 metres in width and is described by Marud (1988a) and Marud and Southam (1988) as a fault *mélange*. It is typified by units that are strongly broken and



Photo 3-5. Serpentinite breccia with harzburgite knockers in a matrix of strongly sheared serpentinite, exposed along the shore of Atlin Lake near the town of Atlin.

fractured, with gouge and rubble zones ranging from centimetres to more than 10 metres in thickness. The fault zone contains irregular blocks and lenses of all the lithologies typical of the Atlin ophiolitic assemblage. These include metamorphosed basalt, diabase, gabbro and ultramafite. Ultramafic rocks are either completely serpentinitized or completely carbonatized. Typically, strongly sheared incohesive serpentinite contains blocks of more competent silica-carbonate-altered ultramafics. Other lithologies within the fault zone include both the feldspar porphyry and melanocratic dike types described earlier, which also occur as irregular pods and lenses up to several tens of metres in size. Northwest-trending cross faults, which appear to offset the fault zone, are a common feature.

It is interpreted that movement on the Pine Creek fault caused both the development of incohesive serpentine and the tectonic entrainment of blocks and lenses of carbonatized and gold mineralized ultramafic rocks developed along the earlier, low-angle structure during, or just following ophiolite obduction. Dike rocks related to the Fourth of July batholith and coeval with carbonate alteration and associated mineralization that postdate obduction (Ash *et al.*, 1992) occur as pods and slivers within the fault zone and support the argument that the fault postdated the mineralizing event. In addition, if the incohesive serpentine had been present during the introduction of the CO<sub>2</sub>-rich mineralizing fluids one would expect that it too would be altered, or at least show some degree of carbonate veining. It does not.



# LITHOGEOCHEMISTRY OF THE ATLIN OPHIOLITIC ASSEMBLAGE

## CHAPTER 4

The lithogeochemistry of the Atlin ophiolitic assemblage was investigated in order to characterize the type and possible origin of the oceanic crustal and upper mantle units. Phase chemical studies were conducted on primary minerals in harzburgites and dunites. Whole-rock major, trace and rare-earth element analyses were obtained for a representative suite of the metabasalts and their petrochemical character evaluated.

### PHASE CHEMISTRY OF THE ULTRAMAFIC ROCKS

A geographically representative suite of ten samples, including five harzburgites and five dunites, was chosen for microprobe analysis of the primary minerals. Locations of the individual samples are illustrated on map (in pocket). Olivine, orthopyroxene and chrome spinel were analyzed in harzburgite; olivine and chrome spinel in dunite. For the silicate phases, two grains were analyzed in each sample, with two-point analyses performed on each grain to test for chemical heterogeneities. Analysis of the chrome spinel grains was more detailed, in many cases involving two-point analysis of the core and rim of individual grains to test for compositional zoning. Only in several of the orthopyroxene grains were chemical heterogeneities detected.

Analyses were conducted using a Cameca SX-50 electron microprobe at the Department of Geology, The University of British Columbia. Spot analyses were made using a beam 1 to 2 microns wide at an operating current of 20 nanoamperes and an accelerating voltage of 15 kilovolts for a counting time of 20 seconds. Natural standards were used and an automated computer correction program, PAP (Pouchou and Pichoir, 1984, 1985), provided instantaneously corrected oxide weight percent values during data acquisition. A complete listing of the analyses obtained for the individual minerals is given in Tables 4-1 to 4-3.

### OLIVINE

Olivine in all samples analyzed is of forsteritic composition. Olivine in harzburgite samples is remarkably homogeneous with a very limited compositional range (Fo<sub>89.5-90.7</sub>). Olivine in the dunites is consistently more magnesian and displays a somewhat broader range in composition between individual samples, with forsterite varying

from 91.8 to 94.2. Nickel content of all samples is relatively uniform, averaging approximately 0.40 weight percent, with no detectable difference between the two rock types.

### ORTHOPYROXENE

The composition of orthopyroxenes is illustrated in Figure 4-1. Five of the data points plot outside the enstatite

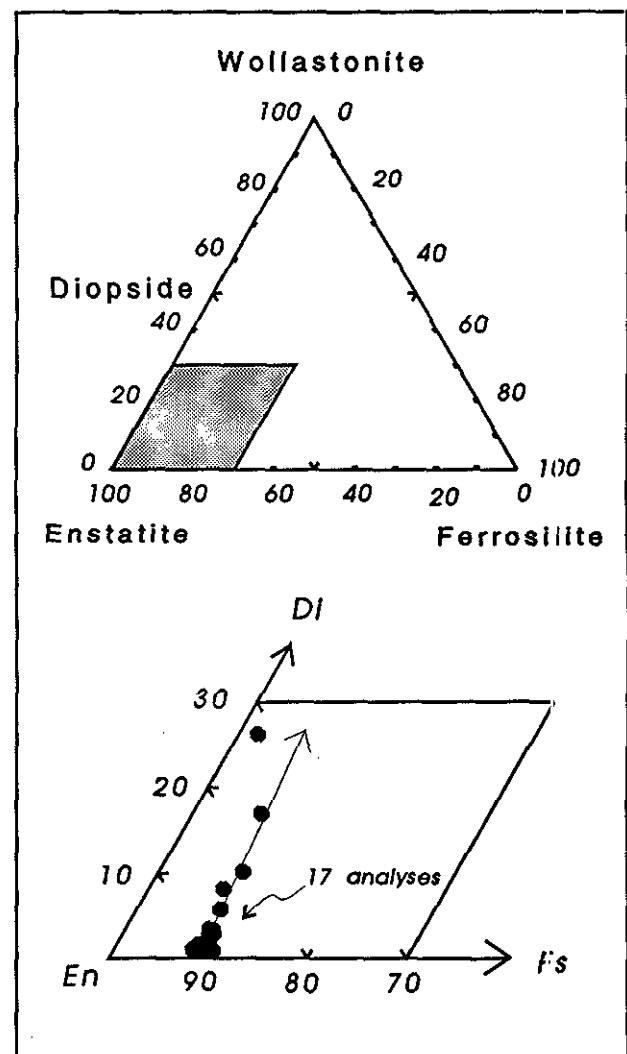


Figure 4-1. Composition of orthopyroxenes from harzburgite in the Atlin ultramafic allochthon.

TABLE 4-1A  
PHASE CHEMISTRY OF OLIVINE IN HARZBURGITE FROM THE ATLIN ULTRAMAFIC ALLOCHTHON

	CAS 6-1-1			CAS 2-1-2			CAS 3-2-2				CAS 10-6				CAS 9-1-4			
	1	2	3	1	2	3	1	2	1	2	1	2	1	2	1	2	1	2
SiO <sub>2</sub>	40.53	40.55	40.51	40.44	40.32	40.58	39.70	39.90	40.30	40.52	40.62	40.41	40.56	40.34	41.11	40.43	41.03	40.66
TiO <sub>2</sub>	0.02	0.02	0.00	0.04	0.03	0.02	0.00	0.03	0.01	0.00	0.02	0.00	0.00	0.03	0.01	0.00	0.01	0.00
MgO	49.49	49.71	49.79	50.43	50.31	50.94	50.08	49.94	50.29	50.54	49.25	49.13	48.73	48.98	50.21	49.60	49.47	49.38
MnO	0.16	0.11	0.09	0.08	0.18	0.13	0.09	0.18	0.09	0.13	0.11	0.14	0.14	0.16	0.10	0.13	0.13	0.15
FeO	9.44	9.30	9.36	9.51	9.05	9.38	9.14	9.44	9.54	9.55	9.43	9.46	9.87	10.14	9.09	9.22	9.14	9.11
NiO	0.37	0.38	0.43	0.43	0.53	0.39	0.44	0.39	0.39	0.28	0.43	0.47	0.47	0.36	0.33	0.41	0.40	0.40
Total	100.01	100.07	100.18	100.93	100.42	101.44	99.45	99.88	100.62	101.02	99.86	99.61	99.77	100.01	100.85	99.79	100.18	99.70
Fo	90.19	90.40	90.37	90.36	90.67	90.52	90.62	90.25	90.30	90.30	90.19	90.11	89.66	89.45	90.69	90.43	90.49	90.47

TABLE 4-1B  
PHASE CHEMISTRY OF OLIVINE IN DUNITE FROM THE ATLIN ULTRAMAFIC ALLOCHTHON

	CAS 8-1-2				CAS 9-1-3				CAS 6-2-2		CAS 3-1-5			
	1	2	1	2	1	2	1	2	1	2	1	2	1	2
SiO <sub>2</sub>	41.41	41.51	41.33	41.41	41.16	41.13	41.66	41.30	40.66	41.29	41.19	41.06	41.05	41.69
TiO <sub>2</sub>	0.00	0.00	0.00	0.00	0.00	0.00	0.01	0.00	0.01	0.00	0.00	0.00	0.01	0.00
MgO	52.53	52.43	52.56	52.66	50.74	51.09	51.26	50.82	51.80	51.46	51.33	51.22	51.03	50.81
MnO	0.10	0.05	0.08	0.10	0.11	0.06	0.06	0.14	0.08	0.08	0.10	0.11	0.11	0.13
FeO	5.89	5.91	5.69	5.72	7.37	7.45	7.31	7.42	7.54	7.54	7.90	7.81	8.06	7.81
NiO	0.42	0.52	0.48	0.44	0.42	0.41	0.39	0.36	0.36	0.35	0.36	0.41	0.48	0.40
Total	100.35	100.42	100.14	100.33	99.80	100.14	100.68	100.04	100.45	100.72	100.88	100.61	100.74	100.84
Fo	93.99	94.00	94.20	94.16	92.36	92.37	92.53	92.29	92.37	92.33	91.95	92.02	91.75	91.94

TABLE 4-2  
PHASE CHEMISTRY OF ORTHOPYROXENE IN HARZBURGITE FROM THE ATLIN ULTRAMAFIC ALLOCHTHON

Sample	CAS 9-1-4				CAS 2-1-2				CAS 6-1				CAS 3-2-2				CAS 10-6			
SiO <sub>2</sub>	55.58	55.64	51.35	55.12	55.66	56.13	55.54	56.00	55.48	54.96	54.95	55.59	55.85	54.74	55.57	55.84	54.49	54.65	54.43	54.26
TiO <sub>2</sub>	0.03	0.02	0.04	0.01	0.01	0.02	0.02	0.00	0.00	0.00	0.03	0.00	0.01	0.02	0.04	0.00	0.06	0.04	0.00	0.04
Fe <sub>2</sub> O <sub>3</sub>	0.00	0.64	3.32	0.50	0.36	0.16	0.56	0.94	0.00	0.09	0.67	0.00	0.00	0.27	0.00	0.06	0.00	0.00	0.18	0.00
Al <sub>2</sub> O <sub>3</sub>	2.82	2.89	5.27	3.56	2.59	2.65	2.60	2.58	2.97	3.38	3.33	3.25	2.56	2.59	2.57	2.65	4.20	4.28	4.23	3.63
Cr <sub>2</sub> O <sub>3</sub>	0.67	0.53	1.09	0.81	0.58	0.68	0.67	0.65	0.71	0.90	1.00	0.92	0.74	0.83	0.74	0.76	0.79	0.77	0.74	0.80
MgO	32.90	33.40	24.65	33.21	32.79	33.57	33.59	34.11	32.69	31.53	30.93	32.59	32.80	27.83	33.20	33.67	32.40	32.18	32.48	29.46
CaO	1.11	0.77	12.55	0.49	1.76	0.89	0.77	0.53	1.50	2.98	4.15	1.77	1.33	8.68	0.70	0.55	0.46	0.47	0.68	5.10
MnO	0.14	0.15	0.04	0.13	0.15	0.10	0.13	0.12	0.14	0.17	0.16	0.15	0.12	0.10	0.15	0.13	0.18	0.12	0.15	0.08
FeO	5.86	5.72	1.13	5.80	5.51	5.91	5.40	5.23	5.90	5.37	4.76	5.64	5.76	4.44	6.08	5.73	6.31	6.06	6.04	5.42
NiO	0.08	0.13	0.08	0.08	0.09	0.09	0.04	0.09	0.07	0.10	0.18	0.09	0.08	0.08	0.15	0.09	0.07	0.09	0.04	0.11
Na <sub>2</sub> O	0.00	0.01	0.04	0.02	0.03	0.01	0.00	0.01	0.01	0.02	0.04	0.01	0.01	0.03	0.01	0.03	0.03	0.02	0.02	0.04
Total	99.19	99.89	99.57	99.73	99.53	100.22	99.31	100.26	99.46	99.49	100.20	100.01	99.25	99.61	99.20	99.50	98.99	98.68	98.98	98.94
En	88.77	89.68	71.80	90.02	88.08	89.32	90.18	90.99	87.97	85.73	84.34	87.83	88.53	75.99	89.25	90.15	89.07	89.43	89.14	81.36
Wo	2.16	1.48	26.28	0.96	3.39	1.71	1.49	1.01	2.91	5.82	8.12	3.42	2.57	17.04	1.35	1.05	0.92	0.93	1.35	10.12
Fs	9.08	8.84	1.92	9.02	8.54	8.98	8.34	8.00	9.12	8.45	7.54	8.75	8.9	6.97	9.4	8.8	10.01	9.64	9.52	8.52

TABLE 4-3A  
PHASE CHEMISTRY OF CHROME-SPINEL IN HARZBURGITE FROM THE ATLIN ULTRAMAFIC ALLOCHTHON

Sample	CAS 9-1-4			CAS 2-1-2				CAS 6-1-2				CAS 3-2-2				CAS 10-6	
	1	2	3	1	2	3	4	1	2	3	4	1	2	3	4	1	2
SiO <sub>2</sub>	0.03	0.05	0.08	0.03	0.00	0.02	0.03	0.031	0.026	0.05	0.03	0.002	0.01	0.01	0.01	0.00	0.02
TiO <sub>2</sub>	0.04	0.03	0.02	0.03	0.02	0.02	0.03	0.012	0.000	0.01	0.04	0.04	0.04	0.01	0.02	0.03	0.03
Fe <sub>2</sub> O <sub>3</sub>	3.05	2.65	2.60	1.20	1.11	1.72	1.33	0.990	0.852	0.74	1.37	2.27	2.27	2.86	2.58	2.43	2.03
Al <sub>2</sub> O <sub>3</sub>	36.82	37.55	38.30	33.34	32.36	32.73	33.16	34.767	35.390	35.54	37.50	29.22	29.35	29.67	30.02	44.98	45.77
Cr <sub>2</sub> O <sub>3</sub>	28.99	28.09	28.01	34.85	36.28	34.81	34.67	33.283	32.440	33.31	31.41	37.86	38.28	37.09	36.56	21.01	20.42
MgO	14.64	15.13	15.41	14.51	14.26	14.28	14.32	15.231	14.851	15.44	16.10	13.66	13.62	13.40	13.46	16.87	17.00
MnO	0.14	0.14	0.08	0.14	0.11	0.18	0.08	0.098	0.140	0.07	0.11	0.15	0.17	0.11	0.13	0.15	0.09
FeO	14.86	13.87	13.89	14.55	14.96	14.68	14.81	13.450	14.046	13.56	13.14	15.08	15.41	15.74	15.51	12.56	12.50
NiO	0.14	0.16	0.20	0.10	0.09	0.14	0.20	0.213	0.173	0.16	0.25	0.10	0.11	0.03	0.13	0.25	0.23
Total	99.71	99.68	101.58	99.75	101.19	101.57	102.63	99.08	99.92	101.88	103.95	99.38	101.25	101.92	102.42	99.28	100.10
Mg	0.635	0.657	0.662	0.637	0.628	0.631	0.631	0.666	0.650	0.668	0.683	0.615	0.609	0.601	0.605	0.7023	0.7057
Fe <sub>2+</sub>	0.361	0.338	0.335	0.359	0.369	0.364	0.366	0.330	0.345	0.329	0.313	0.381	0.387	0.396	0.290	0.2933	0.2912
Fe <sub>3+</sub>	0.067	0.058	0.056	0.027	0.025	0.038	0.030	0.022	0.019	0.016	0.029	0.052	0.051	0.065	0.059	0.0511	0.0426
Al	1.262	1.290	1.300	1.158	1.126	1.143	1.155	1.202	1.225	1.216	1.258	1.041	1.038	1.052	1.067	1.4809	1.5029
Cr	0.667	0.647	0.638	0.812	0.847	0.816	0.810	0.772	0.753	0.764	0.707	0.904	0.908	0.882	0.872	0.464	0.4499
Cr #	34.58	33.40	32.92	41.22	42.93	41.65	41.22	39.11	38.07	38.59	35.98	46.48	46.66	45.60	44.97	23.86	23.04
Mg #	63.76	66.03	66.40	63.96	62.99	63.42	63.29	66.87	65.33	67.00	68.57	61.75	61.14	60.28	67.60	70.54	70.79

TABLE 4-3B  
PHASE CHEMISTRY OF CHROME-SPINEL IN DUNITE FROM THE ATLIN ULTRAMAFIC ALLOCHTHON

Sample	CAS 3-1-5								CAS 8-1-2								
	1	2	3	4	1	2	3	4	1	2	3	4	5	6	7	8	9
SiO <sub>2</sub>	0.05	0.02	0.02	0.03	0.02	0.02	0.04	0.00	0.01	0.04	0.03	0.03	0.02	0.03	0.04	0.01	0.02
TiO <sub>2</sub>	0.05	0.08	0.05	0.08	0.05	0.02	0.07	0.07	0.08	0.07	0.04	0.04	0.06	0.03	0.09	0.04	0.06
Fe <sub>2</sub> O <sub>3</sub>	3.48	3.71	3.59	4.02	3.16	3.60	3.36	3.71	1.48	1.21	1.57	2.55	1.81	1.51	2.59	2.87	2.22
Al <sub>2</sub> O <sub>3</sub>	15.06	14.90	14.88	14.91	14.93	15.00	14.84	15.09	12.99	12.95	12.72	13.03	12.68	12.65	11.63	12.54	12.90
Cr <sub>2</sub> O <sub>3</sub>	51.14	51.04	50.83	50.67	51.46	51.66	51.61	51.21	56.88	57.62	57.14	55.75	56.62	56.75	56.05	55.44	56.43
MgO	9.83	9.79	9.37	9.44	9.72	10.42	10.24	9.88	12.30	12.32	11.85	12.34	11.43	11.18	10.42	11.10	11.57
MnO	0.19	0.23	0.23	0.28	0.23	0.17	0.20	0.18	0.17	0.08	0.18	0.12	0.15	0.17	0.24	0.12	0.18
FeO	18.74	18.76	19.30	19.31	18.81	17.91	18.04	18.86	14.76	14.99	15.45	14.64	16.09	16.38	17.21	16.50	16.09
NiO	0.04	0.00	0.09	0.08	0.07	0.07	0.05	0.06	0.03	0.06	0.12	0.09	0.02	0.03	0.05	0.12	0.09
Total	98.57	98.53	98.36	98.81	98.45	98.87	98.45	99.04	98.71	99.33	99.10	98.57	98.87	98.74	98.33	98.76	99.56
Mg	0.481	0.480	0.461	0.463	0.477	0.507	0.501	0.481	0.596	0.593	0.574	0.598	0.557	0.546	0.516	0.543	0.559
Fe <sub>2+</sub>	0.514	0.516	0.533	0.531	0.518	0.489	0.495	0.515	0.401	0.405	0.420	0.398	0.440	0.449	0.478	0.452	0.436
Fe <sub>3+</sub>	0.086	0.092	0.089	0.099	0.078	0.088	0.083	0.091	0.036	0.029	0.038	0.062	0.045	0.037	0.065	0.071	0.054
Al	0.583	0.577	0.579	0.578	0.579	0.577	0.574	0.581	0.497	0.493	0.487	0.500	0.488	0.489	0.456	0.485	0.493
Cr	1.327	1.327	1.327	1.317	1.339	1.332	1.338	1.323	1.461	1.472	1.470	1.434	1.463	1.471	1.473	1.440	1.448
Cr #	69.48	69.70	69.62	69.50	69.81	69.77	69.98	69.49	74.62	74.91	75.11	74.15	74.99	75.05	76.36	74.81	74.60
Mg #	48.34	48.19	46.38	46.58	47.94	50.90	50.30	48.29	59.78	59.42	57.75	60.04	55.87	54.87	51.91	54.57	56.18

Sample	CAS 6-2-2						CAS 11-1							
	1	2	3	4	5	6	1	2	3	1	2	3	4	
SiO <sub>2</sub>	0.01	0.03	0.016	0.019	0.016	0.027	0.06	0.06	0.07	0.03	0.01	0.00	0.02	
TiO <sub>2</sub>	0.07	0.06	0.071	0.053	0.069	0.054	0.10	0.08	0.06	0.03	0.06	0.08	0.06	
Fe <sub>2</sub> O <sub>3</sub>	2.07	1.80	2.042	2.061	1.605	1.505	1.27	1.45	3.38	2.14	2.18	1.70	1.76	
Al <sub>2</sub> O <sub>3</sub>	16.75	16.82	16.365	17.159	16.589	16.542	12.34	11.93	11.97	5.34	5.28	5.63	5.37	
Cr <sub>2</sub> O <sub>3</sub>	52.25	52.64	52.892	51.864	52.705	52.803	57.73	57.48	55.16	62.77	63.21	62.95	63.42	
MgO	12.82	12.90	12.525	13.046	12.287	12.332	10.81	10.51	9.67	7.16	7.25	7.19	6.95	
MnO	0.11	0.14	0.166	0.124	0.139	0.164	0.29	0.20	0.23	0.33	0.28	0.23	0.26	
FeO	14.59	14.53	15.089	14.253	15.411	15.245	17.18	17.44	18.66	21.35	21.48	21.59	22.01	
NiO	0.02	0.07	0.07	0.061	0.109	0.018	0.03	0.06	0.07	0.05	0.04	0.12	0.04	
Total	98.68	99.00	99.24	98.64	98.93	98.69	99.81	99.21	99.27	99.20	99.80	99.48	99.88	
Mg	0.609	0.611	0.595	0.618	0.585	0.588	0.525	0.515	0.477	0.371	0.373	0.370	0.350	
Fe <sub>2+</sub>	0.389	0.386	0.402	0.379	0.412	0.408	0.468	0.480	0.516	0.620	0.620	0.624	0.636	
Fe <sub>3+</sub>	0.050	0.043	0.049	0.049	0.039	0.036				0.056	0.057	0.044	0.046	
Al	0.629	0.630	0.614	0.643	0.625	0.624	0.474	0.463	0.467	0.218	0.215	0.229	0.219	
Cr	1.317	1.322	1.332	1.304	1.331	1.336	1.488	1.495	1.443	1.722	1.725	1.721	1.732	
Cr #	67.68	67.73	68.45	66.97	68.05	68.16	75.84	76.35	75.55	88.76	88.92	88.26	88.77	
Mg #	61.02	61.28	59.68	61.99	58.68	59.04	52.87	51.76	48.04	37.44	37.56	37.22	35.50	

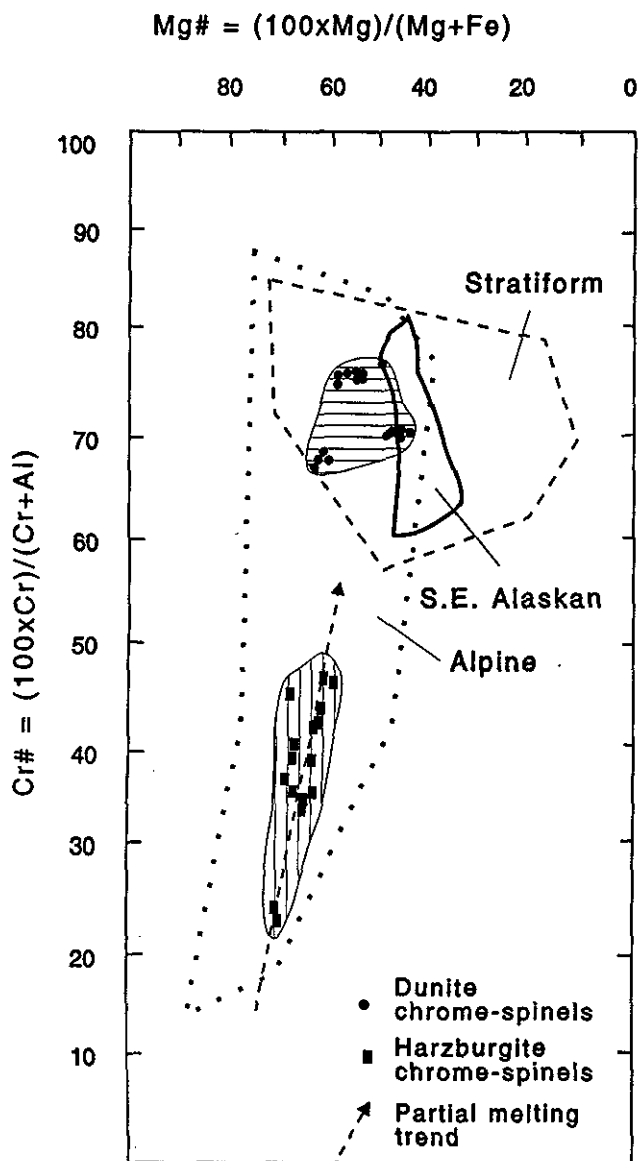


Figure 4-2. Composition of chrome-spinels in harzburgite and dunite from the Atlin ultramafic allochthon compared to compositional fields for alpine-type peridotite (Thayer, 1970), layered intrusions (Irvine, 1967) and southeast Alaskan intrusives (Irvine, 1977).

field and show highly variable wollastonite contents. Compositional variability in these five analyses is suspected to have resulted from simultaneous analysis of both orthopyroxene and contained clinopyroxene exsolution lamellae. Positioning of the beam for spot analysis is restricted to views of the grain in reflected light only, and does not allow for detection and avoidance of these lamellae. This interpretation of a mixed analysis is supported by the fact that they plot along a line between the pyroxene end-members (Figure 4-1). All other orthopyroxenes analyzed have a high magnesian, enstatitic composition (En<sub>87.8-90.2</sub>, averaging En<sub>89.2</sub>).

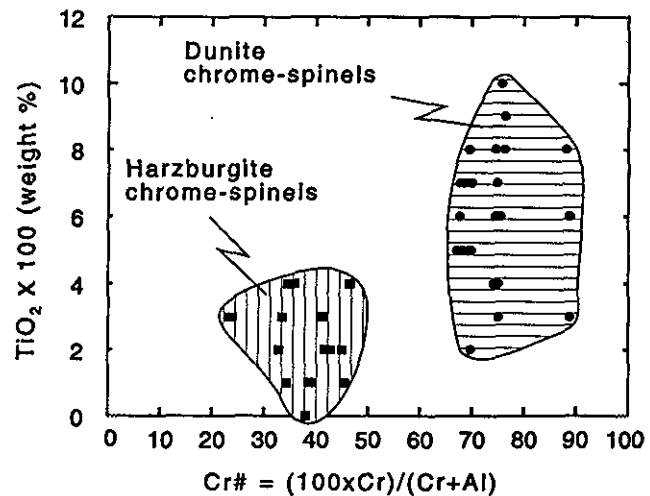


Figure 4-3. Molecular ratio plot of Cr# vs wt% of TiO<sub>2</sub> x 100 for chrome spinels in harzburgites and dunites from the Atlin ultramafic allochthon.

### CHROME SPINEL

Phase chemistry data for chrome spinel from the harzburgite plot within the alpine peridotite field on the Cr#-Mg# face of the spinel prism (Figure 4-2). The compositional variations display a large reciprocal range of chrome and alumina, characterized by a wide range in Cr# (23.0 - 46.7), accompanied by a relatively limited variation in Mg# (60.3 - 68.0). These variations are typical of those found in alpine peridotites (Thayer, 1964, 1969). A collinear variation of increasing Cr# with decreasing Mg# is also apparent, producing a trend characteristic of partial melting (Dick and Fisher, 1984).

All harzburgite chromite plot at the lower end of the compositional field of alpine peridotites. With a maximum Cr# of 46.7, they clearly fall within the abyssal (or mid-ocean ridge) peridotite field and are therefore classified as Type I peridotites with Cr# less than 60 (Dick and Bullen, 1984). The relatively low overall chrome numbers suggest limited degrees of partial melting in the mantle, leaving a relatively fertile mantle residue.

Chrome spinels from the dunite are chemically distinct from those in the harzburgite (Figure 4-3). The Cr# of the dunite chrome spinels is much higher, ranging from 67.0 to 88.9; there is also a wider range in Mg# in the dunite chromite spinels (35.5 - 62.0) compared to the relatively uniform Mg# for chrome spinel in the harzburgite (60.3 - 68.0).

The TiO<sub>2</sub> content of chrome spinels in the two rock types is also strongly variable, with dunite chrome spinels generally higher (Figure 4-3). Chrome spinel in the dunites contains 0.6 weight percent TiO<sub>2</sub> on average, while those in the harzburgite average 0.23%. The chemical and previously described petrological difference between the two chromite types clearly reflects the unique origin of each. The

ehedral chromite of the dunite being magmatic that of the harzburgite metamorphic.

### GEOCHEMISTRY OF THE ATLIN METAVOLCANICS

Geochemical analyses on a representative suite of 17 metavolcanic rocks from the Atlin area were used to classify the metavolcanic units in terms of their paleotectonic eruptive setting. All samples were initially analyzed by atomic absorption (for major elements) and x-ray fluorescence (for Zr, Y, Nb, La, Sc, V, Ni, Cr, Ba, Sr, Ce and Cs). On the basis of these results, five samples were selected for further analyses of the rare-earth elements (REE) by instrumental neutron activation analysis (INAA). The results are listed in Table 4-4.

All Atlin metabasalts sampled are of subalkaline tholeiitic character (Figures 4-4 and 4-5). They plot within the

field of ocean-floor basalts on most discrimination diagrams using high field-strength elements (*i.e.*, Ti-Y-Zr-Nb; Figures 4-6a, b, and c). Therefore, both a mid-ocean ridge or suprasubduction zone setting are potential eruptive environments. Ocean-island, continental and mature calcalkaline island-arc environments are unlikely settings (Pearce and Cann, 1973).

Chondrite-normalized rare-earth element patterns for selected basalts are illustrated in Figure 4-7. Rare-earth abundances are roughly seven to ten times that of chondrite and display a relatively flat distribution pattern. Depletion in lanthanum characterizes most of the samples. Mobilization of this element, due to the effects of sea-floor alteration, is well established (J. Malpas, personal communication, 1991). One sample deviates slightly from the general distribution pattern. It is characterized by slight light REE enrichment and elevated europium content relative to the other

TABLE 4-4  
WHOLE ROCK MAJOR, TRACE AND RARE EARTH ELEMENTAL ABUNDANCES FOR METAVOLCANIC ROCKS IN THE ATLIN AREA

Sample Number	DVL87 30	DVL87 14	MAB88 75	CRE88 3	CRE88 14	CRE88 16	CRE88 34	CRE88 62	CRE88 67	MAB88 122-2	CRE88 263	CRE88 151	CRE88 123	MAB88 241	CRE88 293	CRE88 306	MAJ189 153
SiO <sub>2</sub>	49.35	50.38	48.23	48.09	49.11	50.22	50.84	48.84	44.73	47.36	50.75	50.61	48.86	51.03	48.25	51.50	50.62
TiO <sub>2</sub>	1.54	1.26	1.60	1.25	1.29	1.28	1.27	1.86	2.18	1.31	1.34	1.91	1.30	1.41	1.25	1.53	1.28
Al <sub>2</sub> O <sub>3</sub>	14.11	14.35	14.25	14.04	14.15	14.39	14.77	14.19	14.97	14.73	14.12	13.31	14.68	14.59	14.22	14.49	15.30
Fe <sub>2</sub> O <sub>3</sub>	12.80	11.52	11.85	12.01	11.31	10.55	11.18	13.40	14.48	10.86	12.50	15.12	11.33	10.67	10.29	11.56	11.17
MnO	0.19	0.21	0.17	0.19	0.17	0.18	0.19	0.24	0.18	0.17	0.21	0.24	0.19	0.18	0.19	0.20	0.20
MgO	6.73	6.81	7.30	7.76	6.56	6.06	6.50	6.38	8.02	7.16	6.27	6.47	6.81	6.83	5.60	6.20	6.72
CaO	10.58	12.06	7.80	11.59	6.92	12.14	9.16	9.92	5.48	9.59	9.99	7.21	11.74	11.37	14.01	10.53	9.26
Na <sub>2</sub> O	2.72	2.13	3.23	2.08	3.81	2.87	3.83	2.75	2.59	2.68	2.76	3.46	2.32	2.80	1.91	3.02	3.60
K <sub>2</sub> O	0.25	0.13	0.64	0.16	0.15	0.19	0.34	0.34	0.28	0.32	0.22	0.47	0.17	0.14	0.27	0.33	0.16
P <sub>2</sub> O <sub>5</sub>	0.13	0.11	0.14	0.10	0.10	0.11	0.10	0.14	0.14	0.11	0.10	0.20	0.10	0.14	0.12	0.13	0.12
LOI	1.46	0.54	4.00	2.17	5.57	1.51	1.11	1.08	5.93	5.10	1.96	0.43	1.21	0.80	3.27	0.52	1.28
Total	99.86	99.5	99.21	99.44	99.14	99.5	99.29	99.14	98.98	99.39	100.22	99.43	98.71	99.96	99.38	100.01	99.71
CO <sub>2</sub>	3.58	3.91	0.81	0.15	2.80	0.95	0.18	0.15	1.61	1.92	0.47	0.15	0.15	0.32	2.26	0.36	0
S	0.05	0.20	0.24	0.01	0.02	0.39	0.07	0.06	0.01	0.26	0.03	0.01	0.08	0.10	0.11	0.16	0
FeO	0.57	9.37	8.17	9.06	8.93	8.37	8.24	10.05	11.37	7.73	9.35	11.97	9.07	8.59	8.19	9.21	0
Cr	232	233	265	238	212	229	169	156	328	327	183	155	277	313	245	198	195
Ba	48	14	545	71	123	71	205	40	58	239	34	405	30	50	129	109	44
Sr	126	93	381	101	139	174	185	133	146	244	78	177	184	241	215	189	165
Rb	11	6	14	10	10	10	10	15	10	10	10	10	10	10	10	10	50
Zr	113	85	107	81	70	92	72	114	120	92	70	104	81	105	95	104	88
Y	38	33	34	32	28	37	25	33	27	29	29	32	30	34	30	37	30
Nb	9	10	4	13	8	17	7	8	10	7	5	7	5	7	9	5	10
Ce	25	32	21	21	5	18	5	11	18	10	25	19	11	24	16	14	20
Cs	6	5	5	7	5	5	5	5	5	5	5	5	5	5	5	5	5
La	19	361	15	16	15	17	17	24	21	15	15	19	15	15	17	15	15
Sc	44	46	41	43	37	43	41	43	44	41	40	42	42	41	41	39	40
V	322	308	379	347	332	343	345	418	430	325	376	446	350	324	323	359	309
La		2.5		2.5							2.4	4.9					2.4
Ce		9		8							8	14					9
Nd		7		7							7	11					7
Sm		2.4		2.2							2.4	3.3					2.5
Eu		1.05		0.84							0.81	1.28					0.93
Tb		0.7		0.6							0.7	0.8					0.7
Yb		2.94		2.75							2.77	2.76					2.91
Lu		0.42		0.41							0.42	0.41					0.42

AAS  
XRD  
NIA

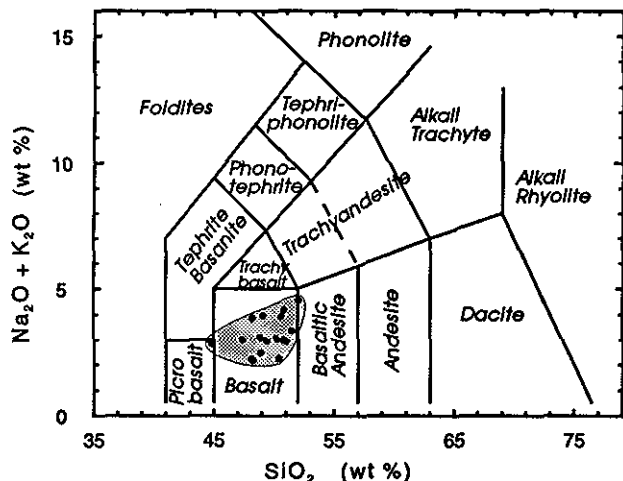


Figure 4-4. Classification of Atlin metabasalts (after Le Maitre, 1984, 1989). AB = alkali basalts, Sub-AB = sub-alkali basalts, TrAn = trachyandesites, B+TB+N = basanites, trachybasanites, nephelinites.

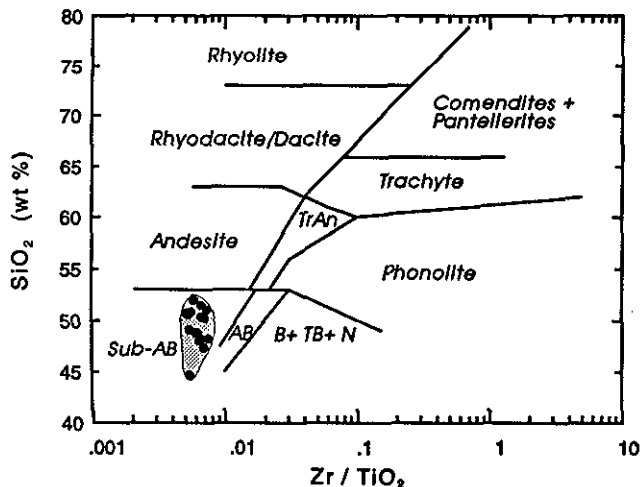


Figure 4-5. Major element discrimination illustrating field of Atlin metabasalts (after Winchester and Floyd, 1977).

samples, suggesting that the deviation is most likely the result of differentiation.

The REE distribution patterns are similar to those characteristic of both mid-ocean-ridge basalts (MORB; Basaltic Volcanism Study Project, 1981) and island-arc tholeiites (IAT; White and Patchett, 1984). These patterns alone, therefore, cannot distinguish between the two potential paleotectonic environments (Jakes and Gill, 1970).

Immobile element covariation diagrams (Ti/V and Cr/Y) can be used to discriminate between the arc tholeiite and mid-ocean-ridge magma types. Ratios of more incompatible to less incompatible elements (e.g. Ti/V, Figure 4-8) illustrate a compositional range for the Atlin metabasalts similar to that for modern ocean-floor basalts. Most of the samples occupy an area of overlap between MORB and IAT

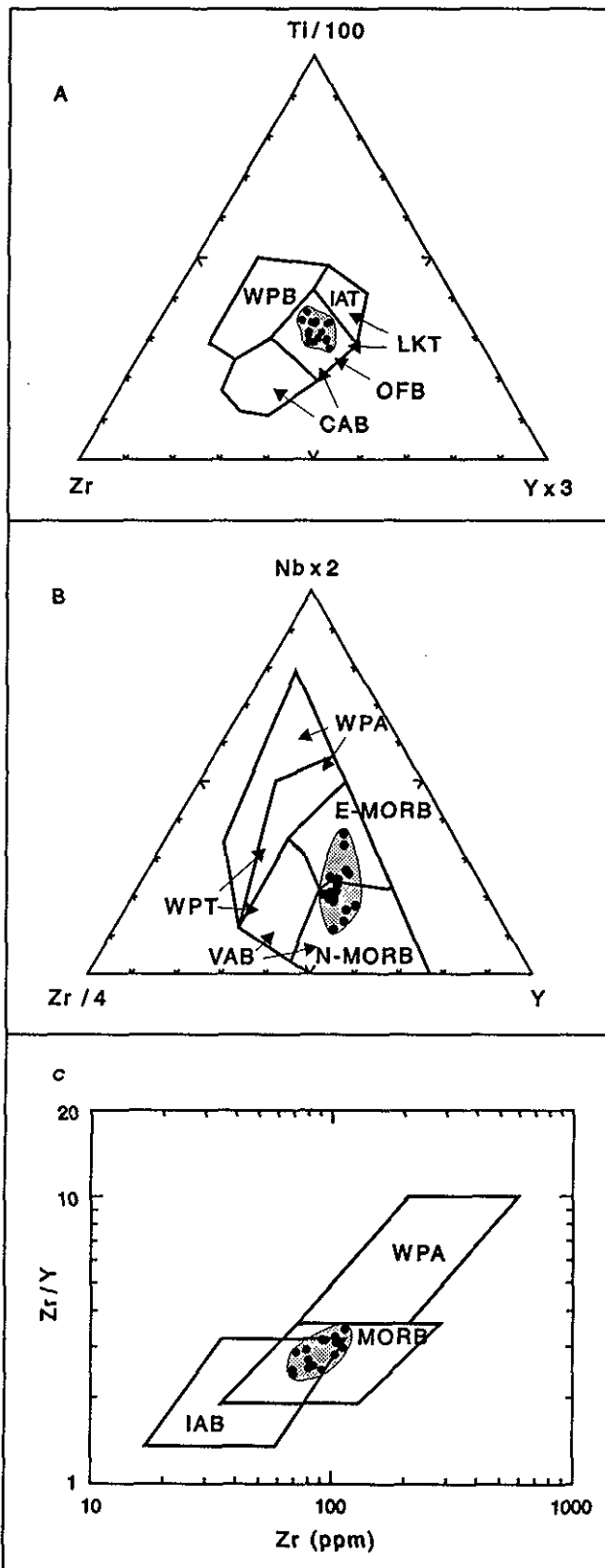


Figure 4-6. Mobile element tectonomagmatic discrimination diagram illustrating field of Atlin metabasalts using (A) Nb-Zr-Y (after Meshede, 1986); (B) Ti-Zr-Y (after Pearce and Cann, 1973); (C) Zr/Y-Zr (after Pearce and Norry, 1979).

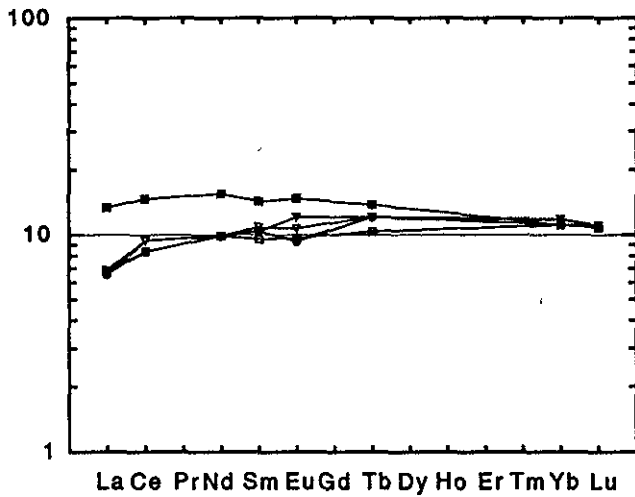


Figure 4-7. Chondrite-normalized rare-earth-element distribution patterns for Atlin metabasalts. Normalization values from Andrews and Ebihara (1982).

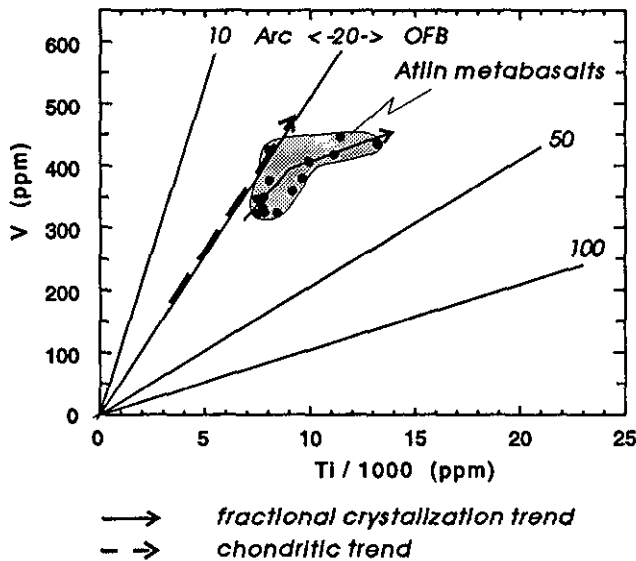


Figure 4-8. Plot of  $Ti/1000$  vs  $V$ , illustrating field of Atlin metabasalts (after Shervais, 1982).

defined by  $(Ti/1000)/V$  ratios between 20 and 27. The samples do, however, display a fractional crystallization trend (solid line with arrow) characteristic of ocean-ridge basalts which is clearly distinct from the "chondritic" trend (broken line) typical of arc tholeiites (Shervais, 1982). The  $Cr/Y$  (compatible/incompatible element) plot is particularly effective in discriminating between the two (Pearce, 1980, 1982; Alabaster *et al.*, 1982). Metabasalts of the Atlin area plot entirely within the MORB field (Figure 4-9). In this diagram the IAT field is displaced toward lower yttrium values at a given chromium concentration, due to the increased depletion of the source region for the generation of tholeiitic magmas as compared to ocean-ridge basalts.

On MORB-normalized multi-element plots (Figure 4-10) metabasalts from the Atlin area display a distribution

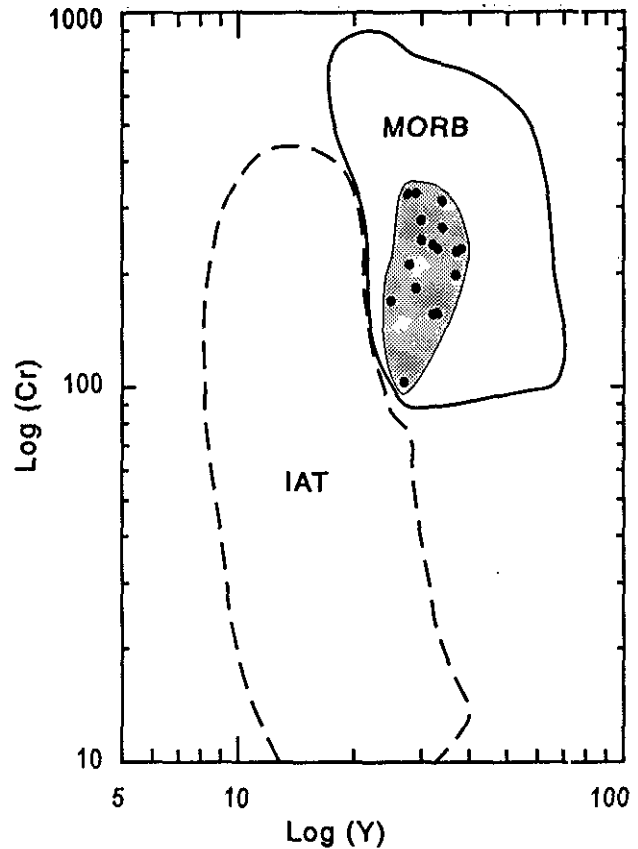


Figure 4-9.  $Cr$  vs  $Y$  discrimination plot illustrating field of Atlin metabasalts (after Pearce, 1982).

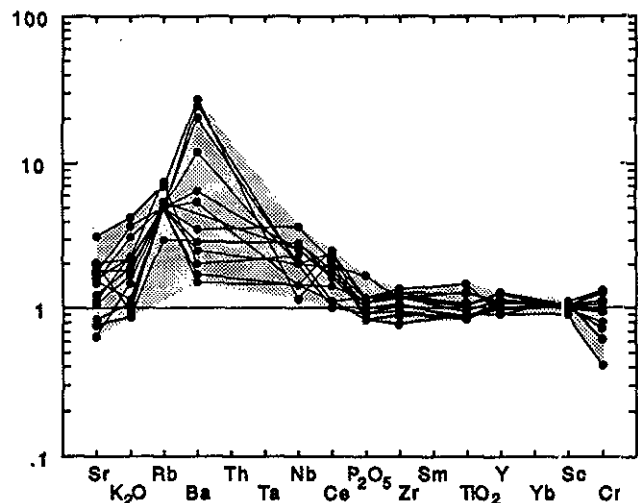


Figure 4-10. MORB normalized multi-element distribution patterns for Atlin metabasalts. Normalization values from Pearce (1982).

pattern indicative of hydrothermally altered mid-ocean-ridge-generated crust. The high field strength (HFS) elements which are considered to be generally immobile during hydrothermal alteration or low-grade metamorphism (Cann, 1970; Pearce and Cann, 1973; Pearce, 1983) display relatively uniform MORB abundances. Abundances of the large

ion lithophile or low field strength (LFS) elements, such as cesium, rubidium, potassium, barium and strontium are highly variable. Sporadic enrichment in a number of the lithophile elements is not considered diagnostic. The mobility of the alkali elements (*i.e.*, Sr, K, Rb and Ba) due to the effect of alteration and metamorphism is well established; and a result of their incompatible nature and mobility in aqueous fluids (Pearce, 1980, 1982, 1983; Pearce and Cann, 1973; Saunders *et al.*, 1980). Barium, which shows the highest variability, is subject to enrichment in secondary mineral assemblages during hydrothermal alteration (Humphries and Thompson, 1978).

The combined evidence provided by applying the various geochemical discriminants to the whole-rock chemical data suggests a mid-ocean ridge paleo-eruptive setting for metabasaltic rocks in the Atlin area. The abundances of the relatively immobile HFS elements are consistent with MORB values. There is neither enrichment of the LFS elements nor depletion of the HFS elements, features attributed to the influence of subduction-derived fluids. The possibility of a suprasubduction zone setting for the Atlin metabasalts is therefore considered unlikely.

### MODELING THE MANTLE SOURCE REGION

Trace element chemistry of metabasalts from the Atlin area can be used as a basis for speculation on the geochemical character of the mantle source region from which they were derived and may also provide supportive evidence for a genetic link between basalts and ultramafic rocks as originally proposed by earlier workers (Aitken, 1959; Monger 1975) due to the close proximity of the two units.

An effective way of modeling both the partial melting and fractional crystallization history of a hypothetical magma is to plot a diagram in which abundances of compatible and incompatible elements are compared, as demonstrated by Pearce (1980, 1982) and outlined below. The diagram of chromium versus yttrium is considered particularly effective for this purpose (Figure 4-10).

Trends followed by chromium and yttrium during the processes of fractional crystallization and partial melting are quite distinct. Yttrium is incompatible with respect to a garnet lherzolite and therefore quickly concentrated into initial melt fractions. Increase melting shows a relative depletion in Y concentration as the bulk of what was initially present is taken away by earlier melt fraction. For this reason its concentration in the melt decreases as melting progresses. Chromium, on the other hand, is compatible and will remain at an almost constant concentration due to buffering by residual chromite, olivine and pyroxene. Therefore, partial-melting trends (for degrees of melting less than 50%) are subparallel to the Y axis, with fractionation trends perpendicular to the partial-melting trend. During fractional crystallization of early mafic phases (olivine, chrome spinel and clinopyroxene) the trend is almost vertical as chromium is very rapidly removed from the melt.

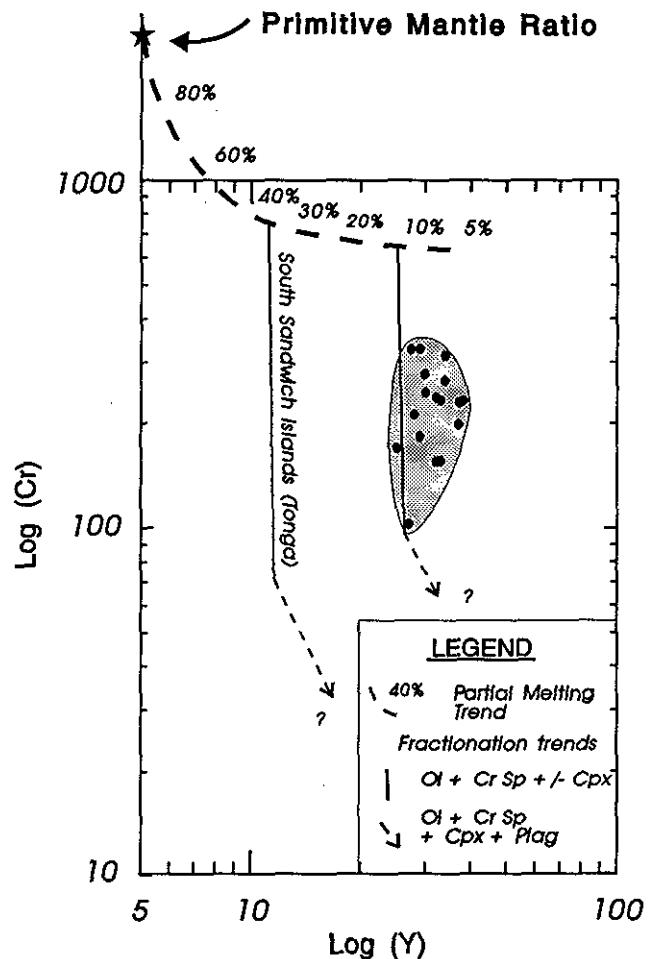


Figure 4-11. Genetic pathways on the Cr-Y plot for derivation of lavas in the Atlin area. Component of partial melting pathway and the petrogenetic pathway of the South Sandwich Islands (includes as an example of a typical island arc tholeiite (IAT) taken from Pearce (1982).

Subsequent crystallization of plagioclase causes the trend to flatten to a slope of -1.

These features are adopted here to model the partial melting and fractional crystallization history of the Atlin metabasalts. The petrogenetic interpretation of the Cr-Y diagram is illustrated by Figure 4-11. Data from the Atlin metabasalts are plotted as in Figure 4-10. The genetic pathway was drawn by starting with the most primitive composition as indicated by the lowest Y content in the basaltic rocks and extrapolating back to the partial melting curve along an olivine-spinel vector. The resultant point of intersection indicates that the primary melt was generated from a mantle source region that was affected by roughly 12-15% partial melting. The variation of a relatively primitive island-arc tholeiitic volcanic suite, from the South Sandwich Islands (data from Pearce, 1982) and a probable petrogenetic pathway connecting it to a source of primordial mantle composition are included for comparison with basalts generated by much higher degrees of partial melting related to subduction.

# CHAPTER 5

# SUMMARY

## ORIGIN OF THE ATLIN ULTRAMAFIC ALLOCHTHON

The combined petrological, chemical and structural data presented for both the harzburgite and basalt units of the Atlin ophiolitic assemblage clearly constrain its environment of formation. The coarse porphyroclastic texture, the folding of metamorphic banding and uncleaved pyroxenite dikes in the harzburgite are consistent with features developed during hypersolidus to subsolidus ductile deformation attributed to asthenospheric flow in the mantle (Nicolas, 1986; Nicolas and Poirier, 1976; Nicolas *et al.*, 1980). The strongly refractory nature and limited compositional range of the primary silicate phases in the harzburgite, the large reciprocal variation of chrome and alumina in accessory chrome spinel and the presence of orthopyroxene-clinopyroxene-spinel clusters, all support an origin by partial melting. The harzburgites are therefore metamorphic in origin and interpreted to represent the depleted residue produced after partial melting and magma genesis in the mantle below an oceanic spreading ridge.

The general podiform shape of the dunite bodies and the consistent parallelism of the long axes of these bodies with metamorphic fabrics in the host harzburgite attest to a genetic relationship with the plastic flow attributed to asthenospheric mantle conditions. Dunite chrome-spinels, in contrast to those in the harzburgite, have well preserved cumulate textures, a broader range in Mg# values and a cluster of high Cr numbers with higher compatible element content (TiO<sub>2</sub>). The distribution and shape of the dunite bodies, combined with the texture and chemistry of associated chrome spinel, are similar to dunites in the mantle section of many ophiolite complexes and are all consistent with the generally accepted interpretation that such dunite bodies are the products of early fractional crystallization from rising basaltic melts generated by partial melting of their residual peridotitic hostrocks (Malpas, 1978; Neary and Brown, 1979; Brown, 1980; Lago *et al.*, 1982; Duke, 1983; Gregory, 1984) as schematically depicted in Figure 5.1. Continued fractional crystallization of these basaltic melts in axial magma chambers above the depleted mantle at the oceanic spreading centre produces the differentiated oceanic plutonic suite. Locally, both the wehrlitic ultramafic cumulates and the gabbros represent dismembered remnants of that suite. Basaltic rocks are equated with the extrusive and possibly hyperbyssal members of an ophiolite.

The chemical signature of basaltic rocks within the Atlin ophiolitic assemblage indicates that they formed from magmas generated by limited degrees of partial melting of a relatively fertile mantle source region. A signature consistent with that of a mid-ocean-ridge paleoeruptive setting. The phase chemical signature of chrome spinel in the harzburgite indicates that it is metamorphic, residual mantle material produced by limited degrees of partial melting. A chemical signature consistent with chrome-spinel in mantle material dredged from mid-ocean-ridge settings (Dick and Fisher, 1984; Dick and Bullen, 1984). It is therefore reasonable to suggest that partial melting of mantle material which produced the residual harzburgite, generated the magma which produced the basaltic rocks. These two units are therefore considered to be genetically related as previously suggested (Aitken, 1949; Monger, 1975).

## EMPLACEMENT OF ATLIN ULTRAMAFIC ALLOCHTHON

The ophiolitic Cache Creek Terrane has been previously interpreted as a Late Triassic accretionary prism or subduction complex related to arc volcanism on Quesnellia (Monger *et al.*, 1982; Monger, 1984; Coney, 1989; Gabrielse and Yorath, 1989). Such an origin is, however, not entirely consistent with the tectonostratigraphic relationships identified in the present map area which indicate that segments of the oceanic crust and depleted upper mantle have been emplaced not only by subduction, but also by obduction processes. This alternative explanation for the emplacement of alpine ultramafic bodies into, or more correctly "onto", the Cache Creek Complex, has critical implications for interpreting the structural setting of the ultramafic rocks and their related lode gold deposits.

The currently accepted mechanism of formation for an accretionary prism or subduction complex involves the build up of material (predominantly sediments) scraped off a subducting oceanic lithosphere above. Many of the features expected in an accretionary prism are present in the lower tectonostratigraphic unit, the Atlin accretionary complex in the present map area. This structurally and lithologically complex sequence of rock types therefore falls within the traditional definition of the Cache Creek Complex. Problems arise, however, when a similar process is invoked to account for the emplacement of the mantle peridotites and associated crustal plutonic rocks of the upper tectonostratigraphic unit, the Atlin ophiolitic assemblage.

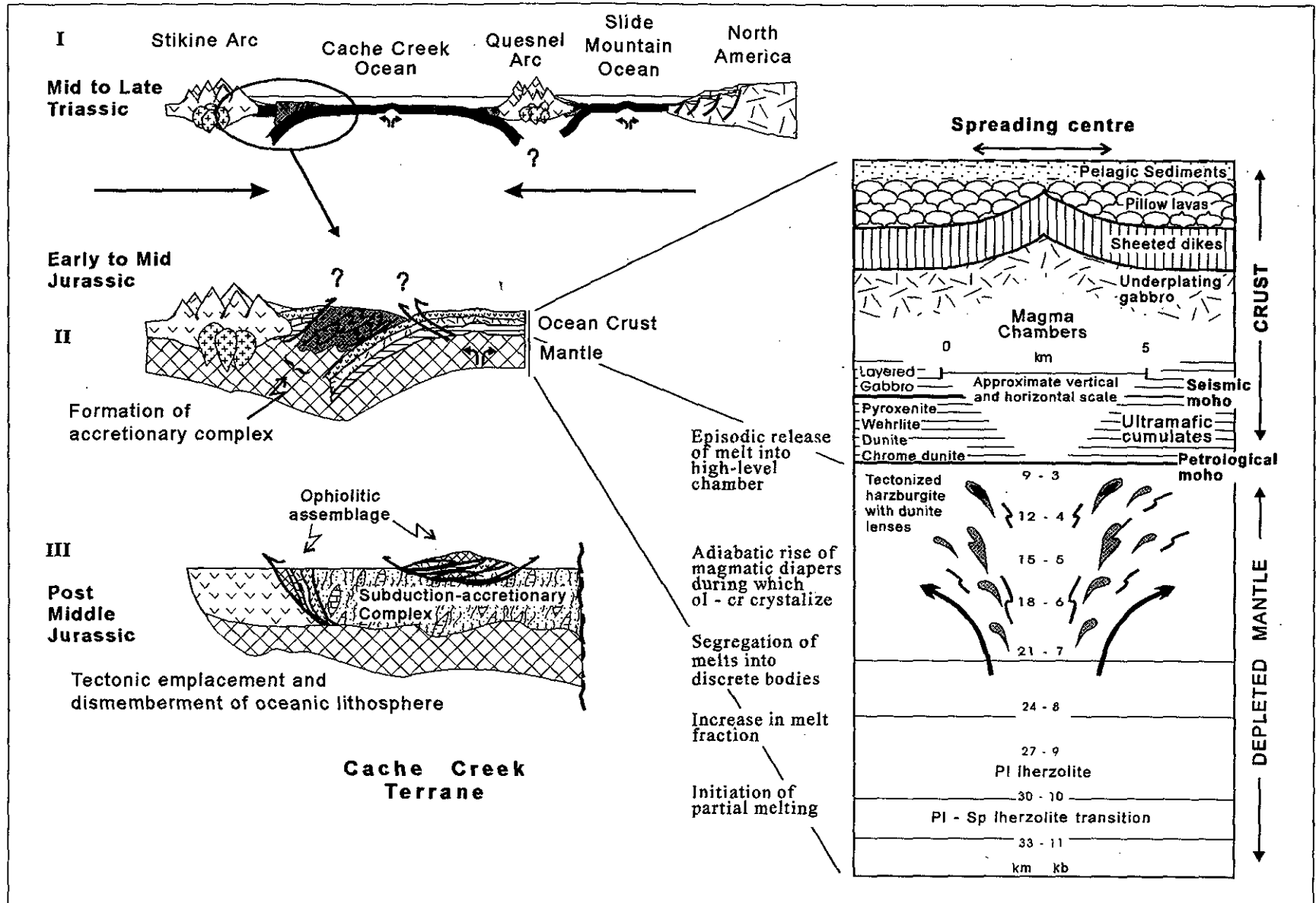


Figure 5-1. Schematic representation of the origin and emplacement process for ophiolitic ultramafic and related rocks in the Atlin area. (Section of oceanic lithosphere modified after Gass, 1980.)

Aubouin (1989) recently reviewed subduction zone characteristics as seen through detailed bathymetric surveys and geophysical studies. He included multichannel seismic profiling and gravimetric as well as magnetic surveys from many of the better studied modern subduction zones. He stressed that the descriptive emphasis of the review was based on facts, not ideas and models. Concerning the effects of subduction on the oceanic crust, he states: "There is no reason to assume that ophiolitic bodies derived from the oceanic lithosphere are incorporated into mountain belts by subduction; they must be obducted during a collisional process."

Incorporation of residual mantle harzburgite that originated at oceanic crustal depths of at least 8 to 10 kilometres into an accretionary complex by the subduction process seems unlikely. In the Atlin area, residual mantle ultramafic rocks overlie imbricated, steeply dipping pelagic sediments with pronounced structural discordance along a regional low-angle fault zone.

Many major ophiolite complexes exhibit post-collisional geometries in which shallow-water sediments are overlain by deep oceanic sediments which are in turn overlain by a slab of oceanic crust and upper mantle (ophiolitic slab; Gealey, 1980).

Structural features which characterize the harzburgite unit provide additional evidence for its mechanism of emplacement. Ductile syn-emplacement fabrics identified in the mantle section indicate that the ultramafic body has been affected by inhomogeneous bulk strain during emplacement in the solid state. The development of serpentinite-bastite mylonite, as identified near the base of the Atlin ultramafic allochthon, is a common feature of the basal ultramafic portions of many ophiolite massifs (Boudier *et al.*, 1982; Karamata, 1980) and represents an integral part of the assemblage of units referred to as the "dynamothermal aureole" (Williams and Smyth, 1973; Malpas, 1973).

That serpentinization is most likely contemporaneous with the development of the mylonite suggests that the body was emplaced relatively cold (less than 500°C; Karamata, 1980) which suggests that the mantle section from which it was detached had travelled a significant distance from the zone of high heat-flow, at the oceanic spreading centre. This relationship is in excellent agreement with the litho-geochemical signature of the ultramafic rocks which indicates

that they are abyssal peridotites formed in a mid-ocean ridge setting.

## CONCLUSIONS

Ultramafic rocks in the Atlin area of northwestern British Columbia consist of both depleted mantle harzburgite and plutonic ultramafic cumulates. Both units form individual thrust sheets, or slices imbricated with primarily basaltic volcanics and lesser diabase and gabbro. Collectively, these units are here referred to as the Atlin ophiolitic assemblage. This assemblage was emplaced tectonically in Middle Jurassic time above a highly varied, steeply to moderately dipping, tectonically intercalated package of fine clastic and pelagic sedimentary rocks with pods and slivers of basaltic volcanic rocks, limestones and ultramafics, named the Atlin accretionary complex.

Recognition of these two distinctive lithotectonic elements with different origins requires a two-fold subdivision of the northern Cache Creek Terrane into: dismembered ophiolitic assemblages, tectonically emplaced by processes of obduction; and accretionary prisms, formed by the process of subduction.

The texture, mineralogy and phase chemistry of the harzburgite are all consistent with an origin as the depleted residue after partial melting and magma genesis in the mantle below an oceanic spreading centre. A characteristically low Cr# for harzburgitic chrome-spinels (consistently less than 50), combined with clinopyroxene content of the peridotite being greater than 5 modal percent in some areas, suggests an abyssal or mid-ocean ridge origin for these ultramafic rocks. Ultramafic rocks formed in such an environment are typically chromite poor (Roberts, 1988) a feature consistent with the lack of alpine-type chromite deposits in ultramafic rocks of the Cache Creek Terrane.

Whole-rock major, trace and REE chemistry of basalts throughout the study area suggest a mid-ocean-ridge eruptive setting for these volcanic rocks. Such an origin is consistent with the suggested setting for the formation of the residual ultramafic rocks and suggests a genetic relationship between the two units. It is suggested that the partial melting of the mantle source region which produced the residual harzburgite also generated the melt from which the basalts crystallized.



## REFERENCES

- Aitken, J.D. (1959): Atlin Map-area; British Columbia; *Geological Survey of Canada*, Memoir 307, 89 pages.
- Alabaster, T., Pearce, J.A. and Malpas, J. (1982): The Volcanic Stratigraphy and Petrogenesis of the Oman Ophiolite Complex; *Contributions to Mineralogy and Petrology*, Volume 81, pages 168-183.
- Andrew, K.P.E. (1985): Fluid Inclusion and Chemical Study of Gold-Quartz Veins in the Atlin Camp, Northwestern British Columbia; unpublished B.Sc. thesis, *The University of British Columbia*, 117 pages.
- Andrews, E. and Ebihara, M. (1982): Solar-system Abundance of the Elements; *Geochimica et Cosmochimica Acta*, Volume 46, pages 2363-2380.
- Ash, C.H. and Arksey, R.L. (1990a): The Atlin Ultramafic Allochthon: Ophiolitic Basement within the Cache Creek Terrane; Tectonic and Metallogenic Significance; in *Geological Fieldwork 1989, B.C. Ministry of Energy, Mines and Petroleum Resources*, Paper 1990-1, pages 365-374.
- Ash, C.H. and Arksey, R.L. (1990b): The Listwanite - Lode Gold Association in British Columbia; in *Geological Fieldwork 1989, B.C. Ministry of Energy, Mines and Petroleum Resources*, Paper 1990-1, pages 359-364.
- Ash, C.H. and Arksey, R.L. (1990c): Geology and Tectonic Setting of the Atlin Ultramafic Allochthon; *B.C. Ministry of Energy, Mines and Petroleum Resources*, Open File 1990-22.
- Ash, C.H., Macdonald, R.W.J. and Arksey, R.L. (1992): Towards a Deposit Model for Ophiolite-related Mesothermal Gold in British Columbia; in *Geological Fieldwork 1991*, Grant, B. and Newell, J.M., Editors, *B.C. Ministry of Energy, Mines and Petroleum Resources*, Paper 1992-1, pages 253-260.
- Ash, C. H., Macdonald R.W.J., Arksey, R.L., Renyolds, P. and Chaudhry, M. (in preparation): Deposit Model for Ophiolite-related Lode Gold Deposit in British Columbia; *B.C. Ministry of Energy, Mines and Petroleum Resources*.
- Aubouin, J. (1989): Some Aspects of Subduction Zones; *Tectonophysics*, Volume 160, pages 1-21.
- Ballantyne, S.B. and MacKinnon, H.F. (1986): Gold in the Atlin Terrane, British Columbia; Abstract in Gold 86, *An International Symposium on the Geology of Gold Deposits*, Chapter, A.M., Editor, *Geological Association of Canada*, pages 16-17.
- Bloodgood, M.A. and Bellefontaine, K.A. (1990): The Geology of the Atlin Area (Dixie Lake and Teresa Island) (104N/6 and parts of 104N/5 and 12); in *Geological Fieldwork 1989, B.C. Ministry of Energy, Mines and Petroleum Resources*, Paper 1990-1, pages 205-215.
- Bloodgood, M.A., Rees, C.J. and Lefebure, D.V. (1989a): Geology and Mineralization of the Atlin Area, Northwestern British Columbia; in *Geological Fieldwork 1988, B.C. Ministry of Energy, Mines and Petroleum Resources*, Paper 1989-1, page 311-322.
- Bloodgood, M.A., Rees, C.J. and Lefebure, D.V. (1989b): Geology of the Atlin Area; *B.C. Ministry of Energy, Mines and Petroleum Resources*, Open File 1989-15a.
- Bozek, J. (1989): Trace Element Geochemistry and Carbonate Mineralogy of the Pictou and Yellowjacket Showings, Atlin, B.C.; unpublished B.Sc. thesis, *Memorial University of Newfoundland*, 103 pages.
- Brown, M. (1980): Textural and Geochemical Evidence for the Origin of Some Chromite Deposits in the Oman Ophiolite; in Ophiolites, Panayiotou, A., Editor; *Proceedings of the International Ophiolite Symposium, Cyprus, 1979, Cyprus Ministry of Agriculture and Natural Resources*, Geological Department, pages 714-721.
- Boudier, F., Nicolas, A. and Bouchez, J.L. (1982): Kinematics of Oceanic Thrusting and Subduction from Basal Sections of Ophiolites; *Nature*, Volume 296, pages 825-828.
- Buisson, G. and Leblanc, M. (1985): Gold in Carbonatized Ultramafic Rocks from Ophiolite Complexes; *Economic Geology*, Volume 80, pages 2028-2029.
- Buisson, G. and Leblanc, M. (1986): Gold-bearing Listwanites (Carbonatized Ultramafic Rocks) from Ophiolite Complexes; in *Metallogeny of Basic and Ultrabasic Rocks*, Gallagher, M.J., Ixer, R.A., Neary, C.R. and Prichard, H.M., Editors, *The Institution of Mining and Metallurgy*, pages 121-131.
- Cann, J.R. (1970): Rb, Sr, Y, Zr and Nb in Some Ocean-floor Basaltic Rocks; *Earth and Planetary Science Letters*, Volume 19, pages 7-11.
- Christopher, P.A. and Pinsent, R.H. (1979): Geology of the Ruby Creek and Boulder Creek Area near Atlin (104N/11W); *B.C. Ministry of Energy, Mines and Petroleum Resources*, Preliminary Map No. 2, with accompanying notes, 10 pages.
- Coleman, R.G. (1977): Ophiolites, Ancient Oceanic Lithosphere?; *Springer-Verlag*, 229 pages.
- Coney, J.P. (1989): Structural Aspects of Suspect Terranes and Accretionary Tectonics in Western North America;

- Journal of Structural Geology*, Volume 11, No. 1/2, pages 107-125.
- Cordey, F. (1990): Comparative Study of Radiolarian Faunas from the Sedimentary Basins of the Insular, Coast and Intermontane Belts; unpublished in house report, 57 pages.
- Cordey, F., Gordey, S.P. and Orchard, M.J. (1991): New Biostratigraphic Data for the Northern Cache Creek Terrane, Teslin Map Area, Southern Yukon; *Geological Survey of Canada*, Current Research Part E, Paper 91-1E, pages 67-76.
- Dawson, K.M. (1988): Radiogenic Age and Isotopic Studies: Report 2; *Geological Survey of Canada*, Paper 88-2.
- Dick, H.J.B. and Bullen, T. (1984): Chrome Spinel as a Petrogenetic Indicator in Abyssal and Alpine-type Peridotites and Spatially Associated Lavas; *Contributions to Mineralogy and Petrology*, Volume 86, pages 54-76.
- Dick, H.J.B. and Fisher, R.L. (1984): Mineralogic Studies of the Residues of Mantle Melting: Abyssal and Alpine-type Peridotites; in *Kimberlites II: The Mantle and Crust-Mantle Relationships*, Kornprobst, J., Editor, *Elsevier*, pages 293-308.
- Duke, J.M. (1983): Ore Deposit Models 7. Magmatic Segregation Deposits of Chromite; *Geoscience Canada*, Volume 10, Number 1, pages 15-24.
- Gass, I.G. (1980): Troodos Massif: Its Role in the Unravelling of the Ophiolite Problem and its Significance in the Understanding of Constructive Plate Margin Processes; in *Ophiolites*, Panayiotou, A., Editor, Proceedings of the International Ophiolite Symposium, Cyprus, 1979, *Cyprus Ministry of Agriculture and Natural Resources*, Geological Department, pages 23-34.
- Gabrielse, H. (1985): Major Dextral Transcurrent Displacements Along the Northern Rocky Mountain Trench and Related Lineaments in North Central British Columbia; *Geological Survey of America Bulletin*, Volume 96, pages 1-14.
- Gabrielse, H. (1991): Late Paleozoic and Mesozoic Terrane Interactions in North-central British Columbia; *Canadian Journal of Earth Sciences*, Volume 28, pages 947-957.
- Gabrielse, H. and Yorath, C.J. (1989): Decade of North American Geology #4. The Cordilleran Origin in Canada; *Geoscience Canada*, Volume 16, Number 2, pages 67-83.
- Gealey, W.K. (1980): Ophiolite Obduction Mechanism; in *Ophiolites*, Proceedings of the International Ophiolite Symposium Cyprus, 1979, Panayiotou, A., Editor, *Cyprus Ministry of Agriculture and Natural Resources*, Geological Survey Department, pages 228-243.
- Gregory, R.T. (1984): Melt Percolation Beneath a Spreading Ridge: Evidence from the Semail Peridotite, Oman; in *Ophiolites and Oceanic Lithosphere*, Gass, I.G., Lip-pard S.J. and Shilton A.W., Editors, *Blackwell*, Oxford, pages 55-62.
- Harte, B. (1977): Rock Nomenclature with Particular Relation to Deformation and Recrystallization Textures in Olivine-bearing Xenoliths; *Journal of Geology*, Volume 85, pages 279-288.
- Hodgson, C.J., Chapman, R.S.G. and MacGeehan, P.J. (1982): Application of Exploration Criteria for Gold Deposits in the Superior Province of the Canadian Cordillera; in *Precious Metals in the Northern Cordillera*, Levinson, A.A., Editor, *Association of Exploration Geochemists*, pages 174-206.
- Hoffman, P.F. (1990): On Accretion of Granite-Greenstone Terranes; in *Greenstone Gold and Crustal Evolution*, Roberts, F., Sheaham P.A. and Green, S.B., Editors, *The NUNA Conference Volume*, pages 32-45.
- Humphries, S.E. and Thompson, G. (1978): Trace Element Mobility During Hydrothermal Alteration of Oceanic Basalts; *Geochimica et Cosmochimica Acta*, Volume 42, pages 127-136.
- Irvine, T.N. (1967): Chromian Spinel as a Petrogenetic Indicator: Part 2, Petrologic Applications; *Canadian Journal of Earth Science*, Volume 4, pages 71-103.
- Irvine, T.N. (1977): Origin of Chromite Layers in the Muskox Intrusion and Other Stratiform Intrusions: A New Interpretation; *Geology*, Volume 5, pages 273-277.
- Jakes, P.J. and Gill, J. (1970): Rare Earth Elements and the Island Arc Tholeiitic Series; *Earth and Planetary Science Letters*, Volume 9, pages 17-28.
- Karamata, S. (1980): Metamorphism Beneath Obducted Ophiolite Slabs; in *Ophiolites*, Proceedings of the International Ophiolite Symposium Cyprus, 1979, Panayiotou, A., Editor, *Cyprus Ministry of Agriculture and Natural Resources*, Geological Survey Department, pages 219-227.
- Lago, B.L., Rabinowicz, M. and Nicolas, A. (1982): Podiform Chromite Ore Bodies: A Genetic Model; *Journal of Petrology*, Volume 23, pages 103-125.
- Lefebure, D.V. and Gunning, M.H. (1988): Yellowjacket; in *Exploration in British Columbia 1987*, Part B, *B.C. Ministry of Energy, Mines and Petroleum Resources*, Pages B87-B95.
- Lefebure, D.V. and Gunning, M.H. (1989): Geological Compilation Map of the Atlin Area; *B.C. Ministry of Energy, Mines and Petroleum Resources*, Open File 1989-24.
- Le Maitre, R.W. (1989): A Classification of Igneous Rocks and Glossary of Terms; *Blackwell*, Oxford, 193 pages.
- Le Maitre, R.W. (1984): A Proposal by the IUGS Subcommittee on the Systematics of Igneous Rocks for a

- Chemical Classification of Volcanic Rocks Based on the Total Alkali Silica (TAS) Diagram; *Australian Journal of Earth Science*, Volume 31, pages 243-255.
- Lueck, B.A. (1985): Geology of Carbonatized Fault Zones on the Anna Claims and their Relationship to Gold Deposits, Atlin, B.C. unpublished B. Sc. thesis, *The University of British Columbia*, 35 pages.
- Malpas, J.G. (1973): The Dynamothermal Aureole of the Bay of Islands Ophiolite Suite; *Canadian Journal of Earth Sciences*, Volume 16, pages 2086-2101.
- Malpas, J.G. (1973): A Restored Section of Oceanic Crust and Mantle in Western Newfoundland; *Geological Society of America*, Northeast Section, Abstracts with Programs, No.2, Volume 5, page 192.
- Malpas, J.G. (1978): Magma Generation in the Upper Mantle, Field Evidence from Ophiolite Suites, and Application to the Generation of Oceanic Lithosphere; *Royal Society of London*, Philosophical Transactions, Volume A. 288, pages 527-546.
- Marud, D.E. (1988a): Summary Report Surface Drilling, Arent 1, Arent 2, Beama and Adjacent Claims, North and South Claim Groups, Yellowjacket Property, Atlin Mining Division, Volume I of III; *B.C. Ministry of Energy, Mines and Petroleum Resources*, Assessment Report 17,295.
- Marud, D.E. and Southam, P. (1988): Summary Report Diamond Drilling, Arent 1, Arent 2 and Adjacent Claims, North and South Claim Groups, Yellowjacket Property, Atlin Mining Division; Volume I of IV; *B.C. Ministry of Energy, Mines and Petroleum Resources*, Assessment Report 18,608.
- McIvor, D. (1988a): Summary Report; Results of Rotary Reverse-circulation Drilling Program on the Pictou Property, Atlin Mining Division; *B.C. Ministry of Energy, Mines and Petroleum Resources*, Assessment Report 17,546.
- McIvor, D. (1988b): Summary Report, Mineral Exploration Activity on the Heart of Gold Property (Porsche, Millionaire, Goldstar 1, Goldstar 2, Anna 1-8 Mining Claims) Atlin Mining District, British Columbia; *B.C. Ministry of Energy, Mines and Petroleum Resources*, Assessment Report 17,997.
- Menzies, M. and Allen, C. (1974): Plagioclase Lherzolite - Residual Mantle Relationships within Two Eastern Mediterranean Ophiolites; *Contributions to Mineralogy and Petrology*, Volume 45, pages 197-213.
- Meschede, M. (1986): A Method of Discriminating Between Different Types of Mid-ocean Ridge Basalts and Continental Tholeiites with the Nb-Zr-Y Diagram; *Chemical Geology*, Volume 56, pages 207-218.
- Mihalynuk, M.G., Smith, M., Lefebure, D.V. and Gabites, J.E. (1992): Age of Emplacement and Basement Character of the Cache Creek Terrane as Constrained by New Isotopic and Geochemical Data; *Canadian Journal of Earth Sciences*, Volume 29, Number 11, pages 2463-2477.
- Monger, J.W.H. (1975): Upper Paleozoic Rocks of the Atlin Terrane; *Geological Survey of Canada*, Paper 74-47, 63 pages.
- Monger, J.W.H. (1977a): Ophiolitic Assemblages in the Canadian Cordillera; in North American Ophiolites, Coleman, R.G. and Irwin, W.P., Editors, *State of Oregon, Department of Geology and Mineral Industries*, Bulletin 95, pages 59-65.
- Monger, J.W.H. (1977b): Upper Paleozoic Rocks of the Western Canadian Cordillera and Their Bearing on the Cordilleran Evolution; *Canadian Journal of Earth Sciences*, Volume 14, pages 1832-1859.
- Monger, J.W.H. (1977c): Upper Paleozoic Rocks of Northwestern British Columbia; *Geological Survey of Canada*, Paper 77-1A, pages 255-262.
- Monger, J.W.H. (1984): Cordilleran Tectonics: A Canadian Perspective; *Bulletin de la Société Géologique de France*, Volume 7.A XXVI, No.2, pages 255-278.
- Monger, J.W.H., Price, R.A. and Tempelman-Kluit, D.J. (1982): Tectonic Accretion and the Origin of the Two Major Plutonic Belts in the Canadian Cordillera; *Geology*, Volume 10, pages 70-75.
- Monger, J.W.H., Souther, J.G. and Gabrielse, H. (1972): Evolution of the Canadian Cordillera: A Plate-tectonic Model; *American Journal of Science*, Volume 272, pages 577-602.
- Neary, C.R. and Brown, M.A. (1979): Chromite from Al'Ays Complex, Saudi Arabia and the Semai Complex, Oman; in Evolution and Mineralization of the Arabian Shield, Al-Shanti, A.M.S., Editor, I.G.A., Bulletin 2, pages 193-205.
- Newton, D.C. (1985): A Study of Carbonate Alteration of Serpentinites Around Au and Ag-bearing Quartz Veins in the Atlin Camp, British Columbia; unpublished B.Sc. thesis, *The University of British Columbia*, 85 pages.
- Nicolas, A. (1986): Structure and Petrology of Peridotites: Clues to their Geodynamic Environment; *Reviews of Geophysics*, Volume 24, No.4, pages 875-895.
- Nicolas, A. and Poirier, J.P. (1976): Crystalline Plasticity and Solid State Flow in Metamorphic Rocks; *J. Wiley-Interscience*, London, 444 pages.
- Nicolas, A. and Violette, J.F. (1982): Mantle Flow at Oceanic Spreading Centers: Models Derived from Ophiolites; *Tectonophysics*, Volume 81, pages 319-339.
- Nicolas, A., Boudier, F. and Bouchez, J. (1980): Interpretation of Peridotite Structures from Ophiolitic and Oceanic Environments; *American Journal of Science*, Volume 280-A, pages 192-190.
- Norrell, G.T., Teixell, A. and Harper, G.D. (1989): Microstructure of Serpentinite Mylonites from the Josephine

- Ophiolite and Serpentinization in Retrogressive Shear Zones, California; *Geological Society of America, Bulletin*, Volume 101, pages 637-682.
- Orchard, M.J. (1991): Conodonts, Time and Terranes: An Overview of the Biostratigraphic Record in the Western Canadian Cordillera; in *Ordovician to Triassic Conodont Paleontology of the Canadian Cordillera*, Orchard, M.J. and McCracken, A.D., Editors, *Geological Survey of Canada, Bulletin* 417, pages 1-25.
- Pearce, J.A. (1980): Geochemical Evidence for the Genesis and Eruptive Setting of Lavas from Tethyan Ophiolites; in *Ophiolites, Proceedings of the International Ophiolite Symposium, Cyprus, 1979*, Panayiotou, A., Editor, *Cyprus Ministry of Agriculture and Natural Resources, Geological Survey Department*, pages 261-272.
- Pearce, J.A. (1982): Trace Element Characteristics of Lavas from Destructive Plate Boundaries; in *Andesites*, Thorpe, R.S., Editor, *John Wiley and Sons*, pages 525-548.
- Pearce, J.A. (1983): Role of the Sub-continental Lithosphere in Magma Genesis at Active Continental Margins; in *Continental Basalts and Mantle Xenoliths*, Hawkesworth, C.J., and Norry, M.J., Editors, *Shiva Publications*, Nantwich, pages 230-249.
- Pearce, J.A. and Cann, J.R. (1973): Tectonic Setting of Basic Volcanic Rocks Determined Using Trace Element Analyses; *Earth and Planetary Science Letters*, Volume 19, pages 290-300.
- Pearce, J.A. and Norry, M.J. (1979): Petrogenetic Implications of Ti, Zr, Y and Nb Variations in Volcanic Rocks; *Contributions to Mineralogy and Petrology*, Volume 69, pages 33-47.
- Pouchou, J.L. and Pichoir, F. (1984): A New Model for Quantitative Analysis: Part I. Application to the Analysis of Homogeneous Samples; *La Recherche Aérospatiale*, Volume 5, pages 47-65.
- Pouchou, J.L. and Pichoir, F. (1985): 'PAP' o(pZ) Procedure for Improved Microanalysis; *Microbeam Analysis*, pages 104-106.
- Raymond, L.A. (1984): Classification of Mélanges; in *Mélanges: Their Nature, Origin, and Significance*, Raymond, L.A., Editor, *Geological Society of America, Special Paper* 198, pages 7-20.
- Rees, C.J. (1989): Pictou; in *Exploration in British Columbia 1988, Part B*, *B.C. Ministry of Energy, Mines and Petroleum Resources*, pages B163-B167.
- Ricketts, R.D., Evenchick, C.A., Anderson, R.G. and Murphy, D.C. (1992): Bowser Basin, Northern British Columbia: Constraints on the Timing of Initial Subsidence and Stikinia-North America Terrane Interactions; *Geology*, Volume 20, pages 1119-1122.
- Roberts, S. (1988): Ophiolitic Chromitite Formation: A Marginal Basin Phenomenon?; *Economic Geology*, Volume 83, pages 1034-1036.
- Saunders, A.D., Tarney, J., March, N.G. and Wood, D.A. (1980): Ophiolites as Ocean Crust or Marginal Basin Crust: A Geochemical Approach; in *Ophiolites, Proceedings of the International Ophiolite Symposium, Cyprus, 1979*, Panayiotou, A., Editor, *Cyprus Ministry of Agriculture and Natural Resources, Geological Survey Department*, pages 193-204.
- Schroeter, T.G., Lund, C. and Carter, G. (1989): Gold Production and Reserves in British Columbia; *B.C. Ministry of Energy, Mines and Petroleum Resources, Open File* 1989-22, 86 pages.
- Shervais, J.W. (1982): Ti-plots and the Petrogenesis of Modern and Ophiolitic Lavas; *Earth and Planetary Science Letters*, Volume 59, pages 101-118.
- Souther, J.G. (1977): Volcanism and Tectonic Environments in the Canadian Cordillera - A Second Look; in *Volcanic Regimes in Canada*, Baragar, W.R.A., Coleman, L.C. and Hall, J.M., Editors, *Geological Association of Canada, Special Paper*, pages 3-24.
- Stevens, R.D., Delabio, R.N. and Lachance, G.R. (1982): Age Determinations and Geological Studies: K-Ar Isotopic Ages, Report 15; *Geological Survey of Canada, Paper* 81-2, 56 pages.
- Streckeisen, A. (1975): To Each Plutonic Rock Its Proper Name; *Earth Science Reviews*, Volume 12, pages 1-33.
- Thayer, T.P. (1964): Principal Features and Origin of Podiform Chromite Deposits, and some Observations on the Guleman-Soridag District, Turkey; *Economic Geology*, Volume 59, pages 1497-1524.
- Thayer, T.P. (1969): Gravity Differentiation and Magmatic Re-emplacment of Podiform Chromite Deposits; *Economic Geology Monograph*, No.4, pages 132-146.
- White, W.M. and Patchett, J. (1984): Hf-Nd-Sr Isotopes and Incompatible Element Abundances in Island-arcs: Implications for Magma Origins and Crust-Mantle Evolution; *Earth and Planetary Science Letters*, Volume 67, pages 167-185.
- Williams, H. and Smyth, W.R. (1973): Metamorphic Aureoles Beneath Ophiolite Suites and Alpine Peridotite: Tectonic Implications with West Newfoundland Examples; *American Journal of Science*, Volume 273, pages 594-621.
- Winchester, J.A. and Floyd, P.A. (1977): Geochemical Discrimination of Different Magma Series and their Differentiation Products Using Immobile Elements; *Chemical Geology*, Volume 20, 325-343.

**BULLETIN 94**  
**GEOLOGY OF THE ATLIN AREA,**  
**NORTHWESTERN**  
**BRITISH COLUMBIA**

NTS 104N/11W, 12E

Geology by C.H. Ash

Scale 1:25 000



**LEGEND**

**QUATERNARY**

Qal Unconsolidated glacial till and poorly sorted alluvium

13 HYDROMAGNESITE: white, powdery with a uniform texture and composition, no bedding or structure evident, thickness ranges from 0.1 to 1.1 metres

**MIDDLE JURASSIC**

**FOURTH OF JULY BATHOLITH**

12 GRANODIORITE: buff-white to dull pink, medium- to coarse-grained, k-feldspar megacrysts, megacrysts up to 2 cm (20-40%) in a medium-grained matrix of quartz, plagioclase, biotite, accessory magnetite and zircon  
 12a FELDSPAR PORPHYRY: buff-white to dull pink fine grained with 15 to 30%, 4 to 9 millimetre feldspar phenocrysts, hornblende phenocrysts from 3 to 6 millimetre varies from trace to 15%; unit typically occurs as 0.5 to 2 metre wide dikes and small stocks

**MISSISSIPPIAN TO MIDDLE JURASSIC**

**SEDIMENTARY ROCKS**

11 WACKE: grey, grey-green weathering, with abundant chert clasts and lesser clasts of argillite, quartz and limestone with the latter typically weathering out on surface, locally well bedded  
 10 SEDIMENTARY TECTONIC BRECCIA: tan to rusty-brown, polymictic with angular to rounded fragments of variably bedded to massive limestone and siltstone from several centimetres to metres in size cemented by iron-magnetite, includes minor chert and basalt fragments

9 LIMESTONE: massive, grey to buff-white, light to dark grey weathering, typically recrystallized  
 8 ARGILLITE: dark grey to black (graphitic), fine grained, typically sheared and flaggy

7 CHERY ARGILLITE: dark to pale grey, silicious siltstone, impure chert, typically massive, locally bedded  
 6 CHERY: varies from dark to light grey buff white to red brown to black, massive to commonly ribboned with thinner argillaceous interbeds, where containing interbeds the unit is labeled 6/7

5a METABASALT: grey-green, typically massive, fine- to medium grained, locally auto-brecciated, to flow-banded to pillowed, variably carbonatized (5-20%) with disseminated pyrite (trace to 10%); minor metabasite, undivided  
 5b CARBONATIZED METABASALT: weathers orange-brown; generally massive to brecciated with quartz as veinlets and space filling breccia; traces to accessory amounts of mariposite

4 METAGABBRO: dark grey to buff white, medium to coarse grained equigranular to locally varietured and variably carbonate altered  
 3a PERIDOTITE (WEHRLITE?): black to dark grey, dull to light grey weathering, typically highly serpentinized, locally displays poikilitic textures on well washed surfaces with calcocrysts from 1 to 3 centimetres in size  
 3b LISTWANITE (carbonatized serpentinite): similar to 1c

**MANTLE ROCKS**

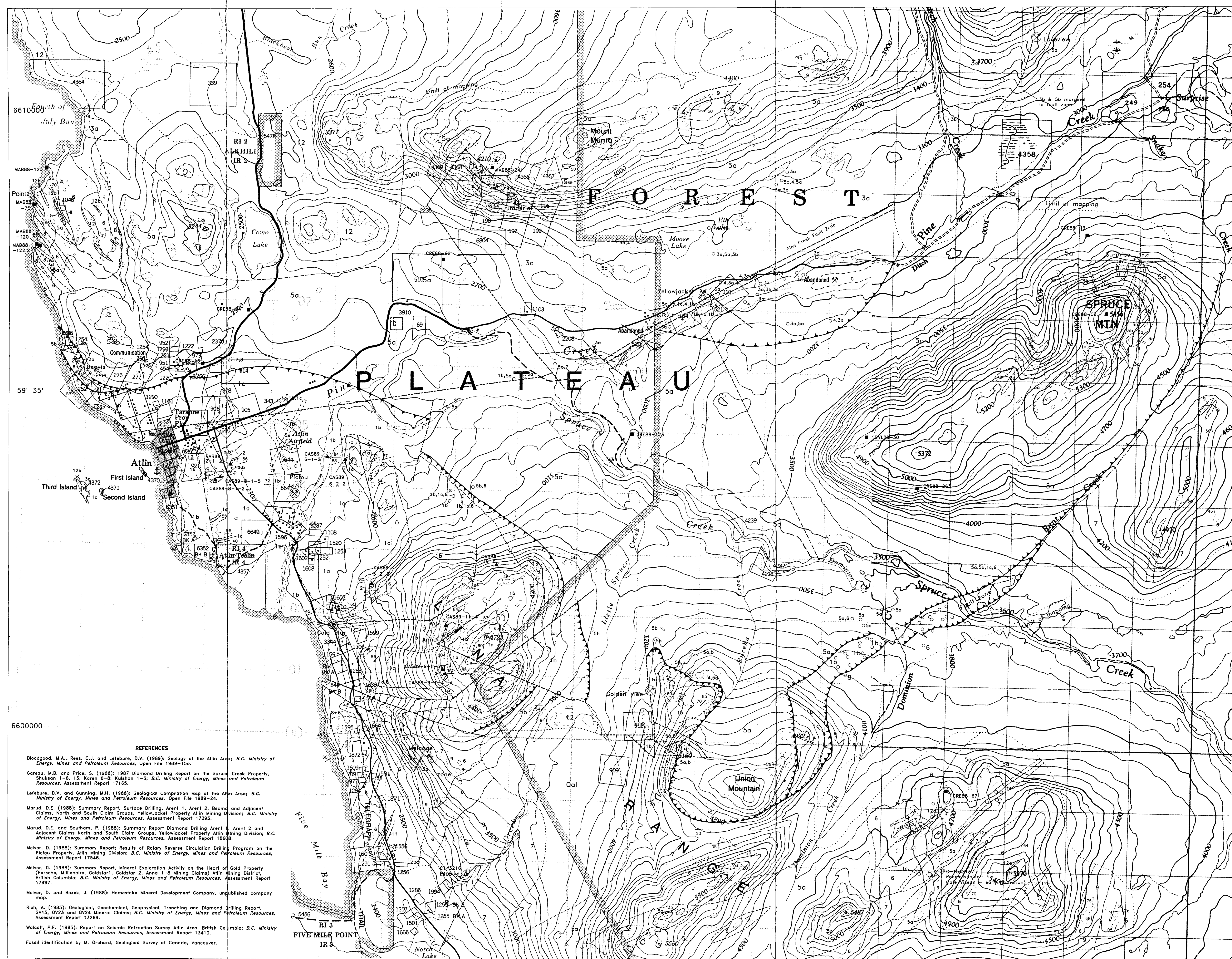
2 DUNITE: dark green, medium-grained equigranular; weathers characteristic tan-brown; variably serpentinized (50 to 100%); occurs as podiform bodies hosted by hornblurgite; trace to 4%, 1-4 mm disseminated chrome-spinel  
 1a HARBURGITE: dark green to black, medium- to coarse-grained porphyroclastic; differential erosion caused by the more resistant orthopyroxene imparts a rough brown weathered surface; accessory chrome-spinel and clinopyroxene; generally 40-60% serpentinized but primary textures are commonly preserved; typically foliated and locally banded  
 1b SERPENTINITE-BASTITE: altered equivalent to 1a; light to dull weathering; locally mylonitic; minor to moderate talc; accessory magnetite and carbonate

**ALTERATION**

1c LISTWANITE (carbonatized serpentinite): buff-white to dull grey, weathers distinctive orange-brown; fault controlled intensity of alteration; quartz stringers and episodic veins (quartziferous); accessory to moderate amounts of malpaisite with higher abundances immediately associated with quartz veins or areas of quartz flooding; sulphides variable (trace to 10%)

**SYMBOLS**

- Geological contact (defined, approximate, inferred, inferred from aeromagnetics).....
- Fault or shear zone (approximate, inferred, inferred from alpha linear).....
- Thrust fault (approximate, inferred, inferred from alpha linear).....
- Tectonic tilting (S1).....
- Tectonic tilting (metamorphic) (S1b).....
- Schistosity-shearing fabric (S2).....
- Bedding.....
- Dike (inclined, vertical, di-diorite).....
- Outcrop location.....
- Drill hole location (lobes indicate down hole progression of units).....
- Local gold showing.....
- Sample location: whole rock geochem.....
- mineral phase chemistry.....
- Trench.....
- Fossil locality with GSC reference number.....



**REFERENCES**

Bloodgood, M.A., Rees, C.J. and Lafabre, D.V. (1989): Geology of the Atlin Area; B.C. Ministry of Energy, Mines and Petroleum Resources, Open File 1989-15a.

Careau, M.B. and Price, S. (1988): 1987 Diamond Drilling Report on the Spruce Creek Property, Shukhan 1-6, 13; Karen 6-8; Kulshan 1-3; B.C. Ministry of Energy, Mines and Petroleum Resources, Assessment Report 17165.

Lafabre, D.V. and Gunning, M.H. (1988): Geological Compilation Map of the Atlin Area; B.C. Ministry of Energy, Mines and Petroleum Resources, Open File 1988-24.

Marud, D.E. (1988): Summary Report, Surface Drilling, Arent 1, Arent 2, Beama and Adjacent Claims, North and South Claim Groups, Yellowjacket Property, Atlin Mining Division; B.C. Ministry of Energy, Mines and Petroleum Resources, Assessment Report 17295.

Marud, D.E. and Southam, P. (1988): Summary Report Diamond Drilling Arent 1, Arent 2 and Adjacent Claims North and South Claim Groups, Yellowjacket Property, Atlin Mining Division; B.C. Ministry of Energy, Mines and Petroleum Resources, Assessment Report 18668.

Mclvor, D. (1988): Summary Report; Results of Rotary Reverse Circulation Drilling Program on the Pictou Property, Atlin Mining Division; B.C. Ministry of Energy, Mines and Petroleum Resources, Assessment Report 17546.

Mclvor, D. (1988): Summary Report, Mineral Exploration Activity on the Heart of Gold Property (Parsche, Milloniere, Gaisstar), Goldstar 2, Anna 1-8 Mining Claims) Atlin Mining District, British Columbia; B.C. Ministry of Energy, Mines and Petroleum Resources, Assessment Report 17997.

Mclvor, D. and Bozek, J. (1988): Homestake Mineral Development Company, unpublished company map.

Rich, A. (1985): Geological, Geochemical, Geophysical, Tracing and Diamond Drilling Report, GV15, GV23 and GV24 Mineral Claims; B.C. Ministry of Energy, Mines and Petroleum Resources, Assessment Report 13269.

Walcott, P.E. (1985): Report on Seismic Refraction Survey Atlin Area, British Columbia; B.C. Ministry of Energy, Mines and Petroleum Resources, Assessment Report 13410.

Fossil identification by M. Orchard, Geological Survey of Canada, Vancouver.